universität wien

MASTERARBEIT / MASTER'S THESIS

Titel der Masterarbeit / Title of the Master's Thesis

„Evaluation of eicosanoid releasates in platelet concentrates consequent to two different pathogen inactivation techniques“

verfasst von / submitted by

Gerhard Hagn BSc

angestrebter akademischer Grad / in partial fulfilment of the requirements for the degree of

Master of Science (MSc)

Wien, 2019 / Vienna 2019

Studienkennzahl lt. Studienblatt / degree programme code as it appears on the student record sheet:	A 066 862
Studienrichtung lt. Studienblatt / degree programme as it appears on the student record sheet:	Masterstudium Chemie
Betreut von / Supervisor:	Univ.-Prof. Dr. Christopher Gerner

Acknowledgements

First of all I would like to thank Univ.-Prof. Dr. Christopher Gerner for giving me the opportunity to work with him and his group on such an interesting project. Since this project is a cooperation with the general hospital of Vienna, I would like to thank Ass.-Prof. Dr. Gerda Leitner as well for giving me permission to work on the project.

But I would like to thank the entire working group, especially Laura Niederstätter, who trained me in eicosanoid analysis, showed me everything from sample preparation to data analysis and provided valuable input. Furthermore I want to express my gratitude to Dr. Astrid Slany, Dr. Besnik Muqaku, Dr. Samuel Meier-Menches, Julia Brunmair, Lukas Janker and Benjamin Neuditschko for always being available for questions. Last but not least I want to thank Peter Frühauf and Dr. Johanna Mader for technical support, discussion and giving advices.

Contents

List of Figures

List of Tables

List of Equations

Abbreviations

AA arachidonic acid

AABG advanced active beam guide

AC alternating current

act activated group

ADP adenosine diphosphate

AP-1 activator protein-1

AQT hyperquad mass filter with advanced quadrupole technology

ATP adenosine triphosphate

AUC area under curve

$CaCl_2$ calcium chloride

CAD compound adsorption device

con control group

COX cyclooxygenase

$cPLA_2$ cytosolic calcium-dependent phospholipase A_2

CsCl cesium-137 chloride

CV coefficient of variation

CYP cytochrome P450

DC direct current

DHA docosahexaenoic acid

DMSO dimethyl sulfoxide

DNA deoxyribonucleic acid

EET epoxyeicosatrienoic acid

EIC extracted ion chromatogram

EPA eicosapentaenoic acid

ESI electrospray ionisation

FA fatty acyls

FWHM full width at half maximum

GC gas chromatography

GL glycerolipids

GP glycerophospholipids

Gy Gray

HCD higher-energy collisional dissociation

HETE hydroxyeicosatetraenoic acid

HHT hydroxyheptadecatrienoic acid

HPETE hydroperoxyeicosatetraenoic acid

HPLC high-performance liquid chromatography

HR-MS high-resolution mass spectrometry

iPLA$_2$ cytosolic calcium-independent phospholipase A_2

LC liquid chromatography

LOD limit of detection

LOX lipoxygenase

LPC lysophosphatidylcholine

LT leukotriene

MAPK mitogen-activated protein kinase

MOA mechanism of action

mRNA messenger ribonucleic acid

MS mass spectrometry

m/z mass-to-charge ratio

OH hydroxy

PAS platelet additive solution

PC phosphatidylcholine

PG prostaglandin

PGI_2 prostacyclin

PK polyketides

PL phospholipase

ppm parts per million

PR prenol lipids

PS phosphatidylserine

PSL platelet storage lesion

PUFA polyunsaturated fatty acid

PVC polyvinyl chloride

RNA ribonucleic acid

RNS reactive nitrogen species

ROS reactive oxygen species

rpm revolutions per minute

SL saccharolipids

S/N signal-to-noise ratio

SP shingolipids

SPE solid-phase extraction

$iPLA_2$ secreted phospholipase A_2

SCC squamous cell carcinoma

ST sterol lipids

TA-GVHD transfusion-associated graft-versus-host disease

TCA tricarboxylic acid

TIC total ion chromatogram

TX thromboxane

UHPLC ultra-high-performance liquid chromatography

UVA ultraviolet A irradiation

VEGF vascular endothelial growth factor

1 Introduction

1.1 Motivation and scope of work

The transmission of pathogens via blood transfusion is still a major threat, thus there are two established standard pathogen inactivation techniques. This study will demonstrate significant differences in the eicosanoid pattern in platelet concentrates consequent to the two diverse ex-vivo procedures and how storage time is effecting this pattern. In cooperation with the general hospital of Vienna, blood samples were taken from 14 different donors, platelet concentrates were generated and analysed before and after pathogen inactivation using liquid chromatography coupled mass spectrometry (LC-MS). Therefore, samples were drawn the first day before treatment and then divided into two sets. Afterwards, one set was treated with cesium-137 chloride (CsCl) and the second set with the INTERCEPT Blood System^{TM} utilizing amotosalen and ultraviolet A irradiation (UVA). The treated samples were stored up to the seventh day to determine possible modifications during the storage of platelet concentrates. In addition to the samples taken at day one, which received no treatment, samples after pathogen inactivation were drawn at day two, five and seven for both inactivation procedures. Furthermore the platelet responsivity on the basis of eicosanoids to in vitro stimulation via ionomycin was investigated.

1.2 Platelets

Platelets are the smallest cells in the blood. These anucleate cytoplasmic fragments derive from megakaryocytes mainly in the bone marrow [2], but also in the lung [3]. Platelets are involved in various physiological and pathophysiological processes like haemostasis and arterial thrombosis [2, 4, 5]. But they are also playing an important role in promoting inflammatory and immune responses [6], tumor growth and metastasis [7, 8]. Thus, platelets are often targeted in bio-analytical and therapeutical approaches as a combination of cyclophosphamide and a thrombin inhibitor resulted in a decrease of tumor growth and metastasis within a mouse tumor model [9].

1.3 Lipids

Due to the immense structural and functional diversity of lipids, they play essential roles in the structure of cells and signal transduction within and between cells [10]. Disturbances in the lipid metabolism are linked to several diseases such as type 2 diabetes [11] and cancer [12]. But lipids are

also involved in various processes of platelet biology like regulating platelet coagulation by diverse eicosanoids, as described in section 1.4.

1.4 Eicosanoids

Eicosanoids are a bioactive subclass of lipids arising from arachidonic acid (AA) and related polyunsaturated fatty acids (PUFAs) oxidation via cyclooxygenase (COX) [13], lipoxygenase (LOX) [14] and cytochrome P450 (CYP) enzymes [15] or via non-enzymatic free radical mechanisms [16]. The term eicosanoid is summing up three clans: Prostanoids (with prostaglandins, prostacyclin and thromboxanes), leukotrienes and epoxides (epoxyeicosatrienoic acids) [17]. Studies could demonstrate the involvement of leukotrienes or prostanoids in regulation of diverse homeostatic and inflammatory processes or angiogenesis [16–18]. They are also involved in various diseases such as cardiovascular diseases [15]. In addition Wang et al. [19] described the role of eicosanoids in cancer especially in epithelial-derived tumors. Among other molecules the reactivity of platelets is also based on eicosanoids. While the COX-1-generated thromboxane (TX)A_2 is mainly responsible for stimulating platelet aggregation, the COX-2-derived prostaglandin (PG)I_2 produced by endothelial cells represents its antagonist and therefore inhibits platelet aggregation [16].

2 Theoretical background

2.1 Platelets, their in vitro activation and pathogen inactivation

2.1.1 Platelets

Platelets were first described by Giulio Bizzozero in 1882 [20]. As mentioned before, these nonnucleated, discoid shaped cells are the smallest cells in mammalian blood (approximately 2 μm in diameter) and derive from megakaryocytes mainly within the bone marrow [2, 21, 22]. A photograph of a platelet and its shape taken with a low-voltage, high-resolution scanning electron microscope is presented in Fig. 1 [21]. Since 2017 we know that platelets are released at high levels in the lungs by megakaryocytes circulating through them [3]. Approximately 100 billion platelets are produced every day by the human body and they are circulating up to 10 days in the bloodstream, which is apparently regulated by their own apoptotic program [23]. Human platelets are containing granules (α, δ, dense and lysosomes), mitochondria and endoplasmic reticulum [7, 24].

Haemostasis, the sensing of injured vessel endothelium and initiating blood clotting to clog the leakage, is the primary physiological role of platelets, which is depicted in Fig. 2 [2, 25]. Platelets are sensing the exposed collagen and extracellular matrix proteins and therefore are adhering to this area, which initiates aggregation of those platelets in combination with neutrophils and red blood cells [2]. Furthermore, these aggregated cells are releasing procoagulant factors such as adenosine diphosphate (ADP) and TXA_2, and also thrombin, which is activating the coagulation cascade. Herein, the adherent, activated platelets are recruiting other platelets [2]. This procoagulant function relies on their ability to turn the negatively charged phosphatidylserine (PS) to the outer membrane followed by activation and localization of the aggregated complexes [26]. The PS-expressing platelet membrane supports the formation of fibrin, which stabilizes platelet-thrombi resulting in a blood clot [2, 4]. A fine balance between pro- and anticoagulation factors like cell-cell interactions, environmental influences or various proteins and lipids are avoiding either haemorrhage or thrombosis [4, 6, 27].

Platelets are also involved in inflammatory processes [22, 28]. They are capable of storing, producing and releasing pro- and anti-inflammatory molecules like cytokines and chemokines, which are chemotactic for neutrophils and monocytes [22]. Thus, platelets are leading lymphocytes, neutrophils and monocytes to inflammation area and are enhancing the inflammatory process.

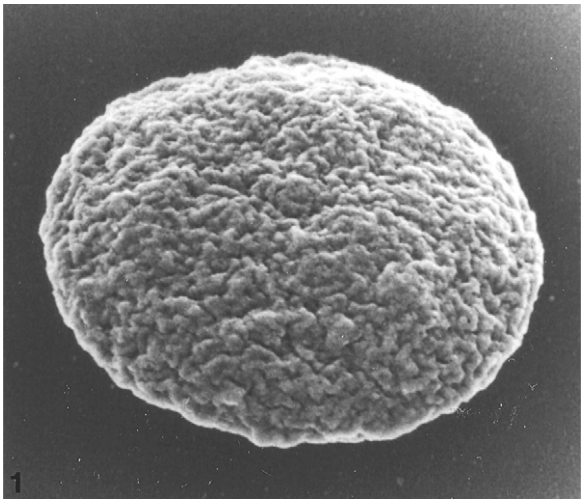

Figure 1: Photograph of platelet presenting its discoid shape recorded with a low-voltage, high-resolution scanning electron microscope [21].

Another field platelets are involved in is angiogenesis [29]. Some essential angiogenesis-regulating agents can be found in platelet-granules [29]. The most potent angiogenesis stimulator vascular endothelial growth factor (VEGF), also present in platelets, benefits vessel wall permeability and attracts endothelial cell sprouting at the beginning of angiogenic response [30]. Because platelet-VEGF is released more significantly in women with early breast cancer, it would serve much better as a biomarker for tumor angiogenesis than serum- or plasma-VEGF [31].

Since wound healing and primary tumor growth are underlying similar mechanistic background-processes, platelets are connected to the latter one [29]. In addition, platelet activation increases metastatic success of embolic tumor cells in vivo via preventing tumor cell clearance by natural killer cells [32].

2.1.2 Platelet in vitro stimulation via ionomycin

The secretome of activated platelets contains more than 300 bioactive molecules from their granules [33]. In vivo stimulation is connected to an increased Ca^{2+} concentration in cytoplasm caused by ionophores, which are supporting the mobilisation of Ca^{2+} from intracellular reservoirs and even the transport of this intracellular Ca^{2+} through the plasma membrane is maintained [34]. The changed Ca^{2+} concentration effects exposure of PS at the outer membrane, which enables quick fibrin formation [26, 35]. Because ionomycin acts as an Ca^{2+} ionophore in terms of inducing rapid shape changes, aggregation

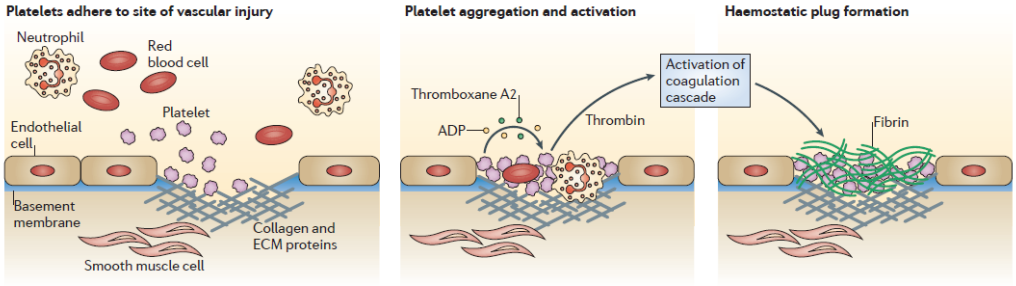

Figure 2: Stages of haemostasis. First, an injured vessel is leading to the exposure of collagen and further extra cellular matrix proteins, which is sensed by platelets and enables adherence to this area. Those activated platelets are releasing pro-coagulant factors like ADP or thromboxane A_2 and they are also producing thrombin. Thrombin is catalysing the activation of the coagulation cascade leading to further platelet recruitment and aggregation. The aggregated platelets, leukocytes and red blood cells are forming the thrombus to clog the leakage, which is stabilised by fibrin formation [2].

and secretion, it can be utilized in combination with calcium chloride ($CaCl_2$) for platelet activation in vitro [34, 35].

2.1.3 Platelet transfusion

A decrease of bleeding by platelet transfusion in thrombocytopenic patients has already been published in 1910 [36]. But the therapeutic benefit disappeared prompt due to quicker vanishing of transfused platelets compared to erythrocytes, thus the conclusion has been drawn that platelets are having a short life span [36]. The first authentic measurements concerning this matter were executed via ex vivo radiolabeled platelets transfused into patients and were able to verify the argumentation on a relatively short life span of human platelets [37]. While erythrocytes tolerate refrigeration, platelet concentrates have to be stored at room temperature, because refrigeration and even 37°C are negatively affecting the viability [23]. The golden standard procedure is room temperature storage up to five days in plastic bags with agitation to allow oxygen exchange subsequent to pathogen inactivation [38].

Since the early 1970s platelet concentrates became widely available, before then the way to get platelets was freshly drawn whole blood [39, 40]. Due to 5 day maximum storage of platelet concentrates to guarantee the safety and efficiency for transfusions, blood banks are not able to store large amounts [41]. To get platelet concentrates for transfusion, whole blood from a

single donor has to be centrifuged or an automated cell separation has been carried out by apheresis to maximize platelet concentration and limit the number of red and white blood cells [41]. Platelet concentrates are utilized today for patients with thrombocytopenia, intensive therapies for haematologic malignancies and solid tumors, but also for surgical and trauma patients [41–43].

Series of biochemical, structural and functional alterations are combined under the term platelet storage lesion (PSL), which covers changes from blood collection, preparation method of the platelet concentrate, storage-conditions, -container and -media (plasma or an additive solution) [43, 44]. These changes are leading to decreased in vivo recovery and thus, the haemostatic capacity within patients after receiving platelet transfusion is reduced as well [45]. For example high centrifugation steps or contact to artificial surfaces during preparation of the concentrates induces platelet activation and fragmentation, which leads to PSL [43]. Also modifications of platelet surface proteins like thrombin receptors or glycoproteins while storage time are decreasing platelet aggregation and are hence effecting PSL [43]. The storage containers are having a big influence on platelet viability as well [45]. The material should allow gas exchange for oxygen or carbon dioxide [46]. The first bags in 1975 were made of polyvinyl chloride (PVC) and approved storage up to 3 days [41, 45]. Second-generation containers were composed of polyolefin and PVC coated inside with tri(2-ethylhexyl)trimellitate, which enlarged the storage period to 5 days [47, 48]. Nowadays bags made of PVC plasticised with butyryl-tri-n-hexyl-citrate are utilized due to their better gaseous permeability resulting in increased in vivo platelet viability after transfusion [49]. The gases, of which bags should enable the exchange through its surface, are taking part in metabolic pathways within platelets [44]. Their main energy source is hydrolysis of adenosine triphosphate (ATP), generated by platelets continuously via the aerobic tricarboxylic acid (TCA) pathway or anaerobic glycolysis [50]. Therefore, storage solutions of platelet concentrates have to buffer the formed lactate with the contained bicarbonate and consequently stabilizing the pH level, which would also influence platelet storage lesion [44].

2.1.4 Pathogen inactivation methods for platelet concentrates

Next to PSL, the risk of bacterial growth is another major issue. To ensure safety of transfusion products in terms of viral and bacterial transmission, different pathogen inactivation procedures are applied nowadays [41]. Storage condition at room temperature also increases risk of bacterial contamination, which may result in transfusion-related sepsis [42, 51]. Concerning globalization in terms of traveling or merchandise trade and newly emerging pathogens, screening techniques can not cover all possible bacterial, viral or other contaminants. Therefore, pathogen inactivation is an important issue [52]. Additionally extension of shelf life from 5 to 7 days can also be achieved by an inactivation of lymphocytes, which are correlating with the development of transfusion-related diseases [53]. Though storage up to 7 days can be achieved technically, platelet concentrates stored for 7 days compared to 5 days stored ones are showing reduced recovery and thus decreased post-transfusion survival [54, 55].

There are different procedures to avoid the development of transfusion-associated graft-versus-host disease (TA-GVHD) by engraftment of allogeneic T lymphocytes in patients, who received transfusions [56]. Herein, donor T lymphocytes can destroy organs, fragile tissue or the bone marrow of the recipient [57]. Although TA-GVHD is rare, the mortality is above 90 percent [56, 57]. Early approaches were executed via irradiation of cellular blood components with γ-rays or X-rays [57]. Recent methods are using molecules that undergo a photochemical reaction induced by UV light [42]. The most common procedures are amotosalen/UVA (INTERCEPT Blood System^{TM}) [58], riboflavin/UVA-UVB (MIRASOL PRT) [59] and UVC (Theraflex-UV) [60].

Irradiation with γ-rays is an established procedure and in 2008 more than 90% of pathogen inactivations were performed using cesium-137 chloride concerning its high reliability and efficiency [61]. CsCl is a compressed, water soluble and easily dispersible powder, which is distributed in the body, when inhaled or ingested [61]. Because of its radioactivity the substance requires strict security measures and the time of radiation has to be adjusted periodically due to CsCl half-life of 30.17 years [61]. The amount of irradiation used for pathogen inactivation by CsCl with 25 Gray (Gy) reduces cell proliferation for example from lymphocytes [62], but is not adequately affecting platelets and granulocytes [56]. Measurements with γ-ray treated samples and their respective control groups have demonstrated a significantly lower pH on day 5 of storage in the treated platelet concentrates, but the pH was in the accepted range [63]. Also a decrease of glucose and an increase of lactate were detected at day 5 in irradiated concentrates, as well as signifi-

cantly higher platelet activation levels from day 1 through day 5 [63]. The study was also able to show that platelets got activated in both irradiated and non-irradiated platelet concentrates consequent to PSL effects [63].

Concerning the described disadvantages of pathogen inactivation by radioactive substances, methods avoiding their usage were requested. Nowadays, protocols based on UV irradiation have displaced them to a great extent [57]. Since 2002 the INTERCEPT Blood System^{TM} is registered and in clinical use for platelet and plasma treatment [58]. Here amotosalen, a synthetic psoralen (see Fig. 3 (A)), reversibly intercalates into deoxyribonucleic acid (DNA) and ribonucleic acid (RNA) and after illumination with long-wavelength UVA light (320-400nm) a covalent cross-link to the pyrimidine bases is formed in a photochemical reaction [57], which is depicted in Fig. 3 (B). Thus, replication of nucleic acids is inhibited, which reduces highly effectively the risk of transmitted bacterial or viral infections and so prevents cellular replication [64].

An important feature of these photochemical treatments is that they are not affecting platelets, so their function remains intact [65]. Amotosalen is inactivating a wide range of pathogens like viruses, bacteria (including spirochetes and protozoa) and leukocytes [58]. Due to its water solubility and less lipophilicity, amotosalen can migrate rapid through cellular membranes, bacterial walls or viral envelopes to intercalate into nucleic acids without interacting with proteins or lipids [58]. Cross-links every 83 base pairs on average are formed between the reactive sites of amotosalen and the pyrimidine bases of the nucleic acids, but also single-stranded forms are targeted and intra-stranded reactions are feasible, which avoids pathogen replication [58]. The final concentration of amotosalen in the container bags with the blood component of 150 μmol/L is UVA illuminated with an intensity of 3 J/cm^2 [58]. After adding amotosalen and illuminating with UVA light, residual amotosalen and free photoproducts are absorbed in the third step by an additional compound adsorption device (CAD) and the pathogen inactivated concentrates are transferred into bags for storage at room temperature for up to 7 days [58]. The three steps of the INTERCEPT Blood System^{TM} procedure are shown in Fig. 4 and so about 40 units per hour can be treated [58].

Since this method is affecting DNA or RNA, a large series of studies on amotosalen alone and in treated platelets or plasma were executed to assure its safety [58]. The most important characteristic of the amotosalen-nucleic acid reaction is its activation only in presence of UVA light, which is making its mechanism of action (MOA) highly specific and controllable [58]. Studies on mice were performed for 39 weeks exposing them 3 times a week with the amount of amotosalen 1,000-fold the human dose rate observing no

A

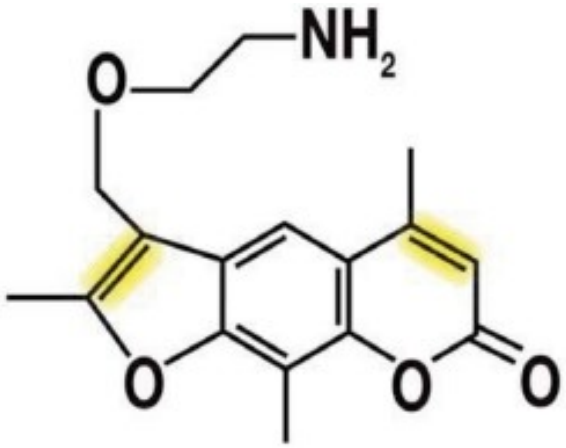

B

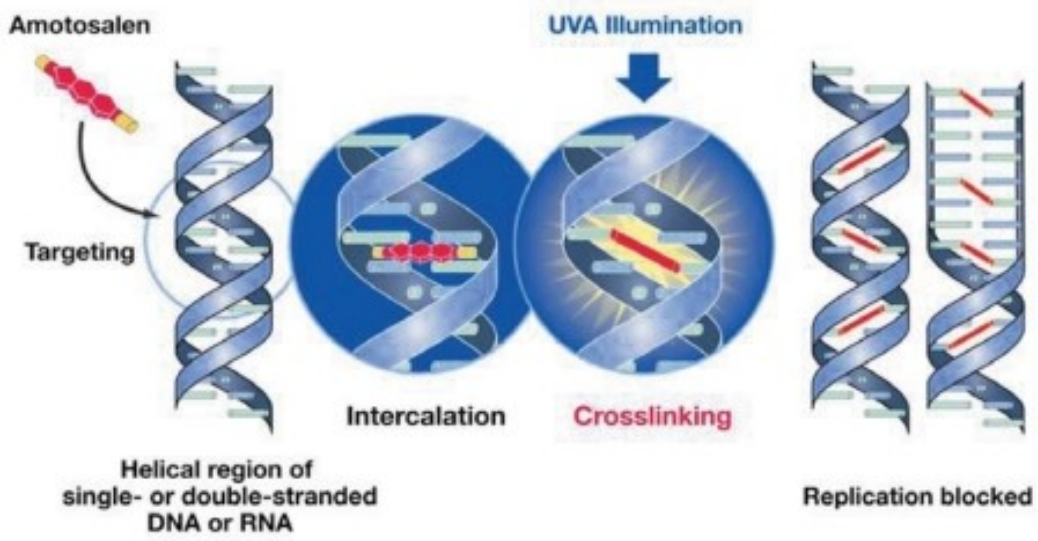

Figure 3: (A) The chemical structure of amotosalen with highlighted reactive sites, when illuminated by UVA. (B) Mechanism of action (MOA) of the INTERCEPT Blood System^{TM}. Pathogen inactivation via amotosalen intercalating into nucleic acid strands and forming a cross-link with pyrimidine bases of DNA or RNA, which avoids proliferation [58].

cancer in any animal [66]. Further toxicological tests on rodents, dogs and primates concerning pharmacological safety, phototoxicity and vein irritation confirmed safeness of this procedure [67].

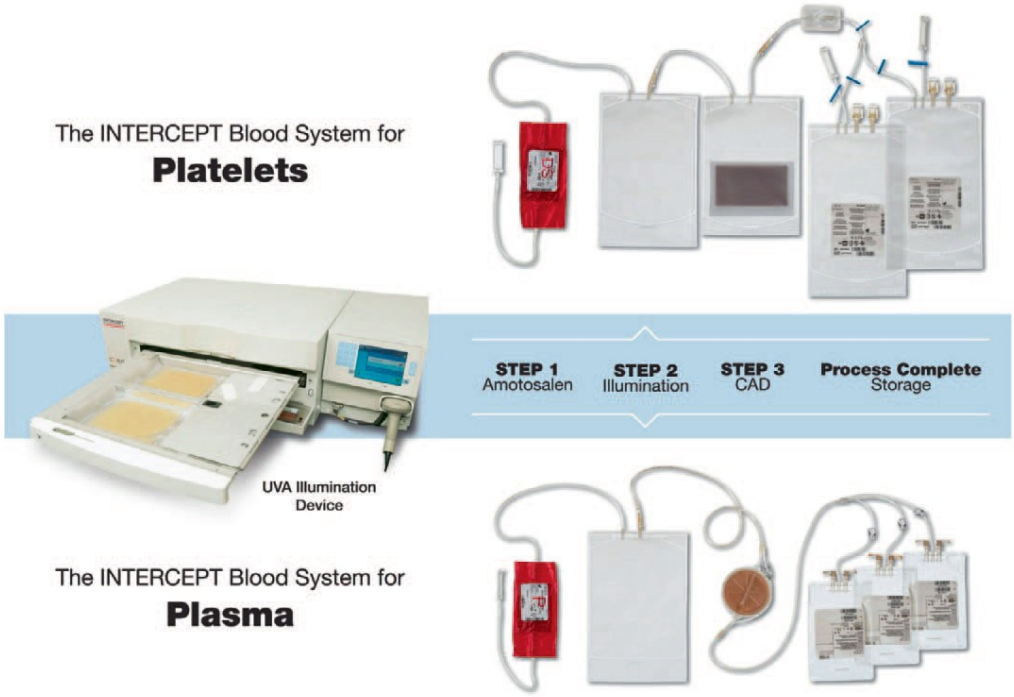

Figure 4: INTERCEPT Blood System^{TM} device for pathogen inactivation of platelets and plasma. In the first step amotosalen is added to the blood component and illuminated with UVA light in the next step. An additional compound adsorption device (CAD) is absorbing residual amotosalen and free photoproducts. Afterwards the pathogen inactivated platelets or plasma can be transferred to the storage containers [58].

2.2 "Omics" technologies and their field of application

2.2.1 The "omics" cascade

"Omics" technologies are trying to picture a wholistic illustration of the molecules in biological samples like cells, cellular components, tissue or organism [68]. The "omic" cascade mapped in Fig. 5 is starting from genome, through transcriptome, proteome and finally to metabolome, where lipids are part of [69]. While genomics, the first step of the cascade, is describing the genotype in detail, the qualitative and quantitative information of metabolomics, the last step, is representing the phenotype, which is reflecting the actual state of the organism [69]. Although lipids are a subgroup of metabolites, completely different working procedures compared to metabolomic approaches are required [70].

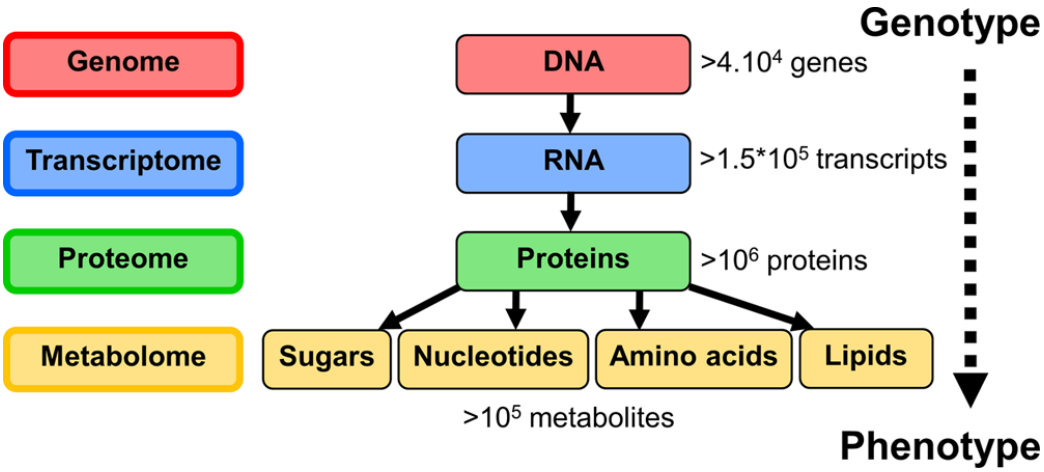

Figure 5: An "omics" cascade overview starting with the first step, genomics, through transcriptomics, proteomics and ending in metabolomics [69, 70].

2.2.2 Lipidomics

Lipids are a class of molecules with an immense structural and functional diversity [71]. Their main biological functions are conserving the membrane integrity and energy storage, but they are also involved in various intra- and intercellular processes, such as signal transduction, apoptosis and membrane trafficking [71, 72]. Thus, disturbances in lipid metabolism may result in several diseases like type 2 diabetes [71], Alzheimer disease [73] and cancer [12].

The LIPID MAPS consortium has developed a comprehensive classification system for lipids, which is sectioning them into the eight classes [71]. Fig. 6 is presenting those eight lipid classes: fatty acyls (FA), glycerolipids (GL), glycerophospholipids (GP), shingolipids (SP), sterol lipids (ST), prenol lipids (PR), saccharolipids (SL) and polyketides (PK) [70, 71]. There is further notation for the different lipid subclasses, e.g. for GLs and GPs the total number of carbon atoms in FAs and the number of double bonds are added to the lipid subclass abbreviation such as PC 36:2, which is standing for a phosphatidylcholine (PC), whose FAs are composed of 36 carbon atoms and 2 double bonds [70]. A more detailed notation separated by an underscore like PC 18:0_18:2 specifies the number of carbon atoms and double bonds of each FA linked to glycerol, without knowing the *sn*-position of the FAs and the separation by a slash, e.g. PC 18:0/18:2, means 18:0 is located at the *sn*-1 and 18:2 at the *sn*-2 position [70]. The prefix "L" indicates the lyso-form of the lipid, for example lysophosphatidylcholine and its abbreviation LPC [70].

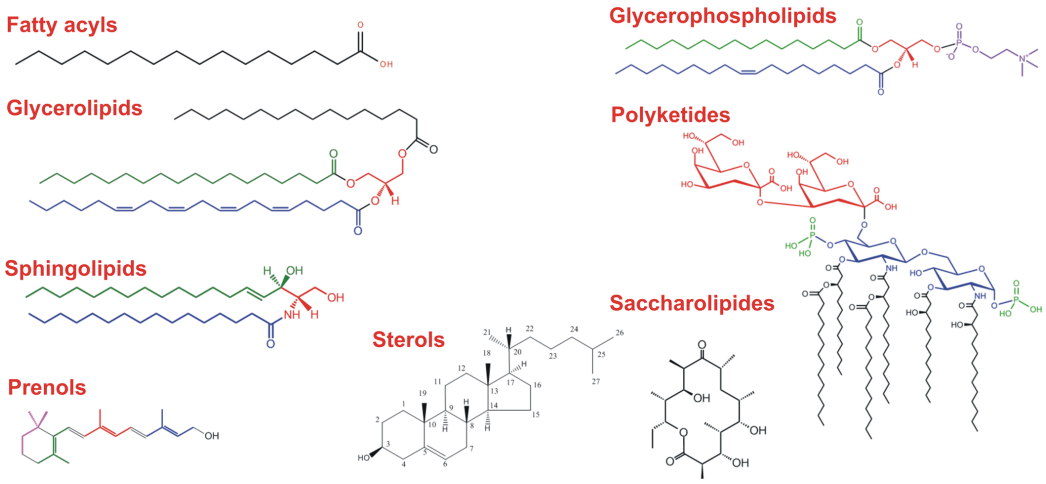

Figure 6: The eight lipid classes defined by the LIPID MAPS consortium and their characteristic chemical structure [70].

Since lipids are found in all cell types, they are also playing various roles in human platelets with respect to structural and signaling functions [10]. Enzymes are managing their formation and metabolism and disturbances in the lipid metabolome are leading to an alteration of platelet functions [10]. As mentioned in section 2.1.2 a structural remodeling of membrane lipids accompanies with platelet activation [10]. 192 FAs and oxidized phospholipids involved in platelet aggregation could have been structurally identified like 12-HETE, TXA_2 or anionic phospholipids [10, 74].

Because of their involvement in diverse key cellular processes the MS based analysis of lipids called lipidomics is gaining in importance [10].

2.2.3 Eicosanoids

The eicosanoid family belongs to the lipid subgroup of FAs and the number of this bioactive group is still growing [17]. These oxygenated C_{18}-C_{22} polyunsaturated fatty acids are mainly generated by the metabolism of the 20 carbon essential FA arachidonic acid, which means that the human body does not produce AA and thus it has to be taken up exogenously from food sources [17, 19, 75, 76]. Another source of AA is the consumption of the essential C_{18} fatty acid linoleic acid, because its metabolism is yielding in AA [15]. Fig. 7 is showing the chemical structure of this polyunsaturated fatty acid with its 4 double bonds in the hairpin conformation [15].

AA can be found for the most part incorporated into membrane phospholipids typically at the *sn*-2 position and not as the free acid, which assures fluidity and flexibility of biological cell membranes [15, 76]. These phospho-

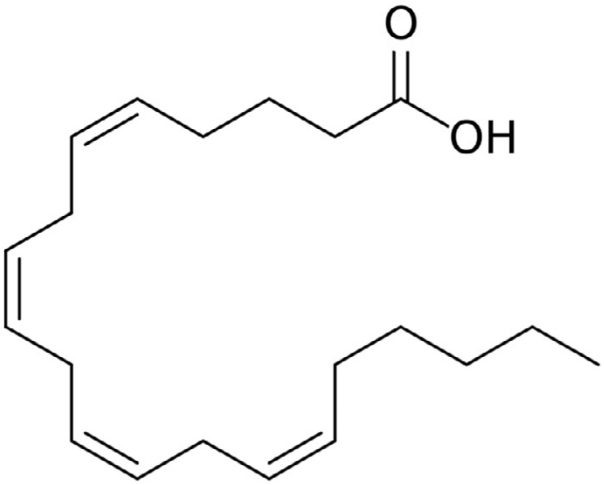

Figure 7: Chemical structure of arachidonic acid, all-*cis*-5, 8, 11, 14-eicosatetraenoic acid [15].

lipids are occurring highly abundant in skeletal muscle, brain, liver, spleen or retina [77], but also at concentrations of about 5 mM in resting cells like platelets, of which 10% is corresponding to the amount of diffusing AA upon activation [78]. At this point a "new" class of enzymes is emerging, phospholipases (PLs) are representing the largest group of lipid-modifying enzymes [79]. There are four groups of this enzyme class with diverse biological function: PLA (PLA_1 and PLA_2), PLB, PLC and PLD, named after the hydrolysed bond of phospholipids as shown in Fig. 8 [79]. While PLA_1 and PLA_2 are catalysing separately the *sn*-1 and *sn*-2 positions, which is leading to the lyso-form of the phospholipid and free fatty acids, the PLB is hydrolysing the linkage at both positions at once [79]. A cleavage of the bond between glycerol and phosphate is induced by PLC generating diacylglycerol and phosphoinositides [79] and the enzyme PLD is splitting the bond between phosphate and the polar head group resulting in phosphatidic acid, which is diagrammed in Fig. 8 [79]. There are many different PLA_2 enzymes, so they are summed up as an own superfamily [80]. These enzymes are well-known for their impact in inflammatory or immune processes via liberating AA from the *sn*-2 position of phospholipids under ischemic conditions and the following AA metabolism forming eicosanoids [76, 79]. Especially three members of the PLA_2 superfamily are participating in eicosanoid production: cytosolic calcium-dependent phospholipase A_2 ($cPLA_2$), cytosolic calcium-independent phospholipase A_2 ($iPLA_2$) and secreted phospholipase A_2 ($sPLA_2$) [16]. While $iPLA_2$ seems to be involved in daily cellular functions like membrane homeostasis and remodeling [81], the calcium-dependent type

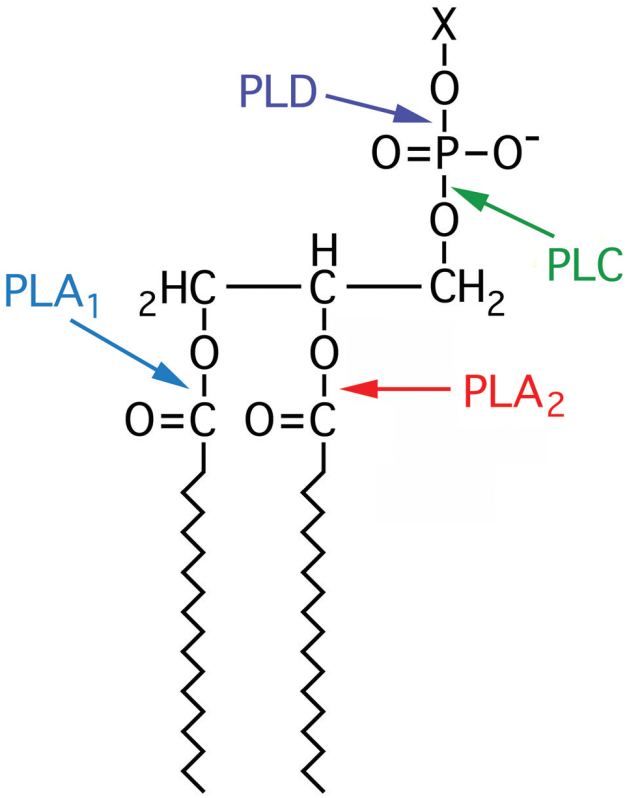

Figure 8: PLA_1 and PLA_2 are catalysing separately the *sn*-1 and *sn*-2 positions leading to a lysophospholipid and the corresponding free FAs and the enzyme PLB is cleaving both *sn* positions at once. PLC is hydrolysing the linkage between glycerol and phosphate, while PLD is breaking the bond between the phosphate and the polar head group [79].

is mostly inactive during homeostatic conditions [82]. Activated by Ca^{2+} ionophores $cPLA_2$ hydrolysis phospholipids leading to AA release [82]. The third member $sPLA_2$ is able to increase the function of $cPLA_2$ to control the intensity of free fatty acids like AA [83].

The eicosanoid generation of free AA is proceeding via four major pathways, of which the first three pathways are named after the enzymes, that are catalysing the committed step: cyclooxygenase, lipoxygenase, cytochrome P450 and anandamide [15, 84]. COX-1 and COX-2 are leading to thromboxane and prostaglandin production, that are participating in inflammatory processes [85]. While the COX-1-mediated TXA_2 primarily produced by platelets is having a pro-coagulant effect on them, the COX-2-mediated prostacyclin (PGI_2) generated by endothelial cells is inhibiting platelet aggregation and an imbalance between these two eicosanoids is linked to car-

diovascular diseases [15]. Enzymes involved in the LOX pathway are LOX-5, LOX-8, LOX-12 and LOX-15, which are generating leukotrienes, lipoxins, hydroxyeicosatetraenoic acids (HETEs) or 8-, 12- and 15-hydroperoxyeicosatetraenoic acid (HPETE) [15, 86]. The LOX enzymes are named after the carbon position, where an oxygen atom is introduced [15]. The two enzymes CYP 450 epoxygenase and CYP 450 ω-hydroxylase of the CYP 450 pathway are catalysing the formation of epoxyeicosatrienoic acids (EETs) and 20-HETE [87]. Endocannabinoids and anandamides are produced in the anandamide pathway by fatty acid amide hydrolases [88]. In addition non-enzymatic oxidative metabolism by reactive oxygen species (ROS) and reactive nitrogen species (RNS) are taking place to autoxidise AA [15]. These metabolic pathways of AA are varying between different tissues and also from cell to cell in one tissue type [15].

But AA is not the only eicosanoid precursor molecule. They are also formed from the essential ω-3 polyunsaturated FAs, docosahexaenoic acid (DHA) and eicosapentaenoic acid (EPA), which are taking part in regulating homeostasis [89]. While in general pro-inflammatory eicosanoids derive from AA, the metabolism of these ω-3 PUFAs is resulting in anti-inflammatory eicosanoids [89]. Therefore, an increased dietary intake of ω-3 PUFAs is recommended to reduce the risk of inflammatory or vascular diseases and cancer [89, 90]. The ratio of these ω-6 and ω-3 PUFAs is essential for regulation of inflammation, pro- and anticoagulation effects in platelets, vasoconstriction and -dilation as well as bronchoconstriction and -dilation [89]. Like arachidonic acid, DHA and EPA are incorporated in membrane phospholipids and mobilised by phospholipase A_2 to generate eicosanoids also via COX and LOX pathways [89]. While the PG-2 family and TXA_2 is derived from AA metabolism, the COX-2 and 5-LOX pathway of EPA is giving rise to series 3 prostaglandins, thromboxane A_3 and series 5 leukotrienes [89]. D-series resolvins, protectins and maresins arise from DHA metabolism [89]. The AA, EPA and DHA pathways plus the MOA of therein formed eicosanoids are depicted in Fig. 9 [89].

Eicosanoids are fulfilling various functions and they are involved in many biochemical mechanisms in the body [17, 19]. Prostaglandins and leukotrienes are playing a role in inflammation and cancer [19]. Especially the pro-inflammatory PGE_2 has been detected in diverse malignancies like colon, lung, breast and head/neck cancer due to COX-2 overexpression [19, 91]. Pro-inflammatory leukotrienes (LTs) such as LTB_4 can also be found at increased levels in colon or prostate cancer [19]. However, these pro-inflammatory eicosanoids are not only enhanced produced by cancer cells, but also by their surrounding cells [19]. These local highly active molecules are controlling tumor progression via regulating cell proliferation, apoptosis, migration and

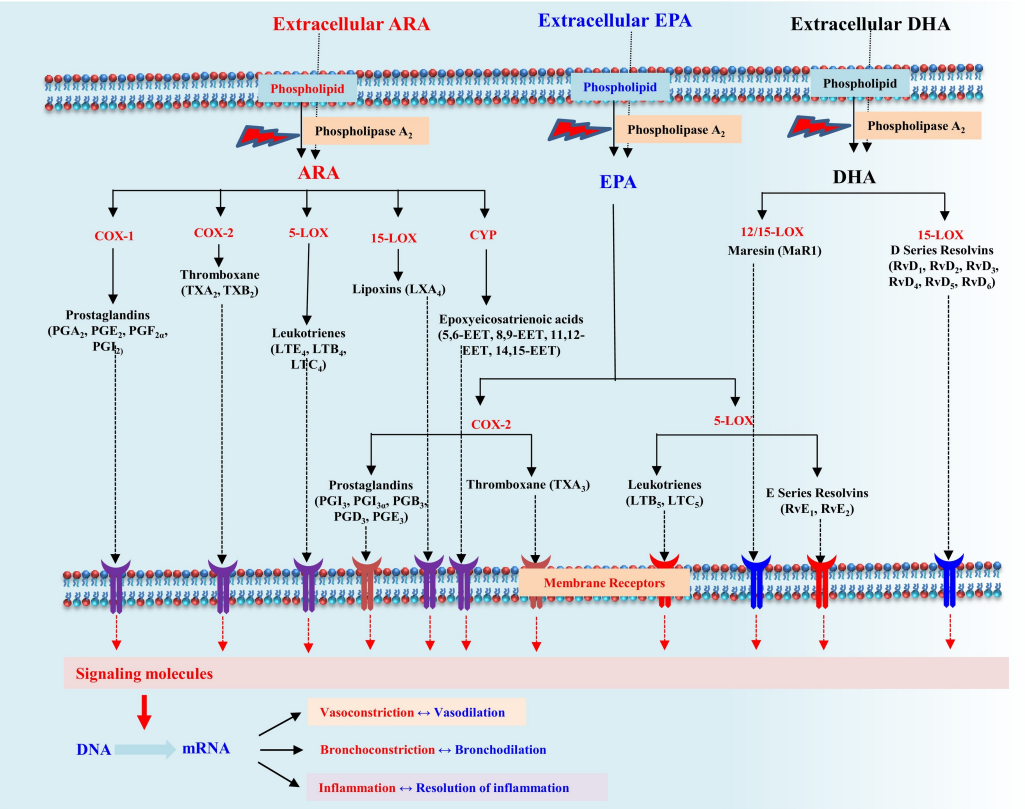

Figure 9: Uptake, storage and release of the eicosanoid precursor molecules AA (arachidonic acid abbreviated in this figure with ARA), EPA and DHA. Formation of eicosanoids via COX, LOX and CYP pathways [89].

invasion [19].

Due to their impact on cellular receptors or ion channels, eicosanoids are playing a part in initiation and propagation of signalling cascades for example in the heart [92]. Via paracrine signalling, eicosanoids like prostacyclin are able to modulate blood flow, contractile state or haemodynamic processes [92].

A participation of eicosanoids in cerebrovascular diseases is known for over 40 years [76]. The enzymes of their metabolic pathways are potential drug targets, because stroke and other neurovascular injuries are derived from an up-regulation [76].

AA and its double bonds are recipient for oxidative reactions, which means oxidative stress for the cells and is an important factor in stroke as well [76]. The oxidative stress is leading to non-enzymatic generation of eicosanoids, which are causing tissue injuries [76]. For example, 9-HETE is derived from the non-enzymatic, free-radical AA oxidation pathway [93]. But eicosanoids are also inducing tissue repair and regeneration during homeostasis [94]. The involvement of this molecule class in cellular processes like cell proliferation, differentiation and angiogenesis are accounting for homeostasis [94]. Especially COX-derived eicosanoids are in charge of tissue regeneration and wound healing controlled by an inflammatory response [94]. Thereby, tissues like liver, lung, kidney or spleen are able to regenerate in parts or even completely after injury [94]. The pattern of these metabolites in acute wounds is depending on the uptaken food as well. The level of oral supplemented EPA and DHA is provoking an alteration of the eicosanoid profile [94].

Eicosanoids are also formed and released by human platelets and many agents of this FA subgroup are able to both stimulate or inhibit platelet reactivity [15, 95, 96]. Platelets activated by eicosanoids are aggregating and forming a thrombus to prevent bleeding [96]. If an inappropriate activation is taking place and the thrombus is generated within the vessel wall, thrombic events like heart attack or stroke could arise subsequently [96]. The processes of platelet activation or inhibition are controlled by the eicosanoids TXA_2 and PGI_2 [96]. While the primary un-metabolised prostanoid TXA_2 has an pro-coagulant effect [96], prostacyclin, the major eicosanoid released by endothelial cells, is acting as counter-balance of TXA_2 by inhibiting platelet aggregation [95]. Upon $cPLA_2$ activation, platelets are producing also significant amounts of PGE_2, PGD_2, 11-, 12- and 15-HETE next to TXA_2 [96]. 15-HETE and its precursor molecule 15-HPETE are blocking the liberation of the anti-coagulant PGI_2 [95, 97, 98]. Stimulated endothelial cells are also releasing 11-HETE, next to 15-HETE and PGI_2, which is a factor in platelet aggregation as well [95, 99]. In contrast to 15-HETE, 11-HETE has not been detected in intact cells [98]. PGD_2 is causing a decrease in platelet activity such as PGI_2 [96]. The impact of PGE_2 on platelet reactivity in vitro is depending on the concentration. While low concentrations of 0.1-10 μM are increasing platelet aggregation, a higher concentration of 100 μM is reducing platelet coagulation [96]. In vitro studies of PGE_2, which is generated by the vessel wall, were indicating anti-coagulating effects due to activation of the prostaglandin E receptors 2 and 4, which are expressed on platelets and are linked to the reduction of platelet aggregation, but also a pro-coagulating effect due to the activation of the prostaglandin E receptors 1 and 3, which are also expressed on platelets and are enhancing platelet

activation [96]. But in vivo the pro-coagulant effect of PGE_2 due to the activation of prostaglandin E receptor 3 is predominated [96]. 12-HETE, the major released eicosanoid by stimulated platelets, and 14-hydroxy-DHA (14-OH-DHA/14-HDHA/14-HDoHE), formed in 12-LOX metabolism of DHA, are both playing an anti-coagulant role [96]. But a pro-coagulant effect of 12-HETE has also been reported [96, 100]. Thus, an unanimous result for the role of 12-HETE in aggregation of platelets has not been reached so far [100]. All EETs at concentrations from 1 to 10 μM are preventing AA induced platelet aggregation and a few of them are also blocking TXB_2 formation by stereospecific inhibition of COX enzymes [101]. The CYP pathway of AA is yielding the anti-coagulant 20-HETE [102]. Neutrophils are producing the 5-LOX-derived metabolite 5-HETE, which is also contributing to platelet aggregation [103]. All pro- and anti-coagulant eicosanoids mentioned here are listed in table 1.

Next to 12-HETE, 12-hydroxyheptadecatrienoic acid (12-HHT) is another major product of activated platelets [10]. The biological function of 12-HHT is still unknown, only its involvement in wound healing has been mentioned [103, 104]. Though a decreased 12-HHT level by a high-dose of aspirin is inducing a wound healing delay [104].

Table 1: Eicosanoids with an impact on platelet aggregation.

pro-coagulant eicosanoids	anti-coagulant eicosanoids
TXA_2 [15, 16, 96]	PGI_2 [15, 16]
TXB_2 [15]	PGD_2 [15, 96]
PGE_2 (at 0.1-10 μM, in vitro; mainly in vivo) [96]	PGE_2 (at 100 μM, in vitro) [96]
15-HETE [95, 97, 99]	14-OH-DHA [96]
15-HPETE [95, 97]	EETs [101]
5-HETE [103]	20-HETE [102]
12-HETE [96, 100]	12-HETE [96, 100]
11-HETE [95, 99]	

2.3 Influence of UVA light on signal pathway activation

90-99% of the solar radiation, which is reaching the surface of the earth, is corresponding to UVA [105]. Benign and malign tumors such as squamous cell carcinomas (SCCs) are caused by this form of radiation as well [105]. While UVB radiation is inducing direct DNA alteration like cross-links within DNA or between DNA and proteins, UVA is generating ROS and is

so indirectly damaging DNA or leading to lipid peroxidation in cell membranes [105]. But UVA is not only causing DNA defects, a tumor promoting effect by the radiation is provoked because of an enhanced gene transcription [105]. Signalling pathways like the p38 mitogen-activated protein kinase (p38 MAPK) can be activated through UVA-induced ROS and the activator protein-1 (AP-1) in this pathway is contributing to transcription and COX-2 expression [105, 106]. Herein, the p38 activity is stabilising the COX-2 messenger ribonucleic acid (mRNA) [105]. AP-1 and COX-2 are supporting tumor promotion by themselves via an up-regulation of VEGF coming along with increased angiogenesis [105]. Additionally an activation of PLA_2 by UVA radiation is taking place in human keratinocytes [105, 107]. Within these cells the radiation is responsible for tumorigenesis, which is based on an increased PGE_2 production leading to an augmented cell growth [105]. The activation of PLA_2 by UVA and the factors supporting tumorigenesis are displayed in Fig. 10 [105].

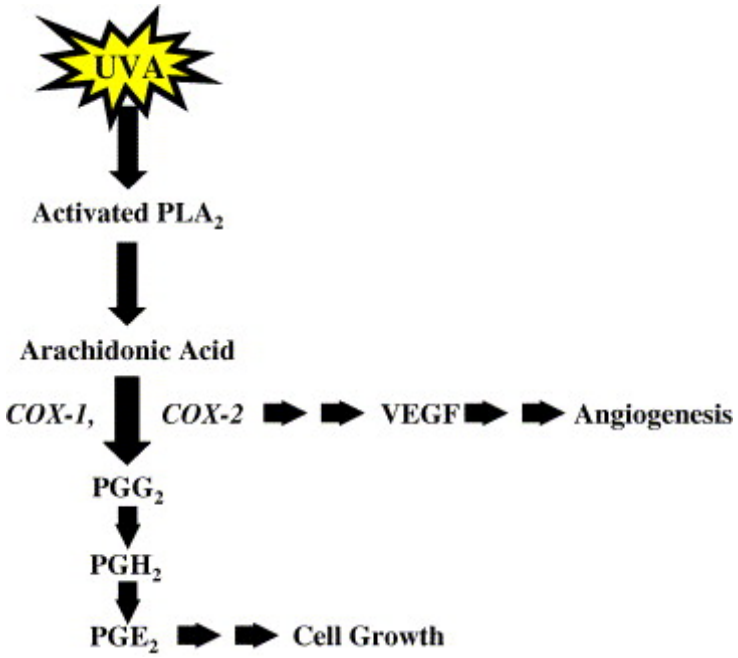

Figure 10: Influence of UVA on tumorigenesis starting from PLA_2 activation and increased COX expression. While VEGF is linked to angiogenesis, PGE_2 derived from AA metabolism is responsible for in vitro cell growth of keratinocytes [105, 107].

2.4 Solid-phase extraction

Eicosanoids are low abundant molecules in biological fluids, therefore solid-phase extraction (SPE) is the preferred technique in sample preparation to isolate and enrich these selected analytes [108, 109]. Additionally a clean-up and an exchange of the medium can be achieved [108]. Nowadays, the application of commercial pre-packed columns are established, but there are also cartridges or disks in use [109, 110]. In SPE the partitioning of the compounds, the sample is containing, is taking place between a liquid and a solid phase [110]. The stationary phase adsorbent materials are based on silica and are related to those utilised in LC [109]. Reversed-phase materials with for example chemically-bonded octadecylsilyl groups commonly termed C_{18} groups are often applied for isolation of eicosanoids [109]. The solid sorbent with its functional groups has to be washed with a suitable solvent (methanol for reversed-phase materials) and conditioned with the same solvent, which the sample is also containing [110]. This enables the correct solvation of the alkyl groups [110]. In the second step the sample solution is loaded on the column [110]. While interfering components are washed through in the next washing step, the analytes are retained during the process due to strong but reversible hydrophobic interactions between analyte molecules and the solid sorbent of the stationary phase [110, 111]. An elution of the selected analyte molecules in the forth and last step of SPE can be achieved by an appropriate solvent [110]. The operating steps of the solid-phase extraction are pictured in Fig. 11 [112].

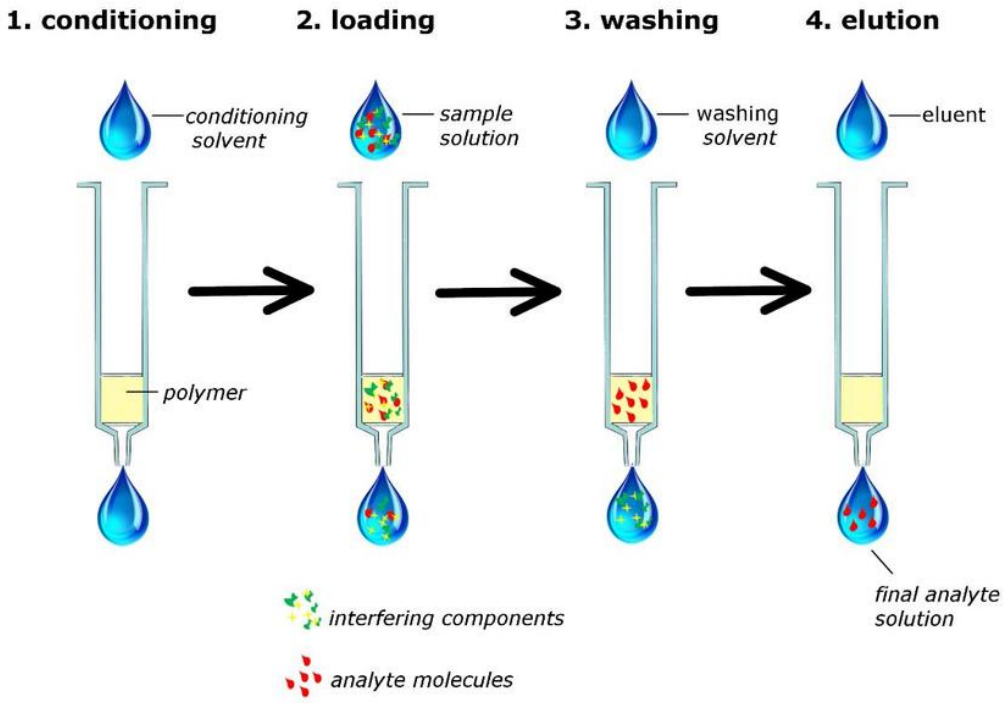

Figure 11: Solid-phase extraction operating steps. Starting with conditioning of the packing material with a certain solvent, through loading the sample solution on the column in the next step and washing through interfering components afterwards. In the end elution of the selected analytes can be achieved by an appropriate solvent [112].

2.5 Liquid Chromatography - Mass Spectrometry

The set-up of LC-MS is fundamentally consisting of a pumping system, an injector and a column connected to the mass spectrometer via an evaporation-ionisation-interface [113]. LC-MS based methods have revolutionised the analysis and quantification of proteins and metabolites including lipids [114]. Also for the identification of eicosanoids in biological samples LC-MS technologies are increasingly used [115].

2.5.1 High-performance liquid chromatography and ultra-high-performance liquid chromatography

Since the 1970s high-performance liquid chromatography (HPLC) is the preferred technique for separation, analysis and purification of any dissolved mixtures containing different compounds [113]. Prior to this gas chromatography (GC) was the tool for the laboratory, but sample volatility, extraction and/or derivatisation before injection and thermal degradation of samples in the GC oven were limiting this method [113].

In HPLC a pumping system is transporting and pressurising the solvent corresponding to the mobile phase from a reservoir into the LC system [113]. If a gradient system with 2 solvents is used, they are mixed to form the mobile phase regulated by a flow controller [113]. The mobile phase is then reaching the injector, of which the loop-and-valve type with 6 ports is the most applied one [113]. The solvent is flowing through another port to the HPLC column, which is the most important part of the LC device and enables separation of the sample components [113]. The sample, which was before reconstituted in the mobile phase starting condition, is injected by a syringe, which can be done automatically by an autosampler, and is arriving at the needle port [113]. In the loading mode depicted in Fig. 12 (A) it is loaded into a small loop and by switching the valve position into the injection mode, the sample gets loaded on the analytical column as shown in Fig. 12 (B) [113].

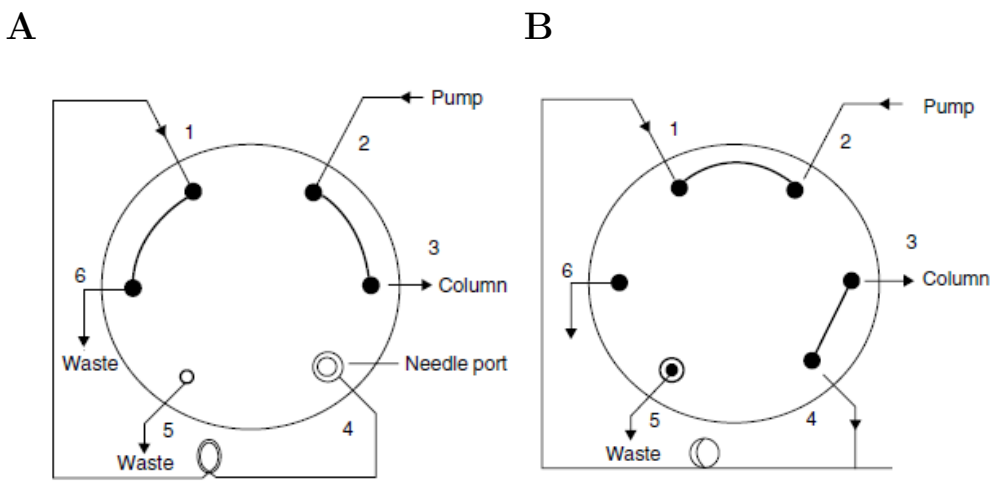

Figure 12: Scheme of HPLC injector system with a 6-port valve in (A) loading mode and (B) injection mode [113].

The separation column is packed with a fine-diameter packing material between two fittings [113]. For the quality of the separation of samples compounds the column packing material type is essential due to the interactions of the stationary phase with the sample molecules [113]. The most common packing material is based on silica with C_{18} functional groups like described in section 2.4 and is representing the reversed phase approach [113]. Here the functional C_{18} groups are interacting with the sample molecules and are retaining them [113]. A simple partition interaction of the sample molecules between the non-polar stationary phase and the polar mobile phase is leading to separation of the sample components [113]. While most polar compounds are eluting first, non-polar compounds are retained longest [113]. The eluted, separated chromatographic peaks are transferred into a detector of various types such as UV, fluorescence or MS [113, 116]. The last hardware component is a computer for data acquisition [113].

In contrast to regular HPLC the more advanced technology is the ultra-high-performance liquid chromatography (UHPLC) facilitating an increased sample throughput [116]. Enhanced efficiency, resolution, sensitivity and speed of analysis can be obtained as a result of higher working pressure, mobile phases at high linear velocities and smaller particle sizes [116, 117]. Here working pressures up to 1200-1400 bar and flow rates between 2 and 5 mL/min are established [116]. Compared to a particle size of the stationary phase of 3-5 μm in classical HPLC, in UHPLC fully porous sub-2-μm particles can be used [116]. An overview of the set-up of an UHPLC system is illustrated in Fig. 13 [118].

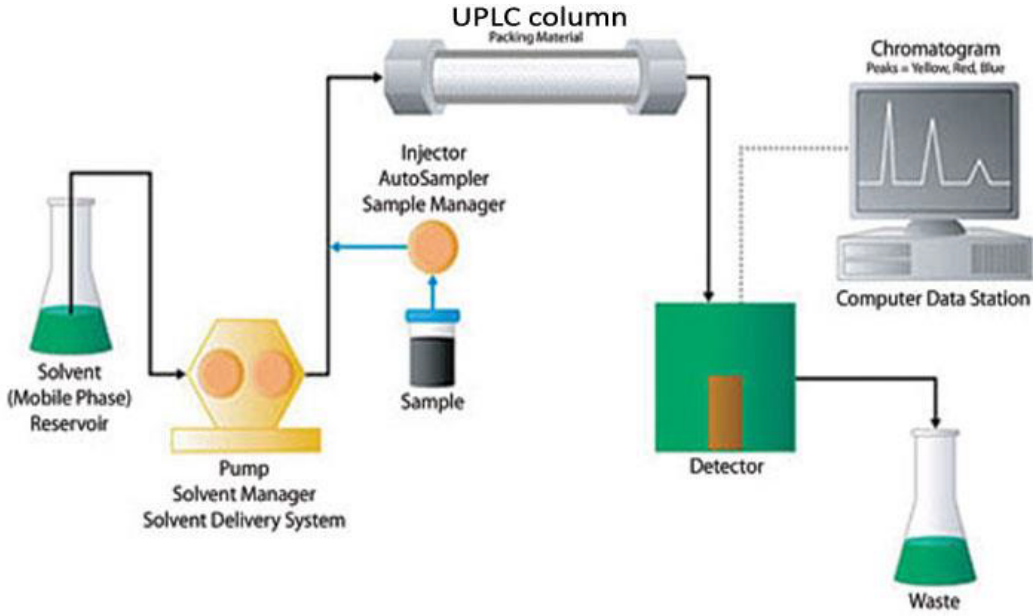

Figure 13: Set-up overview of an UHPLC system with the solvent reservoir, pumping system, sample injection, analytical column, detector and computer for data acquisition [118].

2.5.2 Electrospray ionisation

Before the development of the electrospray ionisation (ESI) there was no way to couple a LC system under high pressure with a mass spectrometer, which is working under high vacuum [119]. In addition mass spectrometry analysis is requiring positively or negatively charged ions and the components in the HPLC eluant are uncharged [119]. Only the development of the ESI in the late 1980s was allowing the ionisation of relevant bio-analytical macromolecules such as proteins, lipids or carbohydrates out of a liquid medium, which was even rewarded with the Nobel Prize in 2002 [119].

There is no direct hardware connection between LC and mass spectrometer, because the eluted peaks would overload the capacity of the vacuum pumps [113]. Therefore, the LC capillary is ending up in the ESI source [113]. The ionisation is taking place in a heated metal capillary tube under a 3-4 kV potential difference and thus enabling both positively and negatively charged ion formation [113]. At the end of the capillary tube the liquid is getting dispersed into highly charged droplets close-by atmospheric pressure followed by conditions causing solvent evaporation [113]. The contracting droplets are spherically shaped, which is based on the repulsion of the same charges and the surface tension [120]. This decrease of droplet size is achieved by

removing the solvent via a combination of heaters, reduced pressure and gas nebulisers [113]. This process is ending up in a Rayleigh explosion leading to single ions [120]. Since the energy in the ESI procedure is not causing a fragmentation of the molecules, electrospray ionisation is part of the "soft ionisation" techniques [113].

2.5.3 Mass spectrometry

After chromatographic separation up to 1200-1400bar for an UPLC system and an ionisation at atmospheric pressure as described in section 2.5.1 and 2.5.2, the ions are entering the MS system [113]. Generally a mass spectrometer can be sectioned into an ion source, a mass analyser and a detector as displayed in Fig. 14 [121]. Therein, a vacuum pumping system is reducing the pressure stepwise up to high vacuum to prevent the ions from collision with gas molecules of the air [113].

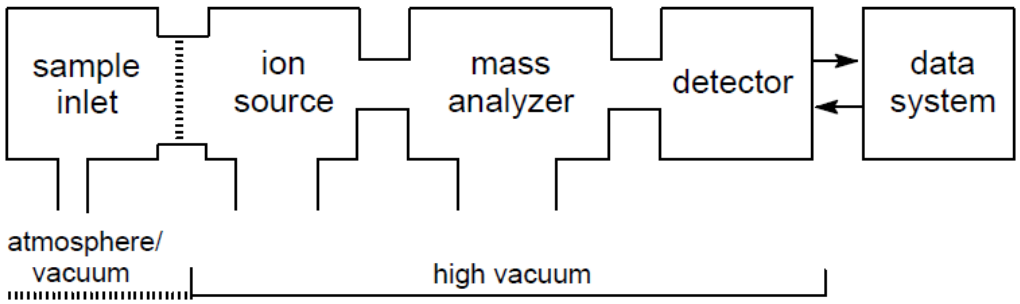

Figure 14: General setting of a mass spectrometer. A sample inlet operating at atmospheric pressure is followed by an ion source, wherein ionisation is taking place at reduced pressure like shown here or at atmospheric pressure. The ion path is then leading via a mass analyser into the detector working at high vacuum. While the ions are getting separated in the mass analyser, these separated ions are recorded in the detector afterwards. Connected to the detector a computer is performing data acquisition [121].

The basic principle of MS is the separation of the ions, which are in turn derived from the prior separated compounds during the LC run time, by their mass-to-charge ratio (m/z) [121]. Mass spectra are two-dimensional with the abscissa representing m/z and the ordinate representing the relative signal intensity correlated with the abundance of the ions [121]. They are continuously recorded during the LC run, which is shown in a third dimension in Fig. 15 [113]. A qualitative and quantitative analysis can be achieved by the m/z values and the relative abundance [121].

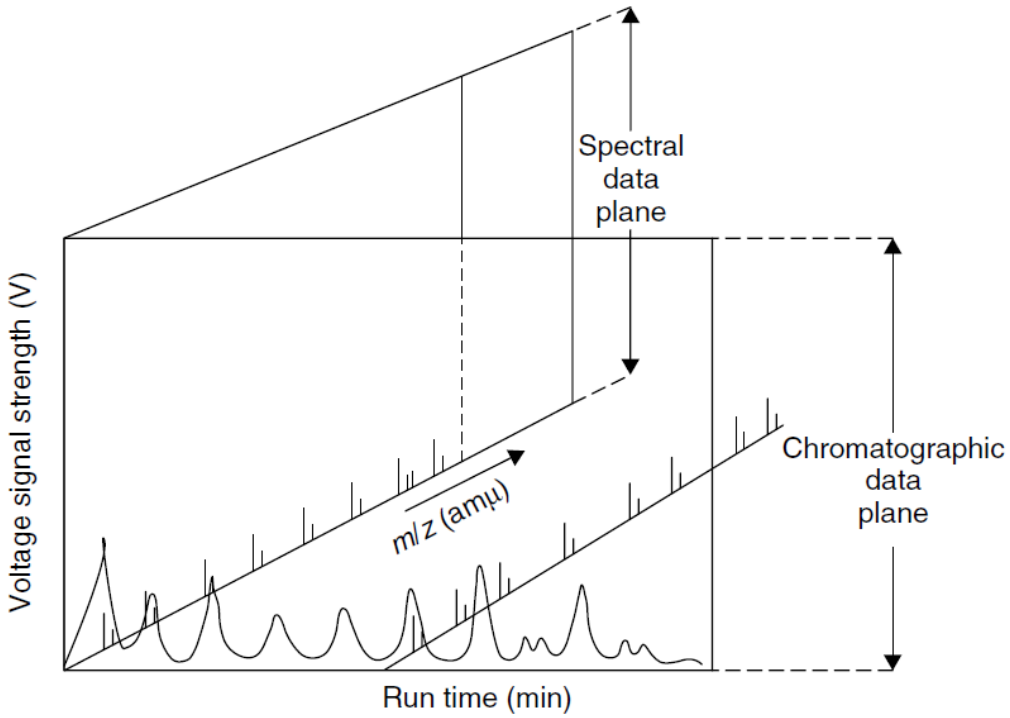

Figure 15: Demonstration of mass spectra recording during LC run time. The three-dimensional array is consisting of a two-dimensional chromatographic plane with the abscissa representing run time and two-dimensional mass spectra with abscissa representing m/z and both planes are sharing the ordinate representing signal strength [113].

The peak with the highest intensity is called *base peak* and due to the fact, that the ordinate is showing the relative intensity, the base peak is always set to 100% [121]. A combination of consecutively recorded single mass spectra of eluted species is termed *ion chromatogram* and enables to follow this species due to its abundance as a function of retention time [121]. While the term *extracted ion chromatogram* (EIC) is summing up a chromatogram generated from the intensity of any selected m/z value as a function of retention time, the *total ion chromatogram* (TIC) is describing the summation of all ion intensities of each mass spectrum as a function of time [121].

The performance of a mass spectrometer is characterised by its sensitivity, detection limit and signal-to-noise ratio [121]. Several factors like efficiency of the ionisation method, extraction of ions from the ion source or transmission to the analyser are effecting the sensitivity [121]. Per definition the limit of detection (LOD) is describing the lowest analyte amount leading to a signal, which can be barely distinguished from the background noise [121]. The

signal quality is directly affected by the signal-to-noise ratio (S/N). Herein, the noise is arising from electronics of the device and consequently it has an impact on signal intensity [121]. But there is also "chemical" noise coming from impurities or potential column bleeding [121].

The *atomic number* Z is representing the number of protons within the nucleus of an element. There are also atoms with the same number of protons, but with varying number of neutrons, and they are termed *isotopes* [121]. Isotopes with the highest intensity are normalised to 100% and thus the isotope abundances can be listed, which enables the sum formula identification of a molecule by its isotopic pattern [121].

In mass spectrometry several types of mass definitions are used. The *nominal mass* is an approximation by summing up the rounded off, integer masses of the most abundant naturally occurring isotope of any element the molecule is containing [121]. *Isotopic mass* is describing the exact mass of any isotope and the mass of a molecule, which is only consisting of the lowest mass isotopes of an element, is termed *mono-isotopic mass* [121].

Ions with a higher level of isotopes than the natural level would be, can be produced and even the labelling at a specific position is feasible [121]. This isotopic labelling is utilized in tracking metabolic pathways, for quantitative analysis via internal standards or for explanation of ion fragmentation mechanisms [121]. Therefore, non-radiating isotopes like ^{2}H, ^{13}C and ^{18}O are preferred [121].

Isotopes can be separated with MS and the resolution is determining the degree of separation [121]. The *mass resolution*, R, is defined as the smallest difference in m/z of a signal, in which separation was able to be achieved [121]. The resolving power of the mass analyser to separate two neighbouring peaks can be calculated with the following equation [121]:

$$R = \frac{m}{\Delta m} = \frac{m/z}{\Delta m/z} \tag{1}$$

An adequate separation is achieved from an intensity value of less than 10 percent between those two regarded peaks, which is also termed the *10% valley definition of resolution*, $R_{10\%}$ [121]. In addition Δm has to be equal to the peak width at 5% peak height, which is explained in Fig. 16 [121]. For a second definition of the resolution the width of a peak at half height is used for calculation and is therefore called *full width at half maximum* (FWHM) shown in Fig. 16 as well [121]. Fig. 17 is demonstrating the impact of resolution on two neighbouring signals [121]. Therefore, peaks at m/z 50, 500 and 1000 were considered with a resolution of 500. While the peaks at m/z 50 are completely separated through the baseline, peak maxima of the

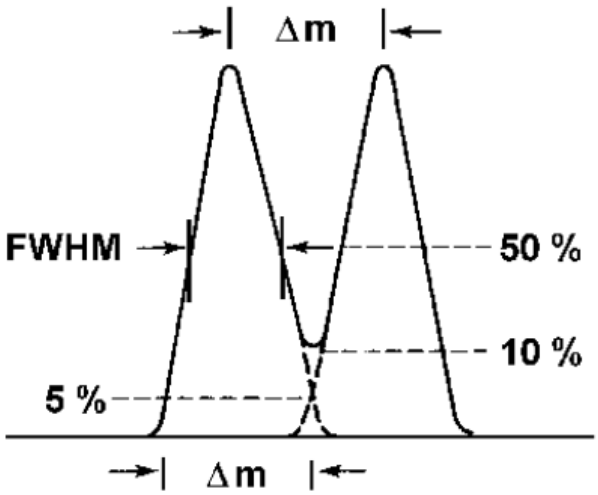

Figure 16: Definitions of resolution between two peaks. *10% valley definition of resolution* and *full width at half maximum definition* (FWHM) [121].

other signals at higher m/z values are shifting together. Especially at m/z 1000 a superposition of both peaks can be observed [121]. A resolution of mass analysers with R = 500-2000 is termed low resolution and R > 5000 is describing a high resolving power [121].

Next to resolution, the *mass accuracy* is another important parameter in MS analysis [121]. Here the *absolute mass accuracy*, Δm/z, is defined as subtraction of the calculated exact mass from the measured accurate mass [121]:

$$\Delta m/z = m/z_{\text{experimental}} - m/z_{\text{calculated}} \tag{2}$$

A fraction of absolute mass accuracy and the mass is yielding in the relative mass accuracy, δm/m, which is dimensionless and given in parts per million (ppm) [121]:

$$\delta m/m = \frac{(\Delta m/z)}{(m/z)} \tag{3}$$

But a measurement should not be accurate alone, it should also be precise to get as close as possible to the true value [121]. While accuracy is describing the deviation of the experimental value from the reference value, *precision* is describing the deviation within a group of identifications [121]. Therein, the terms *repeatability* and *reproducibility* are crucial. The "intra-laboratory" replication of the analysis with the same device is linked to repeatability.

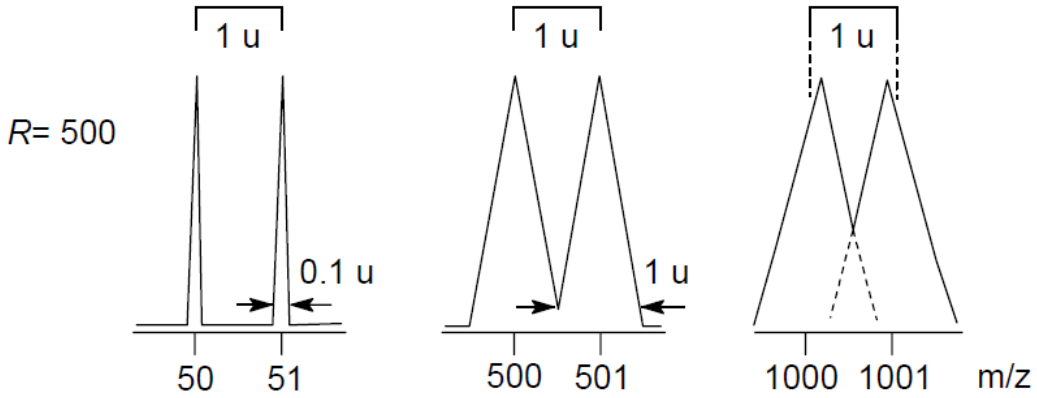

Figure 17: Clarification of the impact of R = 500 using an example of peaks at m/z 50, 500 and 1000. The given resolution is leading to superposition of the peaks at m/z of 1000 [121].

The "inter-laboratory" pendant is called reproducibility, which means, that a measurement repeated in another laboratory by another operator should lead to the same result or conclusion [121].

Measurements with high mass resolution and high mass accuracy are ensured by high-resolution mass spectrometry (HR-MS), which is discussed in section 2.5.4 [121].

2.5.4 Q Exactive™ HF Hybrid Quadrupole-Orbitrap™ Mass Spectrometer

The Q Exactive™ HF is a mass spectrometer with a pre-filter, high-performance quadrupole and an ultra-high-field Orbitrap analyser [122]. With the parent device, the Q Exactive™, proteomics analysis has gained access to a new extent [122]. The number of protein analysed per hour has been significantly increased since its commercial introduction [122]. The equipment configuration of the Q Exactive™ HF Hybrid Quadrupole-Orbitrap™ Mass Spectrometer is shown in Fig. 18 [122]. This hybrid mass spectrometer is consisting of an atmospheric ion source, a stacked-ring ion guide called S-lens, an advanced active beam guide (AABG) representing a low-resolution injection flatapole and a bent flatapole, a hyperquad mass filter with advanced quadrupole technology (AQT) representing a segmented quadrupole mass filter, a C-trap, a higher-energy collisional dissociation (HCD) cell and an Orbitrap mass analyser, displayed in Fig. 18 [122, 123].

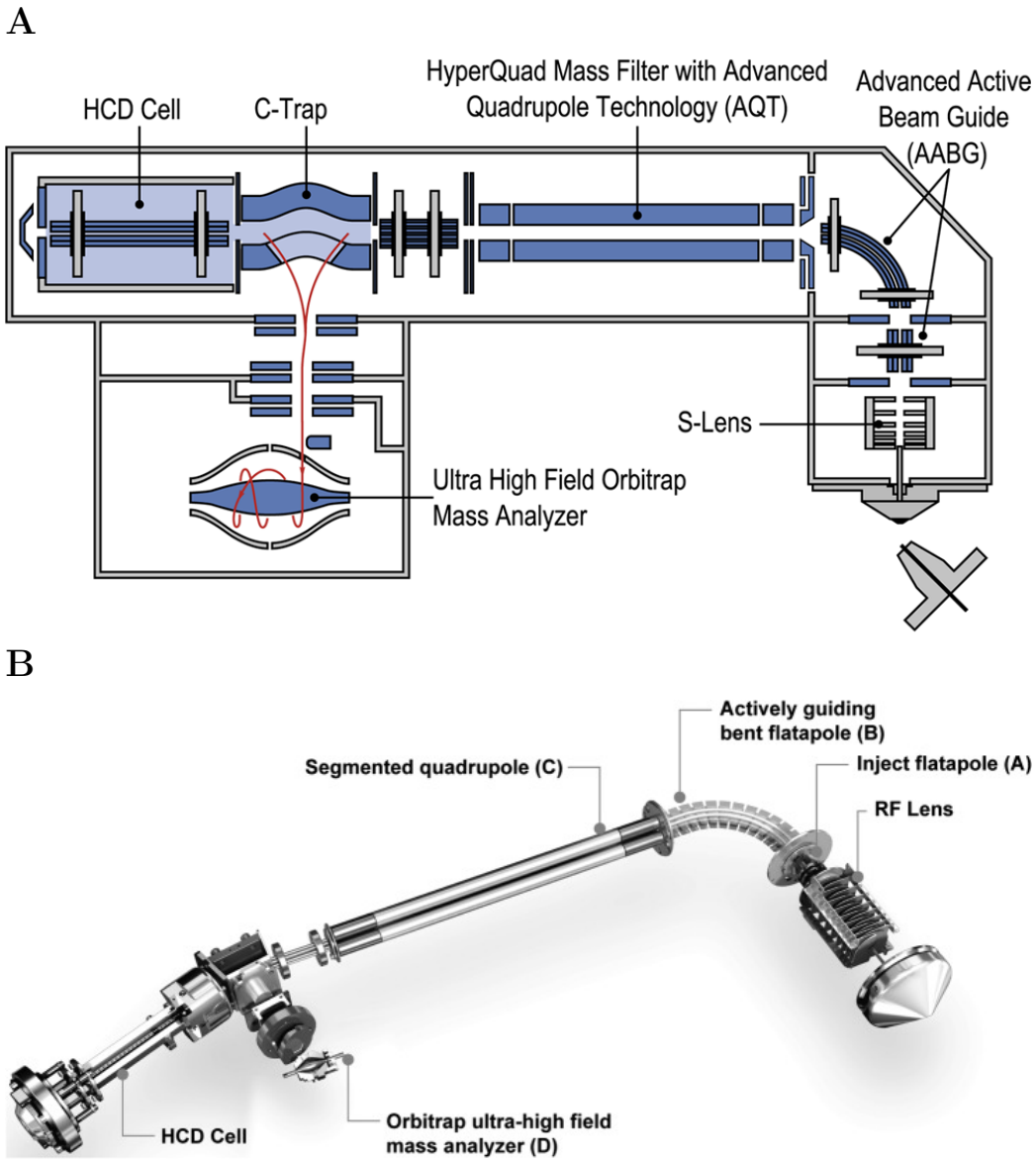

Figure 18: Q Exactive™ HF Hybrid Quadrupole-Orbitrap™ Mass Spectrometer. (A) Scheme and (B) a more realistic illustration of the device with an ion source at atmospheric pressure, a S-lens, an advanced active beam guide with the injection and bent flatapoles, an advanced quadrupole technology respresenting the segmented quadrupole, a transfer octopole, a C-trap/HCD cell combination and the ultra-high field orbitrap mass analyser [122, 123].

After entering the mass spectrometer, solvent droplets, other neutral species and unwanted ions are pre-filtered in the S-lens and the low-resolution injection flatapole in the source region and a bent flatapole [122]. The ions, that made it through the flatapole, are reaching a segmented quadrupole representing the next ion-isolating section, but it is also responsible for ion transmission [122]. The pre-filter elements are preventing contaminants to cover the rods of the quadrupole, which is increasing the robustness of the instrument [122].

An original linear quadrupole is built up of four hyperbolic rod electrodes extended in the z-axis, which can be seen in Fig. 19 [121]. In this connection a positive and a negative potential is applied to respectively two electrodes. The two electrodes with the same potential are arranged vis-à-vis, also shown in Fig. 19 [121]. This is leading to an alternating current (AC) and direct current (DC) component generation and applied periodic voltage plus a periodic change of the sign of the potential are causing attractive and repulsive forces. Thus, ions with a certain m/z value or m/z range, that have entered the quadrupole, can move through the quadrupole on a stable trajectory, while other ions are coming too close to the rods and are getting discharged [121].

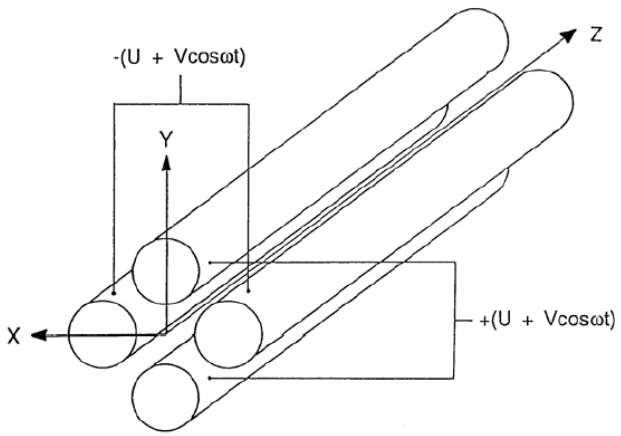

Figure 19: Scheme of a linear quadrupole mass analyser with an arrangement of the hyperbolic rod-like electrodes in the xy-plane and extension in the z-axis [121].

In the Q Exactive™ HF Hybrid Quadrupole-Orbitrap™ Mass Spectrometer an advanced quadrupole technology with a segmented quadrupole mass filter is obstructed to increase ion transmission and more precise precursor isolation efficiency over the isolation window [122]. The last segment of the quadrupole is also effecting an ion transmission in a narrower isolation window [122]. Ions, that have been transmitted the quadrupole on a stable trajectory, are passing an octopole with eight rod electrodes and a steeper potential than in quadrupoles, which is enabling a wide band pass for ions due to a more diffuse m/z cutoff in transmission [121]. An integrated C-trap/HCD collision cell combination is representing the next section. First the octopole is transferring ions, selected in the segmented quadrupole, into the C-trap, a "C"-shaped quadrupole for accumulation and temporary storage of the ions [122, 124]. The storage of ion packets up to about a million charges is taking place in the middle of the trap at low pressure of nitrogen [122, 124]. From here the collected ions are injected into the ultra-high field orbitrap analyser via short, high voltage electric pulses or into the multipole collision cell, where dissociation of ions is occurring with neutral gas molecules at reduced vacuum under a certain collision energy [122, 124]. The fragments are then returning to the C-trap and are afterwards sent to the orbitrap analyser [124]. The analysis of m/z values of product ions after fragmentation is called MS2 and the ions for this fragmentation are selected in a MS1 m/z analysis before and are directly transferred from C-trap into the orbitrap [121].

Orbitrap analysers are permitting high resolving power and accurate mass measurements. They are consisting of two electrodes working at ultra-high vacuum: an outer barrel-like electrode and an central spindle-like electrode [122]. Entering ion packets coming from the C-trap are trapped in an electrostatic field. Herein, electrostatic attraction towards the inner electrode is accompanied by the centrifugal force caused by the initial tangential velocity of the ions, which can be seen in Fig. 18 (A) [121]. The ultra-high field analyser of the Q Exactive™ HF is more compact than in its parent model, the classic Q Exactive™, allowing an enhanced electric field [122]. Ions with different m/z value are oscillating with respective frequencies in the orbitrap and via a fast Fourier transformation their m/z values can be determined [121].

The Q Exactive™ HF Hybrid Quadrupole-Orbitrap™ Mass Spectrometer is representing a system with an increase in robustness, isolation efficiency, ion transmission and resolution. Also higher scan rates up to 17 Hz can be achieved compared to the classic Q Exactive™ [122].

3 Methods and therein used materials or reagents

3.1 Reagents and materials

The chemicals listed in table 2 were used without further purification.

Table 2: List of used chemicals and reagents.

Reagents	Abbreviation	Company
Calcium chloride	$CaCl_2$	Merck KGaA
Ionomycin	-	Merck KGaA
Ethanol (absolute 99.9%)	EtOH	AustrAlco GmbH
Methanol (hypergrade for LC-MS)	MeOH	Merck KGaA
Water (LC-MS grade)	H_2O	VWR International GmbH
Formic acid (for LC-MS, $\geq$ 99%)	FA	VWR International GmbH
Acetonitrile (LC-MS grade)	ACN	Honeywell GmbH
Sodium chloride	NaCl	Merck KGaA
Trisodium citrate dihydrate	Na_3-citrate * 2 H_2O	Merck KGaA
Sodium acetate trihydrate	Na-acetate * 3 H_2O	Merck KGaA
Sodium dihydrogen phosphate dihydrate	NaH_2PO_4 * 2 H_2O	Merck KGaA
Disodium hydrogen phosphate	Na_2HPO_4	Merck KGaA
Potassium chloride	KCl	Merck KGaA
Magnesium chloride hexahydrate	$MgCl_2$ * 6 H_2O	Merck KGaA
Nitrogen (gaseous)	N_2 (g)	-

Deuterated molecules used as internal standards and the company, of which they have been purchased from, are registered in table 3.

Table 3: List of internal standards.

Compound	Company
15S-HETE-d8	Cayman Europe
12S-HETE-d8	Cayman Europe
5-OxoETE-d7	Cayman Europe
11,12-DiHETrE-d11	Cayman Europe
PGE2-d4	Cayman Europe
20-HETE-d6	Cayman Europe
5S-HETE-d8	Cayman Europe
14,15-DiHETrE-d11	Cayman Europe
8-iso-PGF2α-d4	Cayman Europe

Materials and devices used in this work are registered in table 4.

Table 4: List of materials and devices.

Material	Company
Pipetboy ACU classic	VWR International GmbH
Serological pipettes (10 mL, sterile)	Sarstedt
Falcon tubes 15 mL	Corning Science México S.A. de C.V.
Heraeus Megafuge 16R Centrifuge	Thermo Scientific™
miVac Duo concentrator (SpeedVac)	GeneVac Ltd.
Calibrated pipettes (volume ranges of 1-10, 50-200 and 100-1000 μL)	Gilson
Pipette Tips for Gilson	Greiner Bio-One International GmbH
Pasteur Pipettes	-
Strata™-X 33 μm Polymeric Reversed Phase cartridges for SPE (30 mg/1 mL)	Phenomenex Inc.
Glass vials (1.5 mL, screw neck)	Macherey-Nagel GmbH
Glass inlets (200 μL)	Macherey-Nagel GmbH
Screw caps (for 1.5 mL glass vials)	Macherey-Nagel GmbH
VacMaster™ manifold for SPE	Biotage®
Vanquish UPLC System	Thermo Scientific™
Kinetex™ 2.1 mm x 150 mm, 2.6 μm, C_{18}, 100 Å reversed-phase column	Phenomenex Inc.
Q Exactive™ HF Hybrid Quadrupole-Orbitrap™ Mass Spectrometer	Thermo Scientific™

3.2 Experimental design, sample preparation and extraction

As mentioned before, the platelet concentrates were produced from blood samples of 14 different, healthy donors at the general hospital of Vienna and therefrom samples were taken the same day (day 1) without receiving a treatment. Afterwards, one concentrate from each donor was treated with radioactive ^{137}Cs, while another concentrate from each donor was treated with the INTERCEPT Blood System^{TM} utilizing amotosalen and UVA and the concentrates were stored up to day 7. Of these, samples were taken at day 2, 5 and 7.

Up to this point the work was done by our colleagues at the general hospital. We have retrieved the samples at day 1, 2, 5 and 7 and stored the platelet concentrates at room temperature in a dark place till further processing.
The components of the platelet additive solution IIIM (PAS IIIM) and their concentrations are listed in table 5 [1].

Table 5: Composition of the PAS IIIM and the concentration of each additive [1].

Compound	Concentration [mmol/L]
NaCl	69.3
Na_3-citrate * 2 H_2O	10.8
Na-acetate * 3 H_2O	32.5
NaH_2PO_4 * 2 H_2O	6.7
Na_2HPO_4	21.5
KCl	5.0
$MgCl_2$ * 6 H_2O	1.5

3.2.1 Preparation of internal standard mixtures

The deuterated standards are listed in table 3, they have been stored in aliquots at -80°C and were added to the samples after passing through one freeze-thaw cycle. With these standard molecules two different standard mixtures were prepared, of which one was added prior to extraction and one was added prior to the LC-MS analysis. Below the standard mixture added prior to extraction is called "EicosanoidPreMix" and the mixture added prior to the LC-MS analysis is called "EicosanoidPostMix". For the preparation of the EicosanoidPreMix aliquots of the compounds from table 6 were thawed

and the volumes of each deuterated standard stock solution corresponding to table 6 were used and filled up to 500 μL with ACN. This mixture was then split into 70 μL aliquots and they were frozen at -80°C until their use.

Table 6: List of the internal standards used for the preparation of the EicosanoidPreMix plus the used volume of each standard and the final concentration.

Compound	Volume of stock solution [μL]	Final concentration in 500 μL ACN [ng/mL]
15S-HETE-d8	4	200
12S-HETE-d8	4	200
5-OxoETE-d7	12	600
11,12-DiHETrE-d11	4	200
PGE2-d4	8	400
20-HETE-d6	4	200

For the preparation of the EicosanoidPostMix aliquots of the compounds from table 7 were thawed and the volumes of each deuterated standard stock solution corresponding to table 7 were used and filled up to 500 μL with ACN. This mixture was also split into 70 μL aliquots and they were frozen at -80°C until their use.

Table 7: List of the internal standards used for the preparation of the EicosanoidPostMix plus the used volume of each standard and the final concentration.

Compound	Volume of stock solution [μL]	Final concentration in 500 μL ACN [ng/mL]
5S-HETE-d8	4	200
14,15-DiHETrE-d11	4	200
8-iso-PGF2α-d4	8	400

3.2.2 In-vitro cell activation

Two fractions, representing activated platelets and a control group, were derived from each platelet concentrate by transferring with caution respectively 1 mL of the platelet suspension into 15 mL flacon tubes. The platelet activation was performed for 15 min by adding 17.5 μL $CaCl_2$ (1.0725 M; 119 mg in 1 mL H_2O) and 3.33 μL ionomycin (13 mM in dimethyl sulfoxide (DMSO)) only to the 1 mL fraction representing the activated group. After adding $CaCl_2$ and ionomycin these samples were mixed gently. An aliquot of the EicosanoidPreMix, whose preparation has been described in section 3.2.1, was thawed on ice and 5 μL were added after those 15 min to both activated and control fraction. To both fractions 4 mL cold EtOH (-20°C) were added, the falcon tubes were vortex mixed and stored at -20°C overnight.

3.2.3 Solid-phase extraction

The storage of the platelet concentrate diluted 1:5 with cold EtOH at -20°C overnight is leading to a precipitation of proteins. Centrifugation for 30 min at 5000 revolutions per minute (rpm) and 4°C is inducing the formation of a protein pellet and the supernatant containing eicosanoids and other lipids was transferred into a new 15 mL falcon tube. Of these tubes, ethanol was reduced by centrifugation under vacuum at 37°C in a SpeedVac for about 75-105 min to the original volume of 1 mL.

For the solid-phase extraction a VacMaster™ manifold with Strata™-X 33 μm Polymeric Reversed Phase cartridges was used. All reagents and samples were stored on ice during the extraction process.

The C_{18} column material was washed by adding 2 times 1 mL MeOH and conditioning was achieved by adding 2 times 1 mL H_2O, MeOH and H_2O with purity of LC-MS grade. Herein, and during further extraction it had to be ensured, that the column did not dry and the liquid was going through constantly with about one drop every two seconds. After equilibration the sample was completely loaded onto the column using a glass Pasteur pipette due to interaction of some eicosanoids and plastic. In the next step, 2 mL H_2O were added into the falcon, vortex mixed and also loaded onto the column, which was done twice. A last washing step was performed with 1 mL H_2O loaded directly on column. After the liquid went through, the SPE column was disconnected from the vacuum manifold, 0.5 mL of MeOH and 2% FA were added and the elution into a 1.5 mL glass vial was executed manually via gentle pressure of a syringe. The extracted samples were stored at -80°C till further analysis to ensure the same number of freeze-thaw cycles for each sample.

3.3 LC-MS analysis

The preparation for the LC-MS analysis was proceeded by thawing the samples and reducing the solvent under N_2 gas stream lasting about one hour until the samples were completely dried. During the drying phase mobile phase A and mobile phase B were prepared with reagents of LC-MS grade stored at 4°C and thus the following steps were performed on ice. Herein, mobile phase A is consisting of H_2O with 0.2% FA and mobile phase B is consisting of 10% MeOH, 90% ACN and 0.2% FA. Since the initial condition of the LC system is represented by a mixture of mobile phase A and B at a ratio of 65:35, the dried sample is reconstituted in 145 μL of 35% mobile phase B and 5 μL of the EicosanoidPostMix described at section 3.2.1, of which an aliquot was thawed on ice before. After vortex mixing, the reconstituted sample was transferred into a 200 μL V-shaped glass inlet. Another centrifugation step at 2000 rpm and 4°C for 10 min was executed due to further precipitation. Subsequently 120 μL of the supernatant were transferred into a new glass inlet, which was also placed into a glass vial. The glass vial with the inlet containing pellet and residual supernatant was frozen at -80°C for a possible proteomics approach. The 120 μL sample was used for the eicosanoid analysis.

Therefore, the samples were placed in the autosampler of the LC system, a Vanquish ultra-high performance liquid chromatography system from Thermo Scientific™, at 4°C. For analysis a sample volume of 20 μL was injected. To ensure eicosanoid separation a Kinetex™ 2.1 mm x 150 mm, 2.6 μm C_{18}, 100 Å reversed-phase column was installed and the system was operating at a flow rate of 200 μL/min with a lower pressure limit of 2 bar and an upper limit of 800 bar. An already established method with a total run time of 20 min and a gradient flow profile starting at the initial composition of 35% mobile phase B was applied. The exact elution gradient protocol was as follows: 0-1 min at 35% mobile phase B, 1-10 min at 35-90% mobile phase B, 10-10.5 min at 90-99% mobile phase B, 10.5-15.5 min at 99% mobile phase B, 15.5-16 min at 99-35% mobile phase B and a re-equilibration phase at 35% mobile phase B from min 16 up to min 20. Herein, the mobile phase A is consisting of H_2O with 0.2% FA and mobile phase B of 10% MeOH, 90% ACN and 0.2% FA, which has already been described above for the preparation of the reconstitution buffer.

The detection was performed using a Q Exactive™ HF Hybrid Quadrupole-Orbitrap™ Mass Spectrometer from Thermo Scientific™ with an ESI source. Each sample was measured in negative ion mode with a technical replicate. For the identification of eicosanoids, which are belonging with their carboxylic group to the lipid subclass of fatty acids, the negative ion

mode data was consulted. To discover possible carry-over effects 10 μL H_2O were injected after two sample injections.

After receiving MS1 spectra in a full scan, MS2 spectra were obtained subsequent to the HCD fragmentation with a 24 eV collision energy. The following data processing of the attained raw-files containing the spectral information is described in section 3.4.

3.4 Data processing

The relative quantification of the eicosanoids and their precursor molecules is based on the retention time in MS1 spectra and was performed using the FreeStyle™ 1.1 and TraceFinder™ 4.1 Software packages from Thermo Scientific™. The method is already established in our group and the retention times of the deuterated internal standard molecules and the targeted analytes are known, nevertheless the identification was performed by checking the retention times of those molecules and the MS2 spectra via FreeStyle™. Thereby the development of a compound database within the TraceFinder™ software was feasible. This compound database is also containing the exact mass of the molecule plus a mass tolerance of 5 ppm and the corresponding retention time plus an acceptable window of $\pm$ 7.5 sec to search for the appropriate signal. Because of the gradient elution profile, the deuterated standard molecules are so chosen, that their retention times are distributed over the entire gradient and hence they can be adjusted as reference for the residual analytes. Exact masses and retention times of the internal standards, precursor molecules and targeted eicosanoids in their de-protonated form due to negative ion working mode as used in the compound database are listed in table 8. The chemical structures of the internal standard molecules and of the eicosanoids and their precursors in their non-ionised form were generated with ChemDraw Professional 15.0 and can be observed in Fig. 20 and 21. In Fig. 20 the chemical structures of the deuterated internal standard molecules are pictured with the EicosanoidPreMix molecules shown in Fig. 20 (A)-(F) and the EicosanoidPostMix molecules illustrated in Fig. 20 (G)-(I). The chemical structures of the eicosanoids and their precursor molecules are displayed in Fig. 21 with (A) AA, (B) DHA, (C) EPA, (D) 12-HETE, (E) 12-HHT, (F) 15-HETE, (G) 11-HETE, (H) 9-HETE and (I) 5-HETE. These molecules were chosen to observe alterations in the eicosanoid pattern and to check the platelet activation capability after receiving the two different treatments. Since neutrophils are producing 5-HETE, it has been added to the list of investigated molecules to check a possible portion of neutrophils within the platelet concentrates [103].

Table 8: List of the exact masses and retention times of the internal standard molecules, eicosanoid precursor molecules and further analytes in negative ion mode with loss of a hydrogen ion $[M\text{-}H]^-$.

		Compound	Exact mass [Da]	Retention time [min]
Eicosanoid	PreMix	15S-HETE-d8	327.2781	10.15
		12S-HETE-d8	327.2781	10.47
		5-OxoETE-d7	324.2556	11.23
		11,12-DiHETrE-d11	348.3069	9.08
		PGE2-d4	355.2422	5.65
		20-HETE-d6	325.2650	9.64
Eicosanoid	PostMix	5S-HETE-d8	327.2781	10.66
		14,15-DiHETrE-d11	348.3069	8.79
		8-iso-PGF2α-d4	357.2579	4.83
		AA	303.2330	12.70
		EPA	301.2173	12.12
		DHA	327.2330	12.54
		5-HETE	319.2279	10.72
		9-HETE	319.2279	10.63
		11-HETE	319.2279	10.38
		12-HETE	319.2279	10.52
		15-HETE	319.2279	10.21
		12-HHT	279.1966	9.23

To integrate the chromatographically separated peaks in MS1 spectra the ICIS peak detection algorithm was chosen due to its efficiency even at low MS signal levels. A detection strategy for the analyte molecules was defined, wherein the peak with the nearest retention time in the given retention time window should be selected for integration, if it is having a height above $1E^4$. For peak integration of the internal standard molecules the highest peak with an area threshold of 1 was used. In addition a S/N value of at least 3, a minimal peak width of 3 seconds, a multiplet resolution of 5 and an area tail extension of 5 were defined. The positive peak detection was checked manually for each molecule in all samples. Further evaluation was executed with the peak area obtained with the TraceFinder^{TM} software.

The data was exported from the TraceFinder™ software as Microsoft® Office Excel file. The peak areas of the targeted analytes were normalised to the mean peak area of the internal standard molecules. Afterwards the normalised peak area of each sample was averaged with its technical replicate. To clarify the ratio between activated and control group of each molecule at day 1, 2, 5 and 7 (for both treatments on the respective days), the fold change was calculated in [%] as follows [125]:

$$FoldChange = [(B - A)/A] * 100 \tag{4}$$

Herein, B is representing the quantity of the activated group and A the quantity of the control one. While a positive fold change is illustrating an increase after activation, a negative fold change is describing a reduction in the activated state.
For an evaluation of significant differences between the activated and control state of the same sample on the respective days without calculating each sample in particular a paired t-test with two tails has been made. To compare the initial levels of the untreated day 1 and the treated samples at day 2, which were treated at day 1 and stored for one day, a two-tailed paired t-test of the control groups was calculated. Furthermore, a two-tailed paired t-test of the control groups of both treatments at the same day was illustrating significant changes between the initial levels. Results of the t-tests with a p-value below 0.05 were considered as significant change among the two groups of interest. Herein, the intensity of significance was differentiated between p-values below 0.05, 0.01 and 0.005 representing increasing significance.
The coefficient of variation (CV) expressed in percentage of the internal standard molecules was defined as the fraction of standard deviation σ and mean μ multiplied by 100 [126]:

$$CV = [\sigma/\mu] * 100 \tag{5}$$

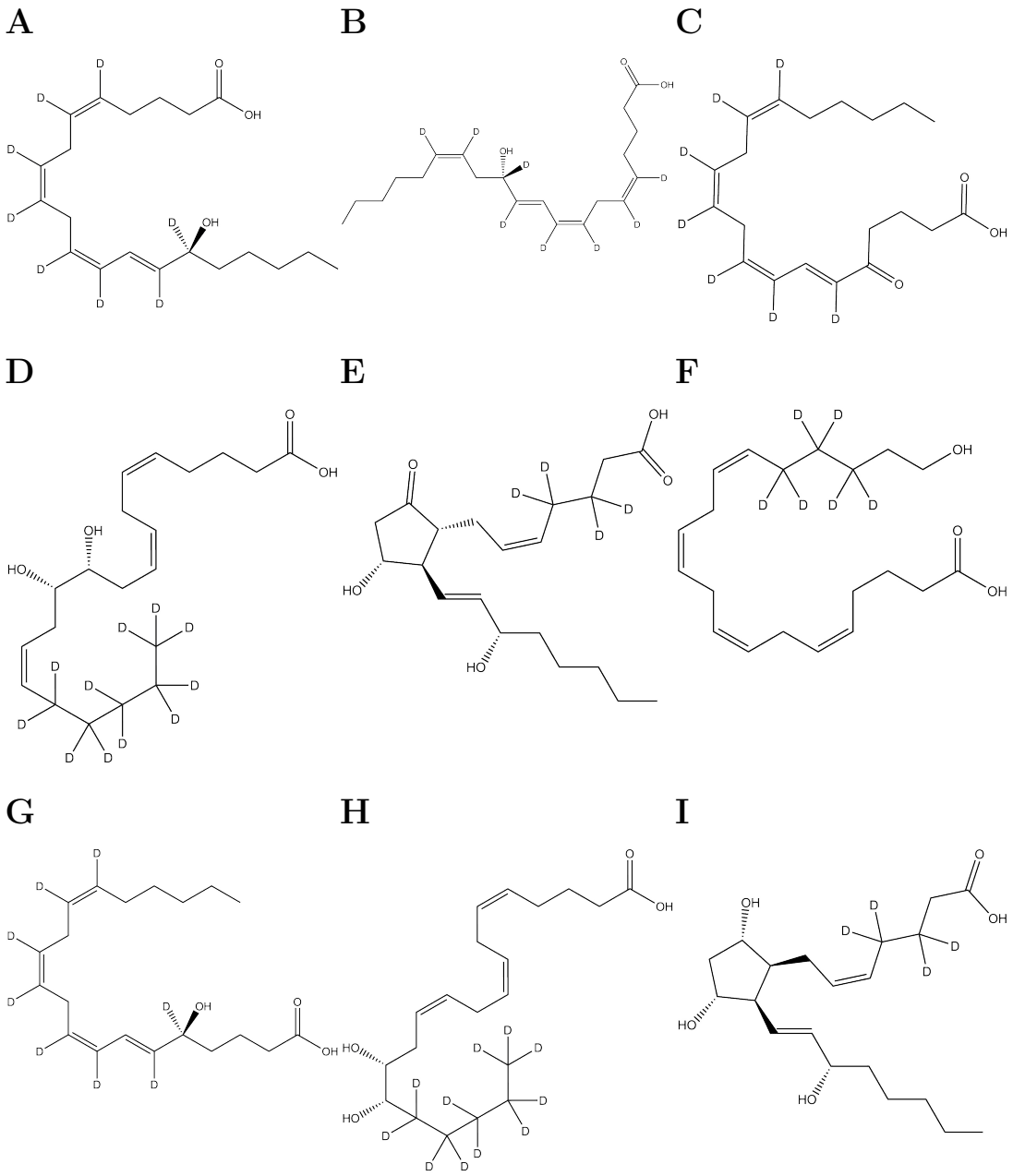

Figure 20: Chemical structures of the internal standard molecules with (A) 15S-HETE-d8, (B) 12S-HETE-d8, (C) 5-OxoETE-d7, (D) 11,12-DiHETrE-d11, (E) PGE2-d4, (F) 20-HETE-d6, (G) 5S-HETE-d8, (H) 14,15-DiHETrE-d11 and (I) 8-iso-PGF2α-d4.

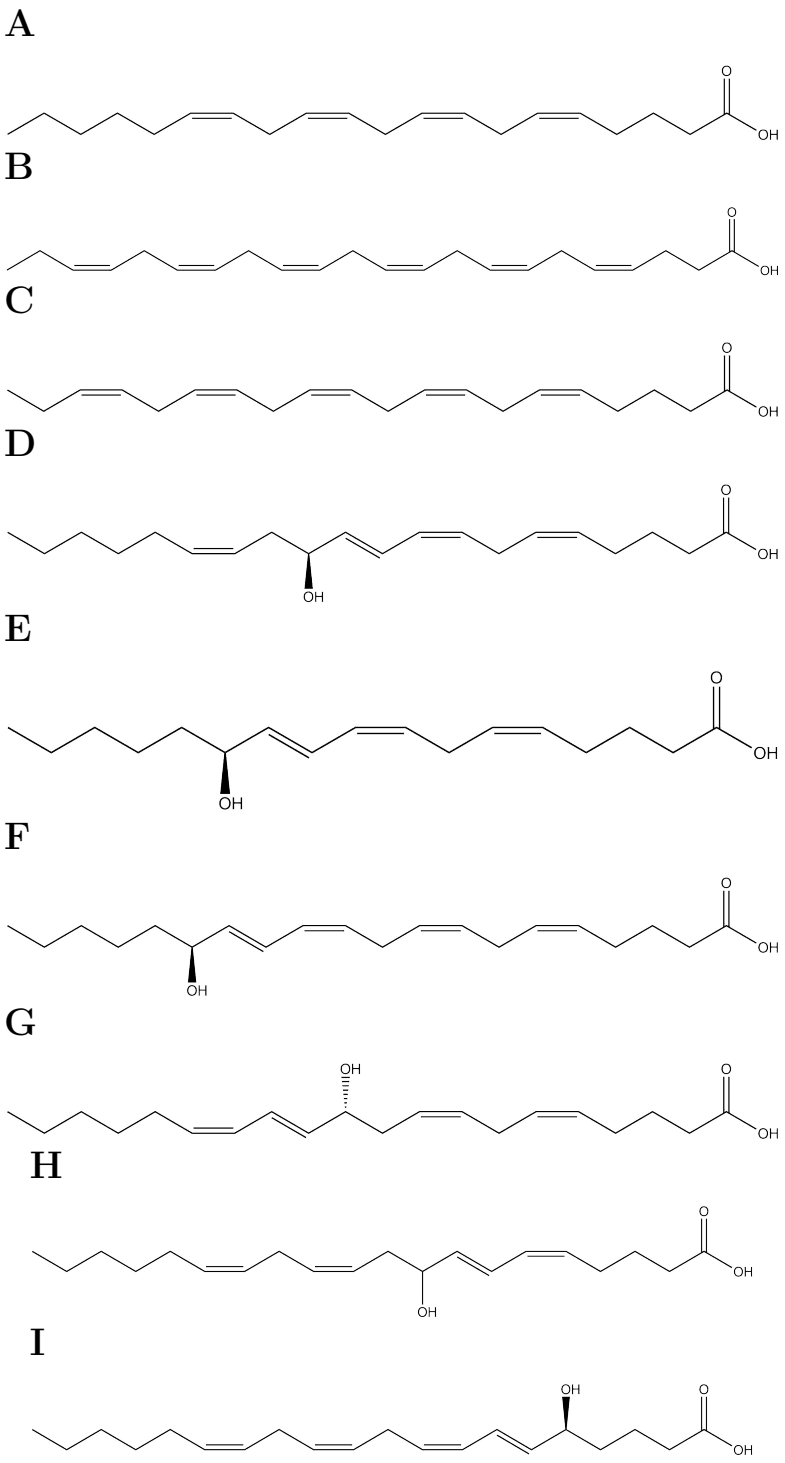

Figure 21: Chemical structures of the investigated eicosanoids and their precursor molecules with (A) AA, (B) DHA, (C) EPA, (D) 12-HETE, (E) 12-HHT, (F) 15-HETE, (G) 11-HETE, (H) 9-HETE and (I) 5-HETE.

4 Results and discussion

The following Figures 23-39 have been generated using Origin®Pro 2019 from OriginLab Corporation. The investigation was focused on eicosanoid precursor molecules AA, DHA and EPA and further eicosanoids of interest 12-HETE, 12-HHT, 15-HETE, 11-HETE and 9-HETE. In the Fig. 23-39 (A) the y-axis is representing the area under curve (AUC), which was calculated by normalising the area of the integrated peak of analyte molecules to the mean area of the standard molecules. Here a logarithmic presentation to the base 10 was chosen due to a large biological variance. The x-axis is showing the day of sample storage, the kind of treatment the samples have received and the state of the cells (control or activated group). The mean value of all donors is presented as bar and the values of the individual donors are presented as dots. Untreated samples of day 1 are depicted in orange with the control group (con) in light orange and the activated group (act) in dark orange. Samples receiving treatment 1 (amotosalen/UVA) are illustrated in blue with the control group in light blue and activated group in dark blue. Samples receiving treatment 2 (^{137}Cs) are pictured in green with the control group in light green and activated group in dark green. Dots in control and activated group of the same donor are connected via lines. A fold change in [%] is shown in Fig. 23-39 (B) and it is describing the difference upon cell activation. Significant changes after activation determined via a paired t-test were tagged with "*" (p-value < 0.05), "**" (p-value < 0.01) and "***" (p-value < 0.005) within Fig. 23-39 (A) and (B). For the comparison of the initial levels from both treatments, a paired t-test of the control groups was calculated as well, which is illustrated in Fig. 23-39 (C). Herein, significant changes are also tagged with "*" (p-value < 0.05), "**" (p-value < 0.01) and "***" (p-value < 0.005).

On the basis of the eicosanoid precursor molecules crucial differences during the storage of the platelets due to the pathogen inactivation treatment could already be observed (see Fig. 23-34). In addition isobaric forms of the investigated precursor molecules could have been identified in the manual check of the integrated peaks in the TraceFinder™ software, which are registered in table 9 as extension of the compound database composition from table 8. As it is shown in table 9, three additional isobaric forms of AA, one additional isobaric form of DHA and five additional isobaric forms of EPA were detected. As mentioned in section 3.4 the retention times of AA, DHA and EPA are known through comparison with commercially available external standards. Therefore, the additional, unfamiliar isobars are named with their rounded off, integer mass and the corresponding retention time divided by an underscore such as in "303_12.76".

Table 9: Extension to table 8 with the exact masses and retention times of detected isobars of the eicosanoid precursor molecules in negative ion mode with loss of a hydrogen ion $[M\text{-}H]^-$.

Compound	Exact mass [Da]	Retention time [min]
AA	303.2330	12.70
303_12.76	303.2330	12.76
303_12.83	303.2330	12.83
303_13.33	303.2330	13.33
DHA	327.2330	12.54
327_12.60	327.2330	12.60
EPA	301.2173	12.12
301_12.20	301.2173	12.20
301_12.45	301.2173	12.45
301_12.66	301.2173	12.66
301_12.87	301.2173	12.87
301_12.96	301.2173	12.96

The CV in percent for the internal standard molecules within the samples is illustrated in Fig. 22. The figure is indicating a difference of the values between the six molecules from the EicosanoidPreMix and the three molecules from the EicosanoidPostMix, which is emerging as CV values between 70 and 85 percent for each of the EicosanoidPreMix standards and 40 to 50 percent for each of the EicosanoidPostMix standard molecules. This effect is arising from spiking the EicosanoidPreMix prior to protein precipitation and SPE, which is leading to higher CV values, while the EicosanoidPostMix is spiked prior to analysis. As mentioned above, the analyte molecules were normalised to the mean area of these standards.

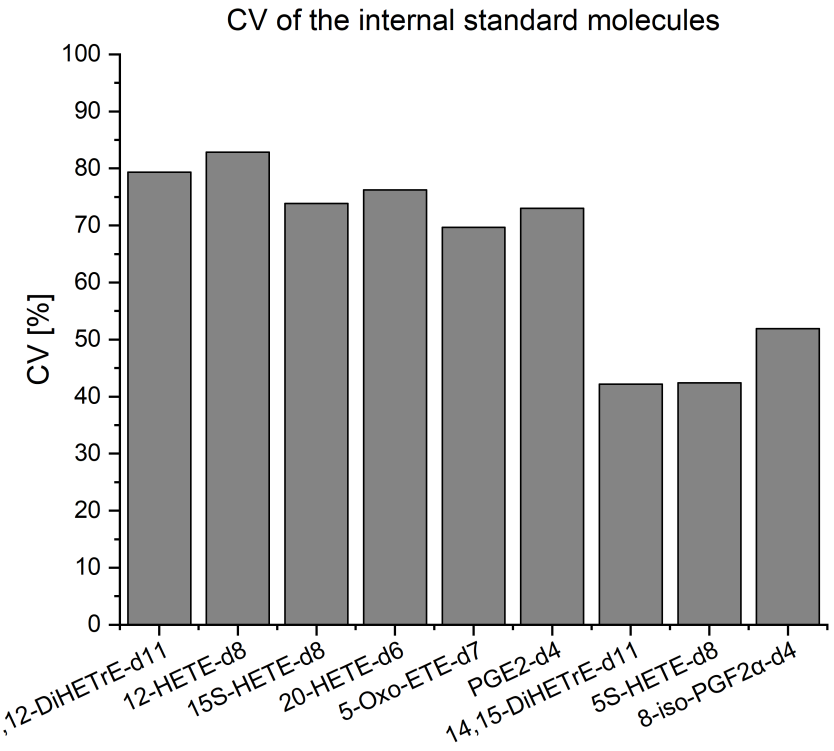

Figure 22: Coefficient of variation of the internal standard molecules within the samples with 11,12-DiHETrE-d11, 12-HETE-d8, 15S-HETE-d8, 20-HETE-d6, 5-Oxo-ETE-d7 and PGE2-d4 from the EicosanoidPreMix and 14,15-DiHETrE-d11, 5S-HETE-d8 and 8-iso-PGF2α-d4 from the EicosanoidPostMix.

AA and three additional isobars. The results of the main eicosanoid precursor, *arachidonic acid*, is depicted in Fig. 23. As Fig. 23 (A) and (B) are showing, a decrease upon activation of about 25 percent can be observed at day 1. Day 2 is showing a different behaviour of the platelets depending on the treatments. While an increase of AA was detected in the activated group of treatment 1 (day 2, blue), treatment 2 is leading to a decreased level in act (day 2, green). On day 5 an increase of about 20 percent in treatment 1 and 25 percent in treatment 2 was observed in the activated platelets. Day 7 is showing a reduction in act of treatment 1 and an increase in treatment 2. Considering the control group initial levels from day 1 up to day 7 a consecutive enhancement can be seen as well. A comparison of the initial levels (control group) from both treatments via a paired t-test is indicating higher levels of AA in treatment 2, which is even significantly enhanced at day 5 and day 7, illustrated in Fig. 23 (C). No significant difference upon the treatment and storage for one day was observed between day 1 and day 2 (see Fig. 23 (C)).

The AA isobar *303_12.76* was only detected in the samples treated with amotosalen/UVA (treatment 1, blue) and was not even detected in the untreated samples collected at day 1, as depicted in Fig. 24 (A). While day 2 and day 7 are indicating a decrease of about 17 and 30 percent in a non-significant way, the activated group at day 5 is remaining constant due to activation (see Fig. 24 (B)).

Another AA isobar, *303_12.83*, was also found in the untreated samples from day 1 and activation was not inducing an enhanced production of this molecule within the platelets, which can be seen in Fig. 25 (A) and (B). But it was also detected in treatment 2. Nevertheless, Fig. 25 (C) is showing significantly higher initial levels at day 2 and day 5 and a not significantly higher mean control group level at day 7 in the UVA-based treatment . The high levels in the control groups of treatment 1 are seeming to prevent a further increase during platelet activation. While the fold change at day 5 is showing a constant level upon activation, it is showing a slight decrease at day 2 and day 7 in Fig. 25 (B). As Fig. 25 (C) indicates, the control group level of treatment 1 at day 2 is significantly enhanced compared to the untreated control group level at day 1. Considering the control group levels at day 1 and at day 2 from treatment 2 in Fig. 25 (C), the mean value at day 2 is slightly increased. The levels at day 2, 5 and 7 in treatment 1 are at a constant level in the not-activated samples, while the intensity of the signal in treatment 2 is consecutively enhancing during storage time from day 2 through day 5 up to day 7 (see Fig. 25 (C)). The fold change in Fig. 25 (B) is denoting a reduction of about 20 percent at day 2 for the samples receiving treatment 2. During the storage time of these samples activation was leading

to an increase of about 40 percent at day 5 and almost 100 percent at day 7.

At a retention time of 13.33 min the last isobar of arachidonic acid, which is called *303_13.33*, was detected. As Fig. 26 (A) is presenting, the isobar was found in the untreated samples at day 1 as in the isobar 303_12.83 from Fig. 25 (A). The initial control levels in the UVA-based treatment 1 are also significantly higher than in treatment 2 as shown in Fig. 26 (C), which is correlating with the results from Fig. 25 (C). Fig. 26 (C) is also illustrating a significantly higher level within the control group of treatment 1 at day 2 than in the control group at day 1, while the levels at day 1 and day 2 from treatment 2 are at a similar level. The fold change in Fig. 26 (B) is showing rather constant or decreased levels for treatment 1, also observed in Fig. 25 (B) for 303_12.83. For 303_13.33 a fold change with an increasing reduction in the activated samples of treatment 1 from day 2 trough day 5 up to day 7 was determined in Fig. 26 (B), while a trend of an increasing level from day 2 up to day 7 for the samples receiving treatment 2 was observed.

Summing up AA and its 3 additional isobars from Fig. 23-26, higher initial levels of AA were observed in treatment 1 comparing the control groups of both treatments. The isobar 303_12.76 was not detected in the untreated samples from day 1 and it was also not detected in treatment 2. The two further AA isobars, 303_12.83 and 303_13.33, were found also at day 1, which means they were not caused by the treatment in the first instance, but the treatments were leading to an increased release of these molecules by the platelets and different behaviour upon storage. Treatment 1 (utilizing amotosalen/UVA) was leading to significantly higher levels in the control state starting already at day 2, in which activation was not effecting an enhanced release of 303_12.83 and 303_13.33. This could mean, that the production of these molecules was used to full capacity. In contrast the values of the control groups of treatment 2 were rising during storage time from day 2 up to day 7. Considering the initial levels of AA and its isobars at day 1 and day 2, significantly enhanced levels were detected within 303_12.83 and 303_13.33 at day 2 in treatment 1, while the levels in treatment 2 were at similar levels to the level in the untreated samples at day 1.

DHA and one additional isobar. The results of *docosahexaenoic acid* are displayed in Fig. 27, in which Fig. 27 (A) and (B) are showing a significant decrease of about 40 percent after activation at day 1. After receiving the treatments, the samples were not showing significant changes upon activation at day 2. Comparing the control group levels of both treatments at the corresponding days, the samples from treatment 2 are indicating higher levels than those from treatment 1 as illustrated in Fig. 27 (C) with signif-

icantly higher values at day 5 and day 7. By comparing day 1 and day 2 in Fig. 27 (C), no significantly enhanced level was determined after receiving the two different treatments. With the fold change a reduction of about 15 percent upon activation of the samples from day 2 receiving treatment 1 and a reduction of about 35 percent for treatment 2 were observed, depicted in Fig. 27 (B). At day 5 samples of both pathogen inactivation procedures were leading to an increase of the level in the activated state, while at day 7 a reduction of about 20 percent was registered for treatment 1 and an enhancement of about 20 percent was registered for treatment 2.

For DHA an additional isobar named *327_12.60* was also identified, the results of which are shown in Fig. 28. This isobar was also detected at day 1 like the two isobars of AA, 303_12.83 and 303_13.33 displayed in Fig. 25-26. Fig. 28 (B) is displaying a reduction of about 45 percent due to platelet activation at the first day, which is correlating to the fold change of DHA from the untreated samples in Fig. 27 (B). The decrease at day 2 for treatment 1 of about 10 percent and for treatment 2 of about 40 percent is behaving similar to the observations of DHA in Fig. 27 (B). At day 5 a slight decrease of about 15 percent in the activated samples of both treatments could be determined, which was also seen at day 7 for treatment 1, while in treatment 2 a constant level after platelet stimulation was recorded. Comparing the control states of both treatments, Fig. 28 (C) is showing a slightly enhanced initial level of treatment 1 at day 2 and a significantly higher level in treatment 1 at day 5. At day 7 the level of treatment 2 was slightly higher than in treatment 1, but the variance of the donors is not allowing an explicit interpretation. By comparing the levels of the control group at day 1 and day 7 of both treatments, an increase of approximately 150 percent in treatment 1 and 250 percent in treatment 2 at day 7. Examining day 2 con and day 7 con, an enhancement of 100 percent for treatment 1 and 200 percent for treatment 2 could be observed. The paired t-test between the untreated day 1 and the two differently treated day 2 samples was not leading to significant changes upon the treatment and storage up to the second day.

EPA and five additional isobars. The last eicosanoid precursor of interest was *eicosapentaenoic acid*, of which results are depicted in Fig. 29. In Fig. 29 (A) can be seen a significant reduction of the level upon activation at day 1, which is becoming apparent in Fig. 29 (B) with a negative fold change of about 45 percent. In the UVA-based treatment (treatment 1) significantly higher initial levels were determined from day 2 through day 5 up to day 7 as shown in Fig. 29 (C). A significantly increased control group level upon treating via amotosalen/UVA with subsequently one day storage

in contrast to the untreated day 1 was ascertained in Fig. 29 (C). Comparing the levels within the control groups in treatment 1 respectively treatment 2, an increase starting from day 2 up to day 7 can be seen in Fig. 29 (C) as well. Because of the high initial levels in treatment 1 the activation of the platelets was not affecting a further increase at day 2 and day 5, and at day 7 a reduction of about 25 percent was denoted, which arises from Fig. 29 (B). For treatment 2 a negative fold change was recorded at day 2 of about 30 percent, while day 5 is showing an increase of 20 percent in the activated state. The value at day 7 in treatment 2 is keeping constant.

Like AA and DHA, isobars of EPA were detected as well. The results of the first additional isobar, *301_ 12.20*, are illustrated in Fig. 30. Within this isobar the levels in the control groups of treatment 1 are all significantly higher compared to those in treatment 2 (see Fig. 30 (C)). Therefore, activation has no impact on the levels as Fig. 30 (B) is pointing out quite constant levels in treatment 1 through all days. For treatment 2 a negative fold change of 30 percent was recorded at day 2, while at day 5 an increase of 30 percent could be determined like illustrated in Fig. 30 (B). At day 7 platelet activation was inducing an enhancement of about 90 percent in treatment 2. A comparison of the control groups in treated samples at day 2, 5 and 7 with the untreated samples from day 1 is indicating a four-fold significantly increased level at day 2, a seven-fold increased level at day 5 and a nine-fold higher level at day 7 in the amotosalen/UVA treated samples, while the levels of day 2 and day 7 in the cesium-based pathogen inactivated samples are arranged in the area of day 1 and only at day 5 a two-fold higher level could be observed, which was not significantly enhanced (arising from Fig. 30 (A) and (C)).

Fig. 31 is picturing the results of the next detected EPA isobar, *301_ 12.45*. Here the sub-figures (A) and (B) are showing a decrease of 20 percent due to platelet activation at the first day. Like EPA and the isobar 301_12.20 from Fig. 29-30, the initial levels of this isobar are more intense within treatment 1 at the corresponding days with a significant difference between the two techniques at all days as Fig. 31 (C) is indicating. Upon activation the samples from treatment 1 are having a negative fold change of about 25 percent and even a significant decrease at day 2 and about 15 percent at day 5 and day 7, which is shown in Fig. 31 (A) and (B). This seems to correlate with the assumption made in observations before, that platelets with already high initial levels are used to full capacity, thus activation is not leading to further increasing levels but rather to a constant level or a reduction in the activated state. For 301_12.45 the level after treating the samples is rising at day 2 with a significantly enhanced level in the UVA-based treatment 1 and it is further increasing at day 5 within both treatments. Comparing day

5 with day 7, a decrease during storage can be observed for both treatments derived from Fig. 31 (C).

301_12.66 is representing another isobar of EPA and its results are shown in Fig. 32. At day 1 a significant reduction in the activated samples could be monitored, as shown in Fig. 32 (A) and (B). Arising from Fig. 32 (C) the initial levels in treatment 1 are slightly higher than in treatment 2 at day 2 and significantly higher at day 5 and day 7. At day 2 and day 5 for both treatments an almost constant level in the activated state could be observed with a negative fold change below 10 percent, which can be considered as constant value (see Fig. 32 (B)). While at day 7 a negative fold change of 15 percent was registered for treatment 1, activation was leading to an increase of about 60 percent for treatment 2. The comparison of day 1 with day 2 is showing a significantly higher level for treatment 1, while for treatment 2 an approximately constant level was observed (see Fig. 32 (C)).

Results of the next EPA isobar, *301_12.87*, are pictured in Fig. 33. As Fig. 33 (A) and (B) are indicating, the activation of the cells at day 1 is not leading to an increase of the level. The comparison of the initial levels in Fig. 33 (C) are showing higher levels in treatment 1 like it was observed in EPA and the isobars discussed so far from Fig. 29-32. In addition, a significantly higher level could be detected at day 7 for 301_12.87 in treatment 1. After treating the samples and storage till day 2, a constant level was observed for treatment 2, while a not significantly increased control group level for treatment 2 was determined at day 2 (see Fig. 33 (C)). Fig. 33 (C) is also presenting an enhancement from day 2 to day 5 with a following reduced level at day 7 in both treatments. Considering the fold change from Fig. 33 (B) a negative fold change of about 20 percent could be ascertained for treatment 1 at day 2, while treatment 2 is indicating an increase of about 80 percent due to platelet activation. At day 5 a negative fold change of about 30 percent was monitored in treatment 1 and a decrease of 20 percent in treatment 2, while activation was keeping the level in treatment 1 constant at day 7 and was causing a positive fold change of 20 percent in treatment 2.

Fig. 34 is showing the results of the EPA isobar *301_12.96*, which was eluting last. At day 1 an about 35 percent decreased level in the activated state could be observed, as can be seen in Fig. 34 (A) and (B). Significantly higher initial levels in treatment 1 compared to those of treatment 2 over all days and a significantly enhanced level after the UVA-based treatment at day 2 compared to day 1 are arising from Fig. 34 (C). Platelet stimulation of the samples treated via amotosalen/UVA was leading to a negative fold change over all days with significantly decreased levels of about 55 percent in the activated state at day 2 and day 7 (see Fig. 34 (A) and (B)).

Summing up DHA, EPA and their isobars shown in Fig. 27-34, signifi-

cantly reduced levels due to platelet activation of the untreated samples at day 1 could be detected for the two eicosanoid precursor molecules DHA and EPA. In contrast to DHA, the initial levels of the control groups of EPA and its isobars are higher in treatment 1 with significantly increased levels over all days in 301_12.20, 301_12.45 and 301_12.96, which is depicted in Fig. 30 (C), 31 (C) and 34 (C). Only Fig. 32 (C) is presenting a not so clear ratio between both treatments for 301_12.66. Considering the control group levels at day 1 and day 2 from both treatments, no significant increase was determined for DHA and 327_12.60, while the levels of EPA and four of the five additional isobaric forms (301_12.20, 301_12.45, 301_12.66 and 301_12.96) were significantly more intense for treatment 1 at day 2 as depicted in Fig. 27-34 (C).

Eicosanoids of interest. 12-HETE is one of the major released eicosanoid molecules by stimulated platelets, of which results are illustrated in Fig. 35 [10]. Therefore, activation of the untreated cells at day 1 is leading to a significant increase as depicted in Fig. 35 (A), which is correlating to a positive fold change of about 30 percent in Fig. 35 (B). At day 2 samples of both treatments are showing a significant enhancement in the activated state, which was not detected the following days. As Fig. 35 (C) is indicating, the initial control group levels are of a very similar intensity, but activation is leading in treatment 1 to an increase of about 30 percent, while in treatment 2 a positive fold change between 80 and 90 percent could be denoted (see Fig. 35 (B)). At day 5 and day 7 significantly higher control group levels were observed in treatment 2 with similar levels of the corresponding treatment at day 5 and day 7, illustrated in Fig. 35 (C). The fold change from Fig. 35 (B) is displaying an increase of about 30 percent for treatment 1 at day 5 and a constant level in view of treatment 2. Also an enhancement of 30 percent for treatment 1 was recorded at day 7, while activation of treatment 2 at day 7 was resulting in a 110 percent enhancement in the level of 12-HETE. Comparing the level of the control state at day 1 with those of the treated and afterwards stored samples, the levels of the treated samples are increased in a significant way at day 2 within both treatments (see Fig. 35 (C)).

Results of 12-HHT, another major product of activated platelets, are pictured in Fig. 36. Activation was causing a significant increase of about 70 percent in the untreated samples at day 1, as shown in Fig. 36 (A) and (B). Although in treatment 1 at day 2 the positive fold change between 10 and 20 percent was recorded, the t-test in Fig. 36 (A) was showing a significant change. Fig. 36 (C) is indicating similar levels of the control groups of both treatments at day 2, as it was seen for 12-HETE in Fig. 35 (C), but the

variance of the individual donors is higher in treatment 2 for 12-HHT. Also for 12-HHT the increase at day 2 due to platelet stimulation was more intense in treatment 2 with almost 50 percent than in treatment 1 (see Fig. 36 (B)). With regard to day 5, a higher initial level in treatment 2 was detected with a significantly positive fold change of about 40 percent, while activation of the samples treated with UVA was leading to an increase of 20 percent. At day 7 there was no difference in the level of the activated state from treatment 1, but for treatment 2 an enhancement between 100 and 110 percent due to activation was observed, as pictured in Fig. 36 (B). Comparing the control states at day 7 in Fig. 36 (C), a significantly enhanced level was observed for treatment 2. But the paired t-test is also indicating a significantly higher level after treating the samples with amotosalen/UVA, which is arising from Fig. 36 (C).

Activated platelets are also producing significant amounts of 15-HETE and Fig. 37 (A) is showing a significantly higher level in the activated state of the untreated platelets at day 1 compared to the stored samples after receiving the different treatments. Due to the high levels in treatment 1 at day 2, 5 and 7 activation is not resulting in further increased levels, while for treatment 2 at day 2 and day 7 a positive fold change of about 30 and 60 percent was found (see Fig. 37 (B)). The level of treatment 2 at day 5 was kept constant. Comparing control groups of both treatments at the corresponding days, higher levels for treatment 1 could be observed with significant differences at all days, as depicted in Fig. 37 (C). Regarding the control state level at day 1 and day 2, samples of both treatments are significantly higher than at day 1 (see Fig. 37 (C)).

The results of 11-HETE are illustrated in Fig. 38. In Fig. 38 (A) and (B) can be seen, that activation of the untreated samples at day 1 is keeping the level constant to the control group level. Considering the control group levels at day 1 and day 2 in Fig. 38 (C), a significantly enhanced level was determined for treatment 1, the level of treatment 2 kept constant to the level at day 1. The comparison of the control groups of both treatments in Fig. 38 (C) is indicating significantly higher levels in the UVA-based treatment 1 over all days. Therefore, platelet stimulation is not causing increased release of 11-HETE, which can be derived from the fold change of treatment 1 in Fig. 38 (B). At day 2 a positive fold change of about 30 percent was recorded, while at day 5 the value was kept constant due to platelet activation and at day 7 an increase of 70 percent was ascertained.

Results of 9-HETE are pictured in Fig. 39 and subfigure (A) is indicating, that the molecule was not detected at day 1. After treating the samples, it could be detected in treatment 1 within control and activated state at day 2. As the fold change in Fig. 39 (B) is displaying, platelet activation at day 2

was leading to a significant increase of 65 percent (see Fig. 39 (A)). 9-HETE was also at day 5 only found in treatment 1. Here, a positive fold change of about 170 percent due to platelet stimulation could be ascertained, which was not significant (see Fig. 39 (B)). At day 7 the molecule was identified within four donors, of which dots of two donors respectively are overlapping, in the control group of treatment 1 and within one donor in the corresponding activated samples, but it was also detected within one activated sample from treatment 2 at day 7, as illustrated in Fig. 39 (A). Considering Fig. 39 (B), a decrease of 80 percent was determined in treatment 1 at day 7. Due to the identification of 9-HETE in only one activated sample, the fold change at day 7 for treatment 1 should not be interpreted too strictly.

Summing up the results of 9-, 11-, 12- and 15-HETE and 12-HHT from Fig. 35-39, platelet activation is leading to significantly higher levels in the activated states at day 1 and day 2 within both treatments according to the results of 12-HETE in Fig. 35 (A). Relating to 12-HETE, 12-HHT, 15-HETE and 11-HETE, depicted in Fig. 35-38, changes in the levels of the control groups were observed between day 2 and day 5, while the levels were considered as constant from day 5 to day 7 within each treatment. Similar initial levels of 12-HETE and 12-HHT for both treatments at day 2 are shown in Fig. 35 and 36. During storage time the levels of 12-HETE and 12-HHT are higher in treatment 2 at day 5 and day 7. In contrast to that, 15-HETE and 11-HETE production is more enhanced in treatment 1 than in treatment 2 starting already at day 2 after pathogen inactivation techniques were applied, as pictured in Fig. 37 and 38. 9-HETE was detected in the control and activated samples of treatment 1 over all days and in only one sample of the activated state of treatment 2 at day 7, which is depicted in Fig. 39. Considering the production of 9-HETE, the treatment of platelet concentrates with UVA seems to induce free-radical, oxidative stress to the cells causing non-enzymatic eicosanoid formation [93].

By comparing the levels of the control states at day 1 and at day 2, after receiving the two different treatments and one day storage time, significantly higher levels were observed for 11-, 12- and 15-HETE and 12-HHT in the amotosalen/UVA-based treatment (treatment 1) and for 12- and 15-HETE in the Cs-based treatment (treatment 2) as shown in Fig. 35-38 (C). Since 11-, 12- and 15-HETE and 12-HHT are enzymatically generated eicosanoids and the control group levels of all these molecules are significantly increased at day 2 in treatment 1, the UVA-based treatment seems to affect the enzymatic activity. The influence of UVA light on signal pathway activation leading to eicosanoid production has already been described in section 2.3.

5-HETE was detected in four samples, which could be connected with a marginal contamination of the platelet concentrates with neutrophils.

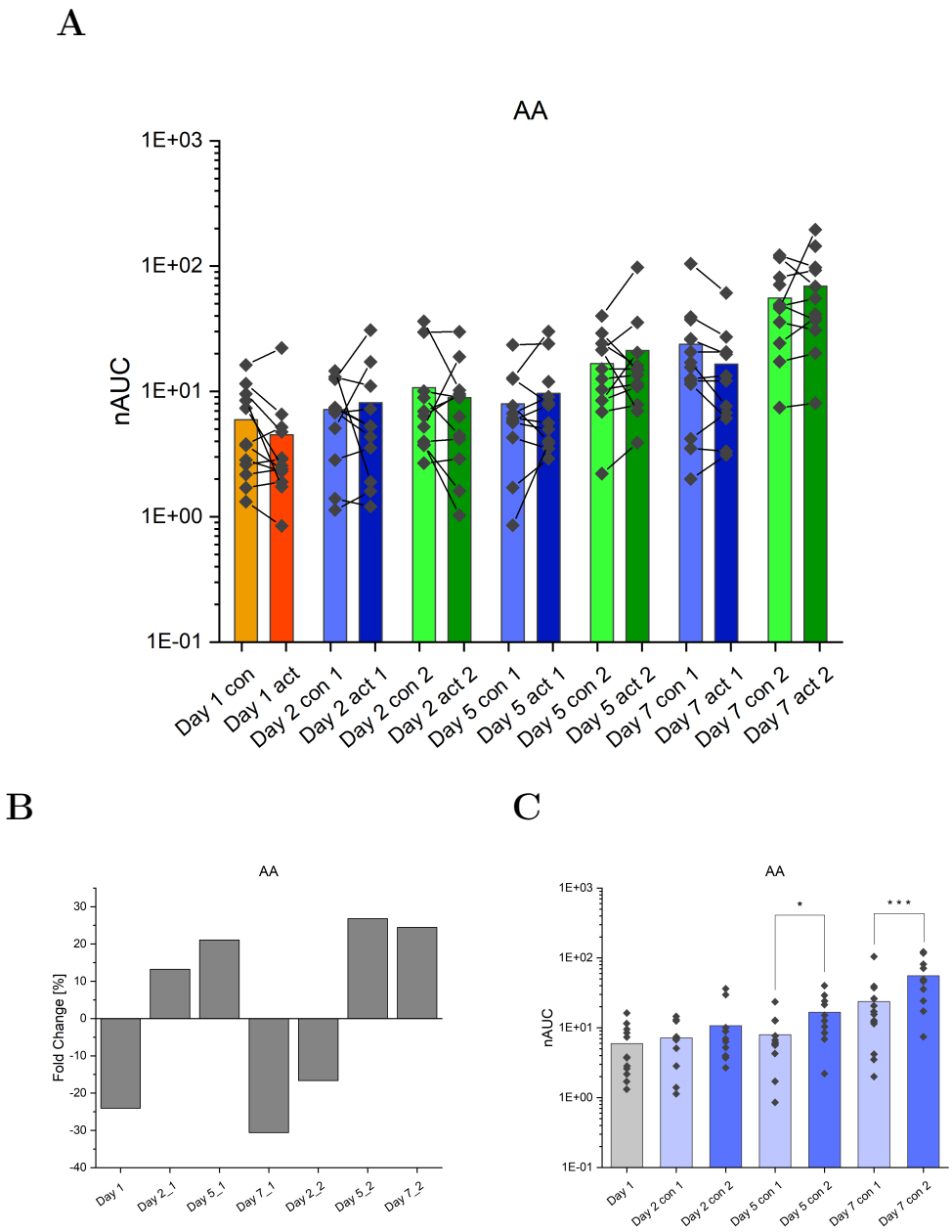

Figure 23: Results of AA. (A) Bars: Normalised mean peak area of all donors. Dots: Peak area of individual donors. Day 1: con (light orange), act (dark orange). Treatment 1 at day 2, 5 and 7: con (light blue), act (dark blue). Treatment 2 at day 2, 5 and 7: con (light green), act (dark green). Lines are connecting con and act of the same donor. (B) Fold change: Difference in act compared to con. (C) Result of paired t-test of con from both treatments. Significant changes are tagged with "*" (p-value < 0.05), "**" (p-value < 0.01) and "***" (p-value < 0.005).

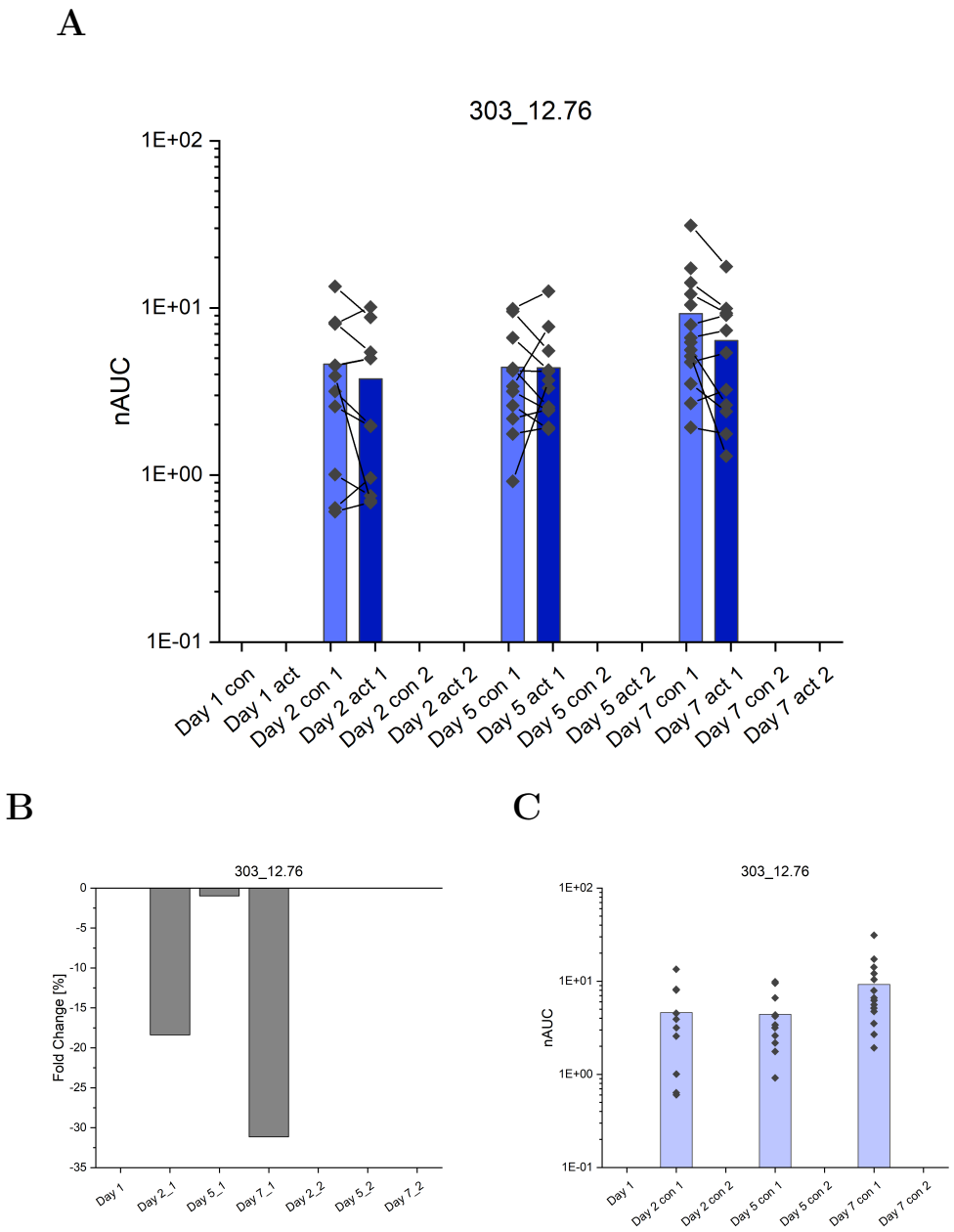

Figure 24: Result of 303_12.76. (A) Bars: Normalised mean peak area of all donors. Dots: Peak area of individual donors. Day 1: con (light orange), act (dark orange). Treatment 1 at day 2, 5 and 7: con (light blue), act (dark blue). Treatment 2 at day 2, 5 and 7: con (light green), act (dark green). Lines are connecting con and act of the same donor. (B) Fold change: Difference in act compared to con. (C) Result of paired t-test of con from both treatments. Significant changes are tagged with "*" (p-value < 0.05), "**" (p-value < 0.01) and "***" (p-value < 0.005).

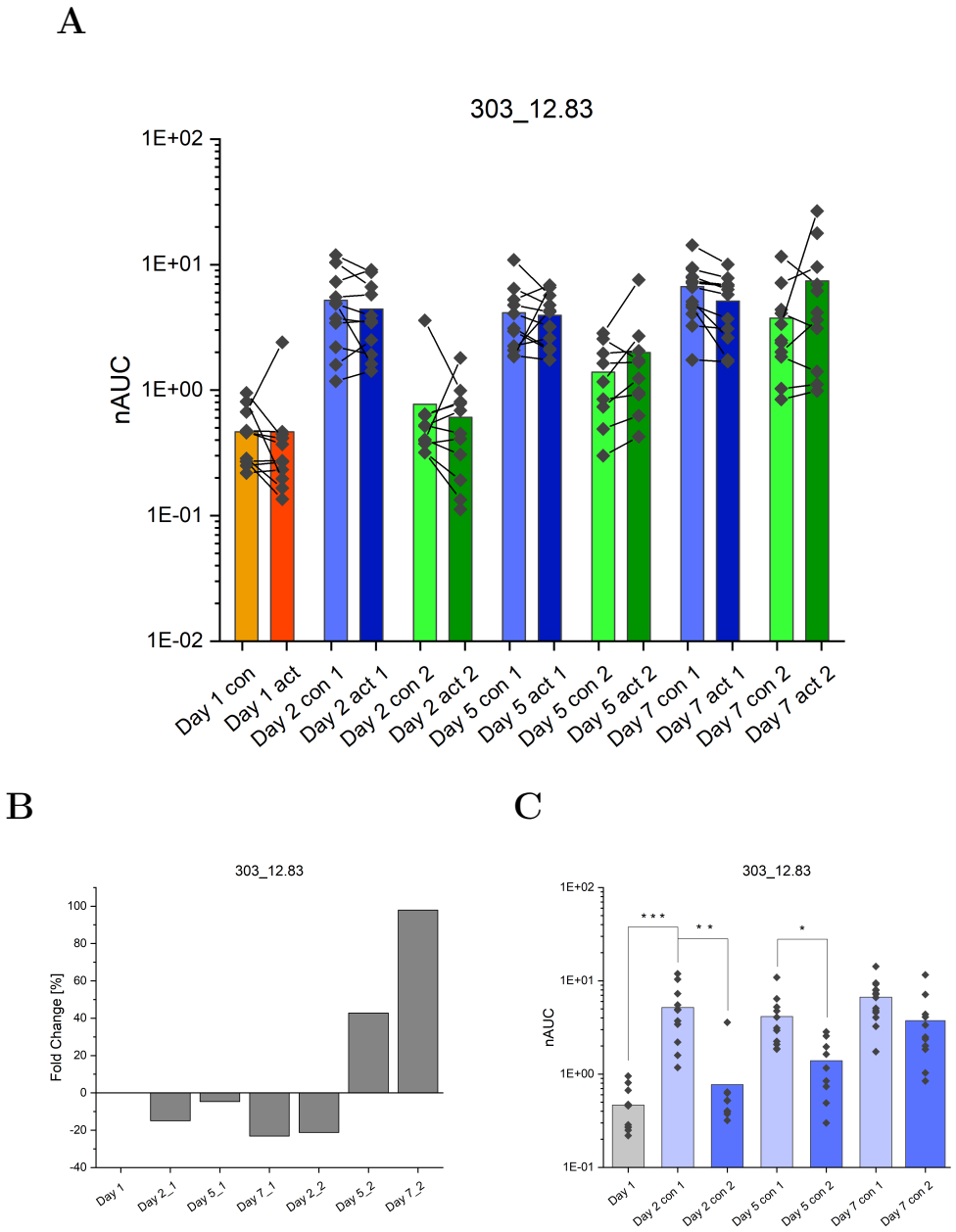

Figure 25: Result of 303_12.83. (A) Bars: Normalised mean peak area of all donors. Dots: Peak area of individual donors. Day 1: con (light orange), act (dark orange). Treatment 1 at day 2, 5 and 7: con (light blue), act (dark blue). Treatment 2 at day 2, 5 and 7: con (light green), act (dark green). Lines are connecting con and act of the same donor. (B) Fold change: Difference in act compared to con. (C) Result of paired t-test of con from both treatments. Significant changes are tagged with "*" (p-value < 0.05), "**" (p-value < 0.01) and "***" (p-value < 0.005).

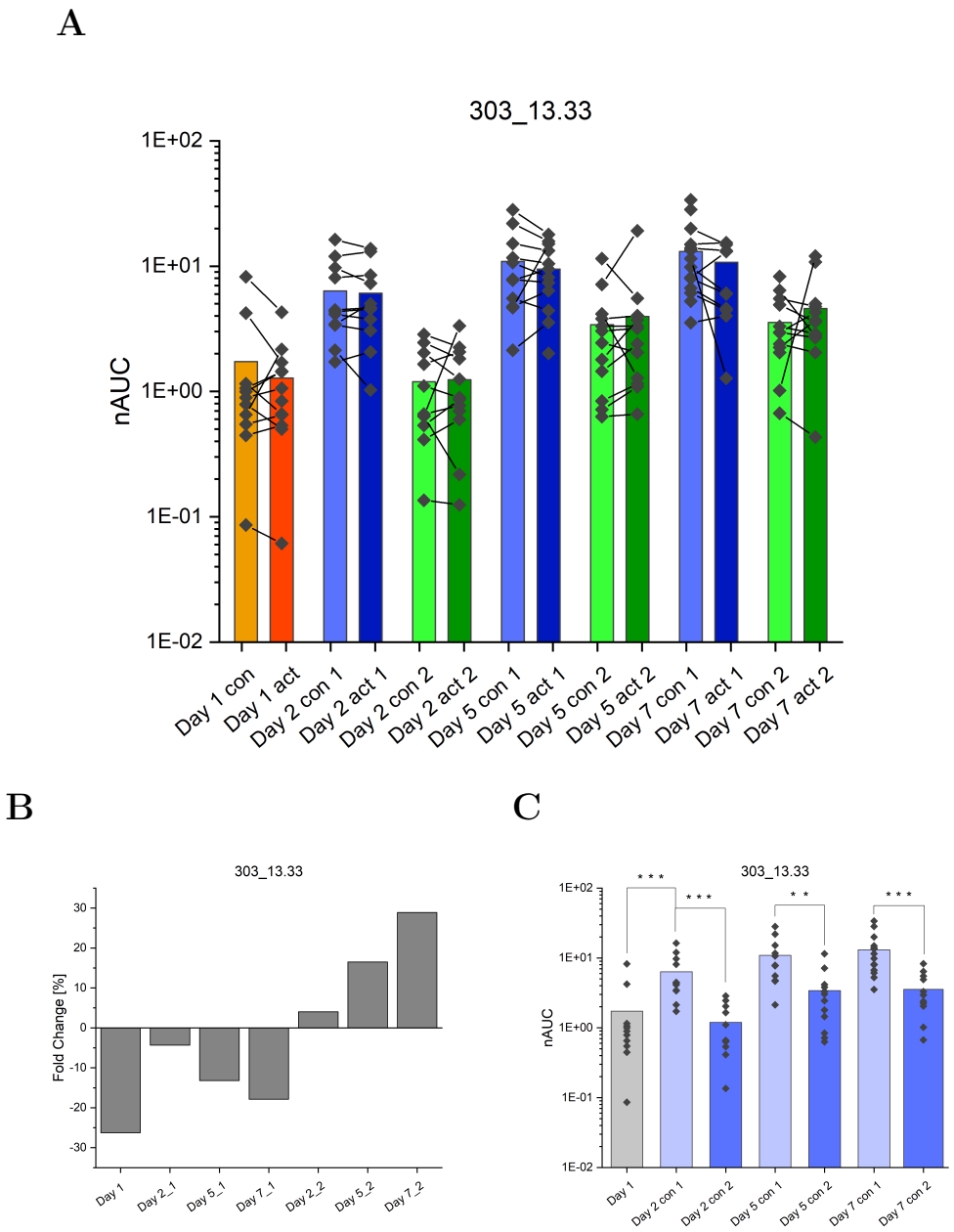

Figure 26: Result of 303_13.33. (A) Bars: Normalised mean peak area of all donors. Dots: Peak area of individual donors. Day 1: con (light orange), act (dark orange). Treatment 1 at day 2, 5 and 7: con (light blue), act (dark blue). Treatment 2 at day 2, 5 and 7: con (light green), act (dark green). Lines are connecting con and act of the same donor. (B) Fold change: Difference in act compared to con. (C) Result of paired t-test of con from both treatments. Significant changes are tagged with "*" (p-value < 0.05), "**" (p-value < 0.01) and "***" (p-value < 0.005).

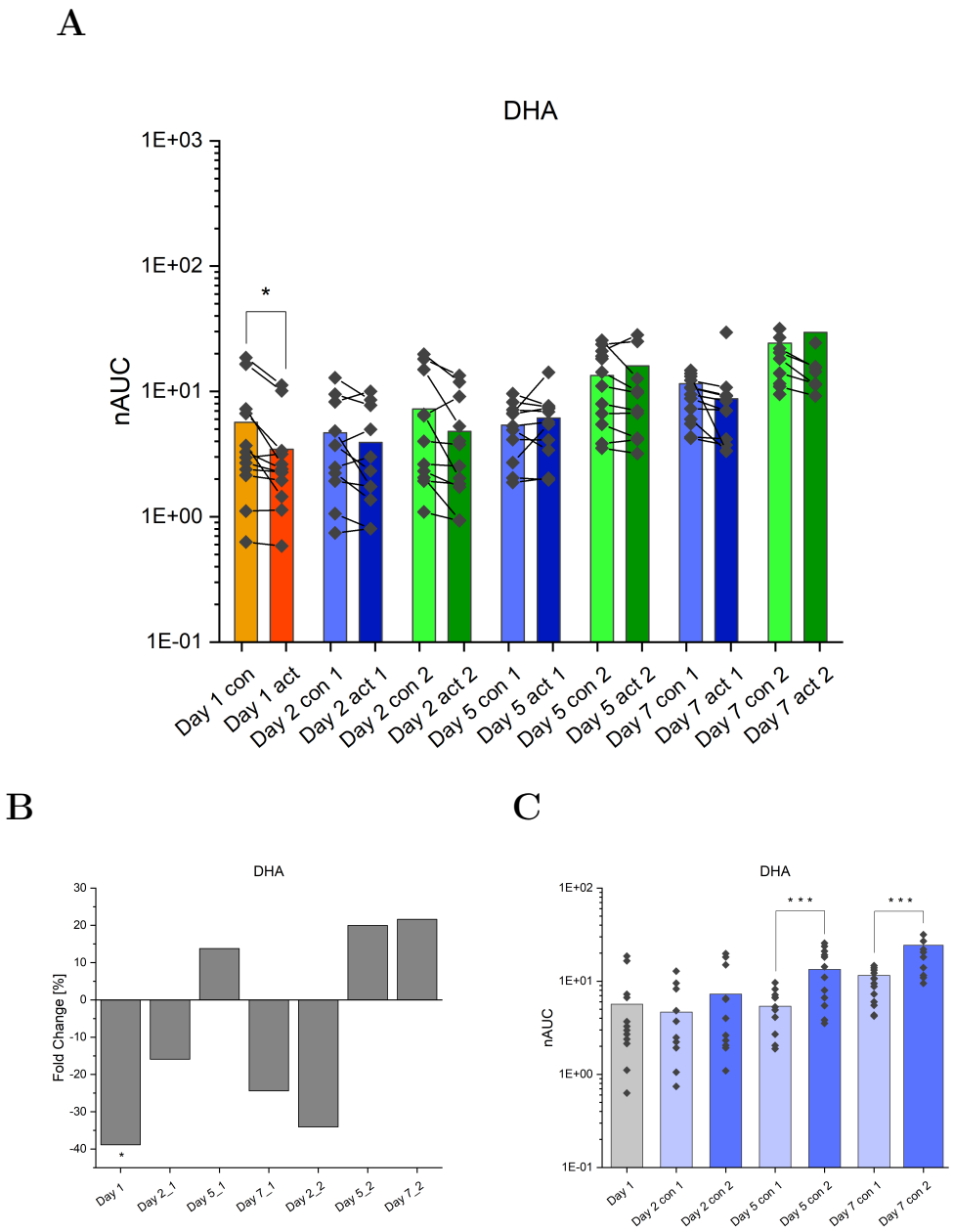

Figure 27: Result of DHA. (A) Bars: Normalised mean peak area of all donors. Dots: Peak area of individual donors. Day 1: con (light orange), act (dark orange). Treatment 1 at day 2, 5 and 7: con (light blue), act (dark blue). Treatment 2 at day 2, 5 and 7: con (light green), act (dark green). Lines are connecting con and act of the same donor. (B) Fold change: Difference in act compared to con. (C) Result of paired t-test of con from both treatments. Significant changes are tagged with "*" (p-value < 0.05), "**" (p-value < 0.01) and "***" (p-value < 0.005).

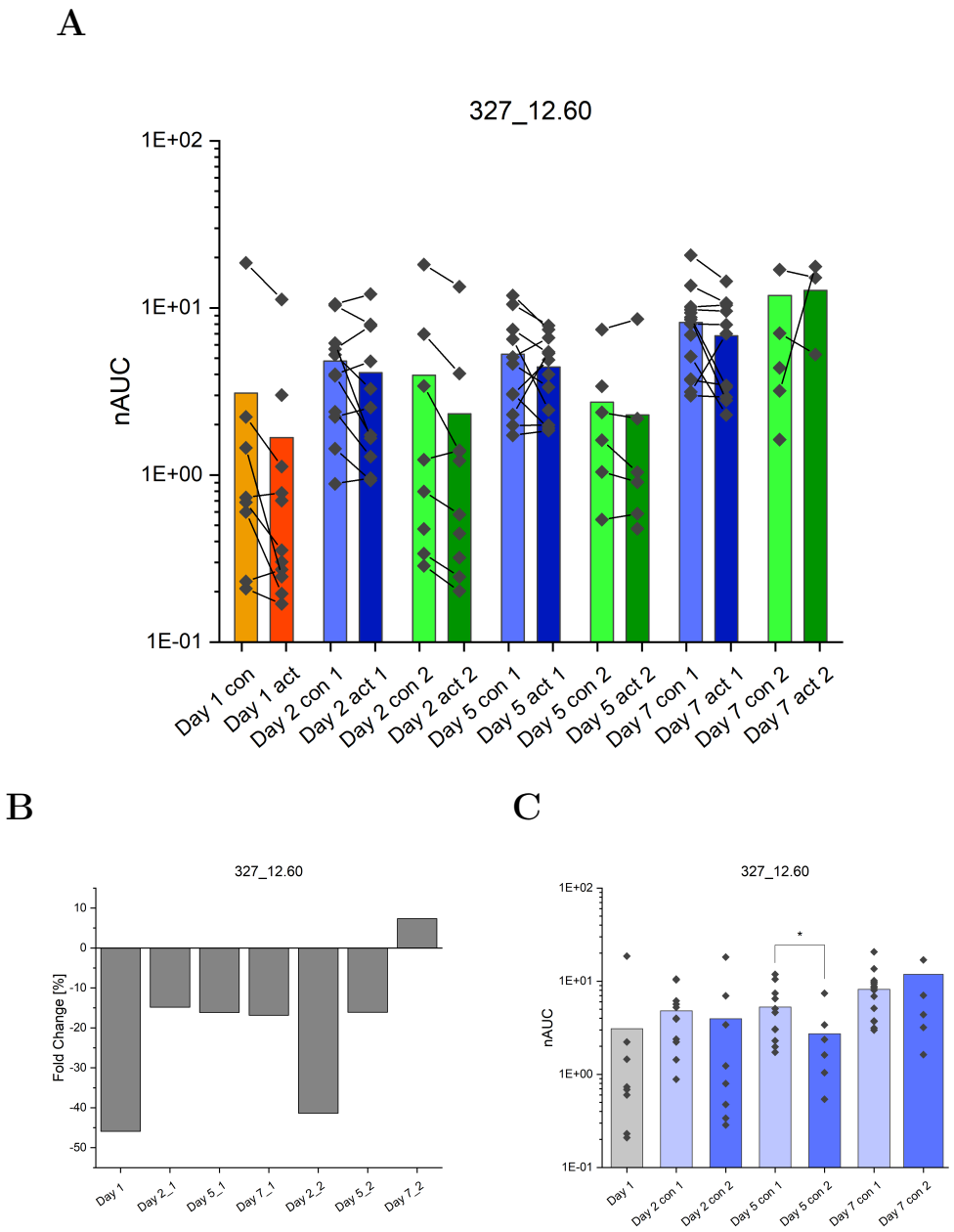

Figure 28: Result of 327_12.60. (A) Bars: Normalised mean peak area of all donors. Dots: Peak area of individual donors. Day 1: con (light orange), act (dark orange). Treatment 1 at day 2, 5 and 7: con (light blue), act (dark blue). Treatment 2 at day 2, 5 and 7: con (light green), act (dark green). Lines are connecting con and act of the same donor. (B) Fold change: Difference in act compared to con. (C) Result of paired t-test of con from both treatments. Significant changes are tagged with "*" (p-value < 0.05), "**" (p-value < 0.01) and "***" (p-value < 0.005).

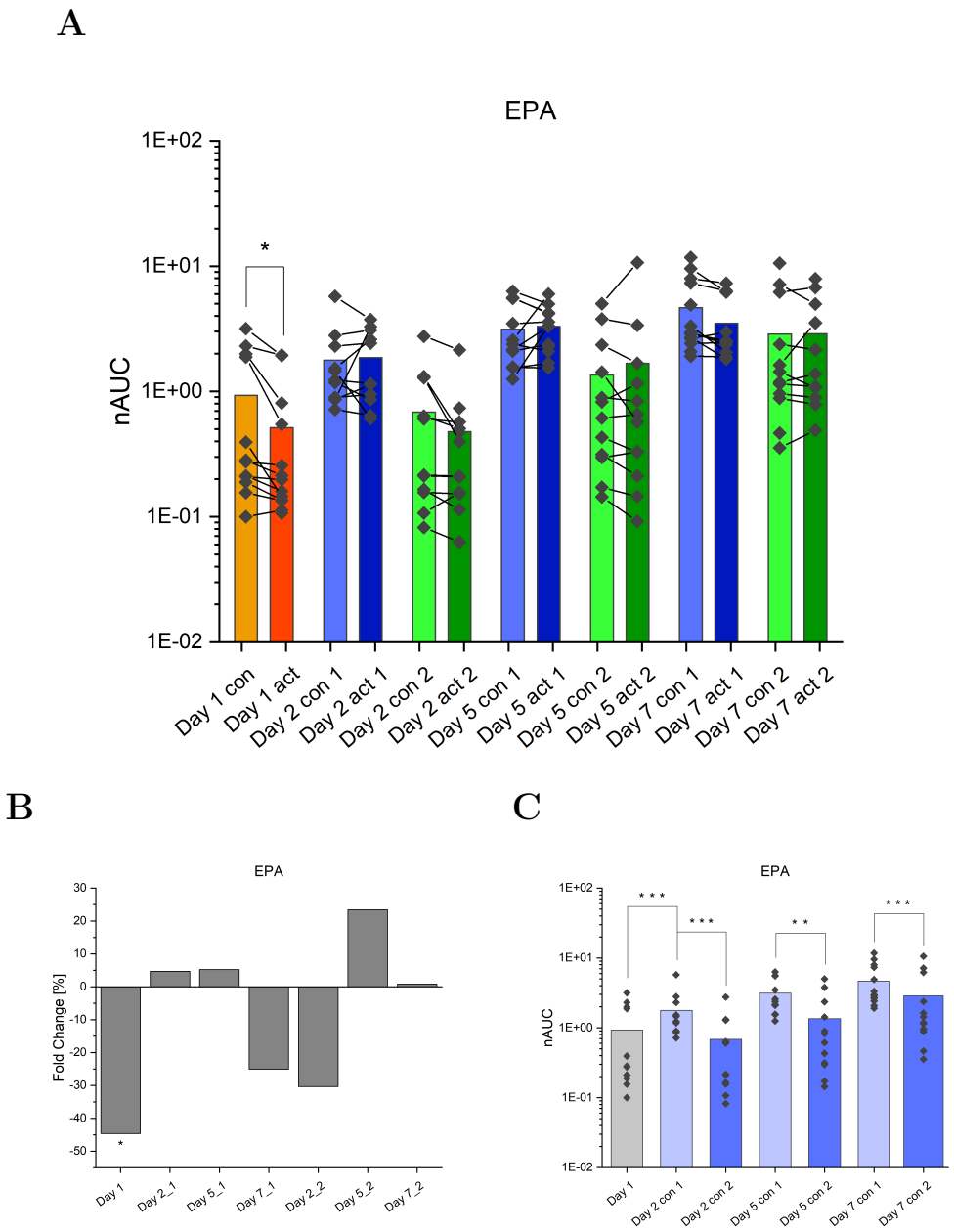

Figure 29: Result of EPA. (A) Bars: Normalised mean peak area of all donors. Dots: Peak area of individual donors. Day 1: con (light orange), act (dark orange). Treatment 1 at day 2, 5 and 7: con (light blue), act (dark blue). Treatment 2 at day 2, 5 and 7: con (light green), act (dark green). Lines are connecting con and act of the same donor. (B) Fold change: Difference in act compared to con. (C) Result of paired t-test of con from both treatments. Significant changes are tagged with "*" (p-value < 0.05), "**" (p-value < 0.01) and "***" (p-value < 0.005).

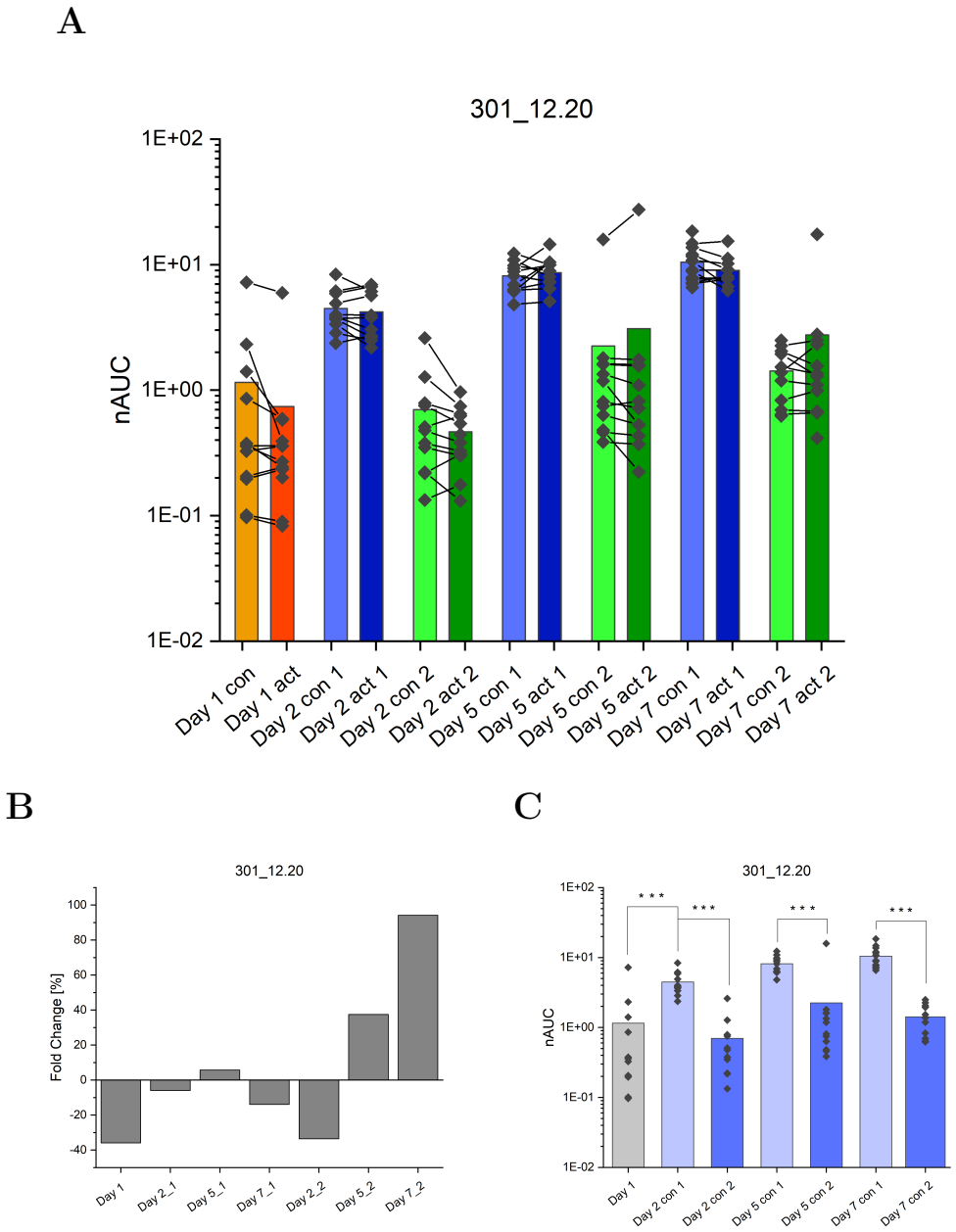

Figure 30: Result of 301_12.20. (A) Bars: Normalised mean peak area of all donors. Dots: Peak area of individual donors. Day 1: con (light orange), act (dark orange). Treatment 1 at day 2, 5 and 7: con (light blue), act (dark blue). Treatment 2 at day 2, 5 and 7: con (light green), act (dark green). Lines are connecting con and act of the same donor. (B) Fold change: Difference in act compared to con. (C) Result of paired t-test of con from both treatments. Significant changes are tagged with "*" (p-value < 0.05), "**" (p-value < 0.01) and "***" (p-value < 0.005).

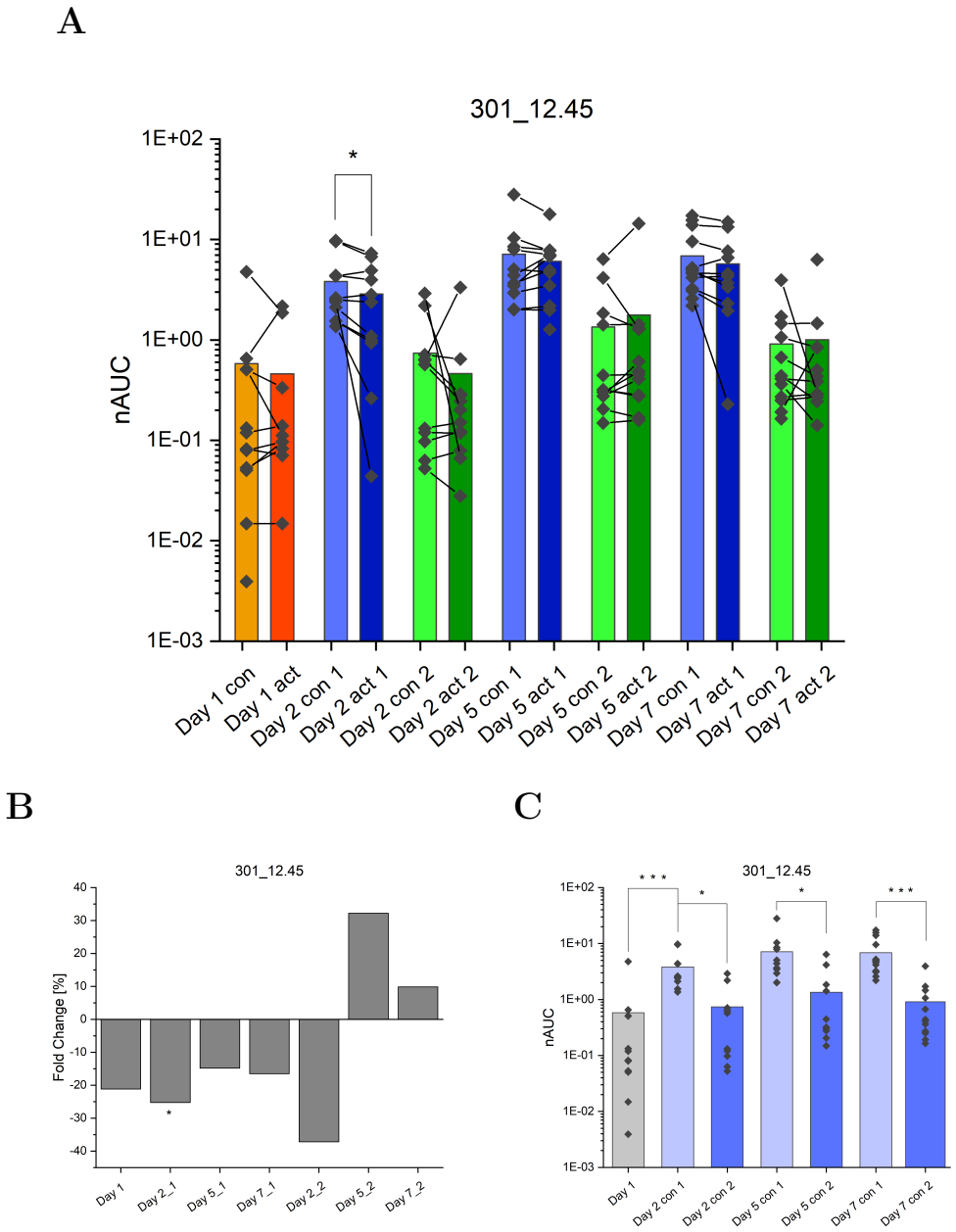

Figure 31: Result of 301_12.45. (A) Bars: Normalised mean peak area of all donors. Dots: Peak area of individual donors. Day 1: con (light orange), act (dark orange). Treatment 1 at day 2, 5 and 7: con (light blue), act (dark blue). Treatment 2 at day 2, 5 and 7: con (light green), act (dark green). Lines are connecting con and act of the same donor. (B) Fold change: Difference in act compared to con. (C) Result of paired t-test of con from both treatments. Significant changes are tagged with "*" (p-value < 0.05), "**" (p-value < 0.01) and "***" (p-value < 0.005).

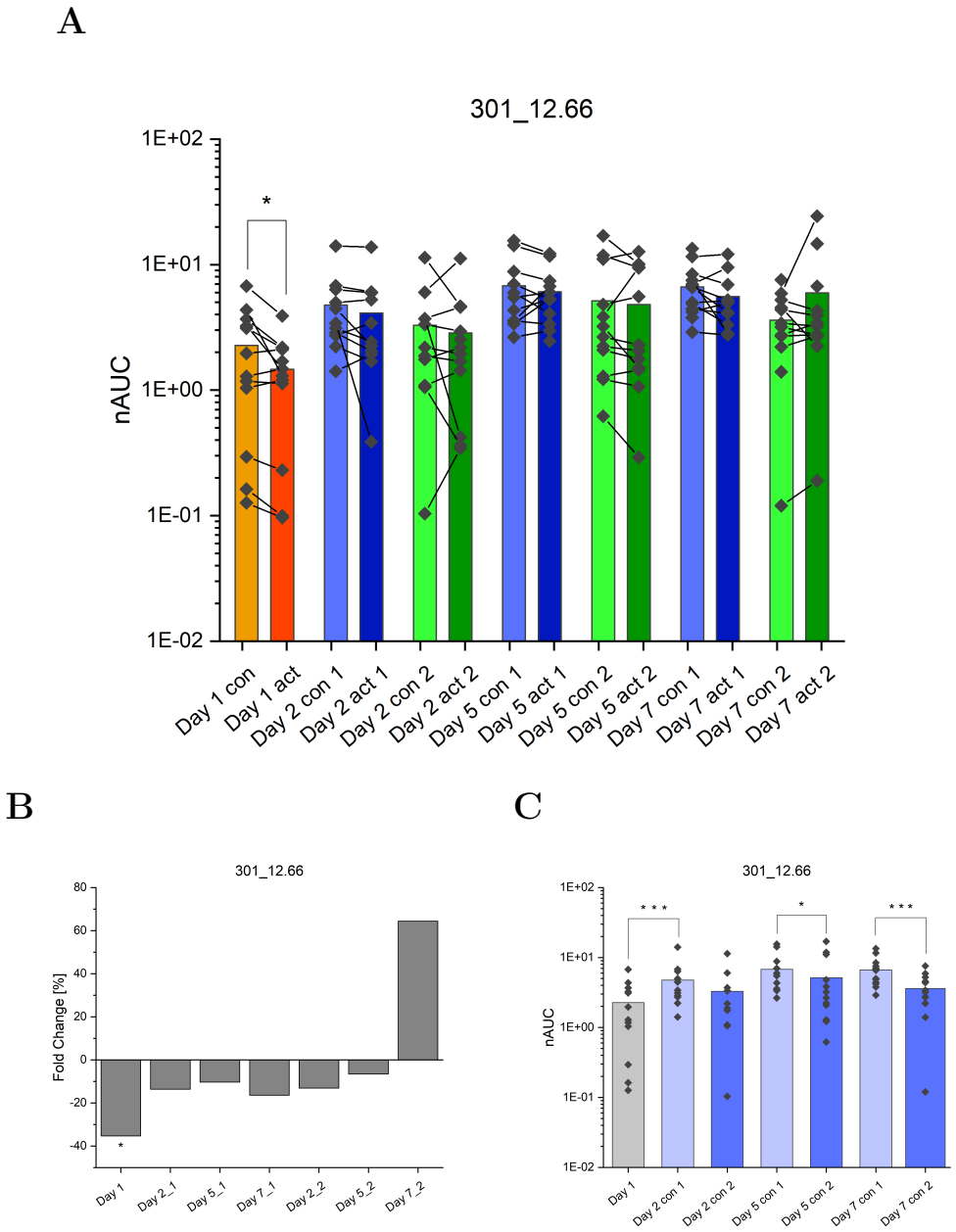

Figure 32: Result of 301_12.66. (A) Bars: Normalised mean peak area of all donors. Dots: Peak area of individual donors. Day 1: con (light orange), act (dark orange). Treatment 1 at day 2, 5 and 7: con (light blue), act (dark blue). Treatment 2 at day 2, 5 and 7: con (light green), act (dark green). Lines are connecting con and act of the same donor. (B) Fold change: Difference in act compared to con. (C) Result of paired t-test of con from both treatments. Significant changes are tagged with "*" (p-value < 0.05), "**" (p-value < 0.01) and "***" (p-value < 0.005).

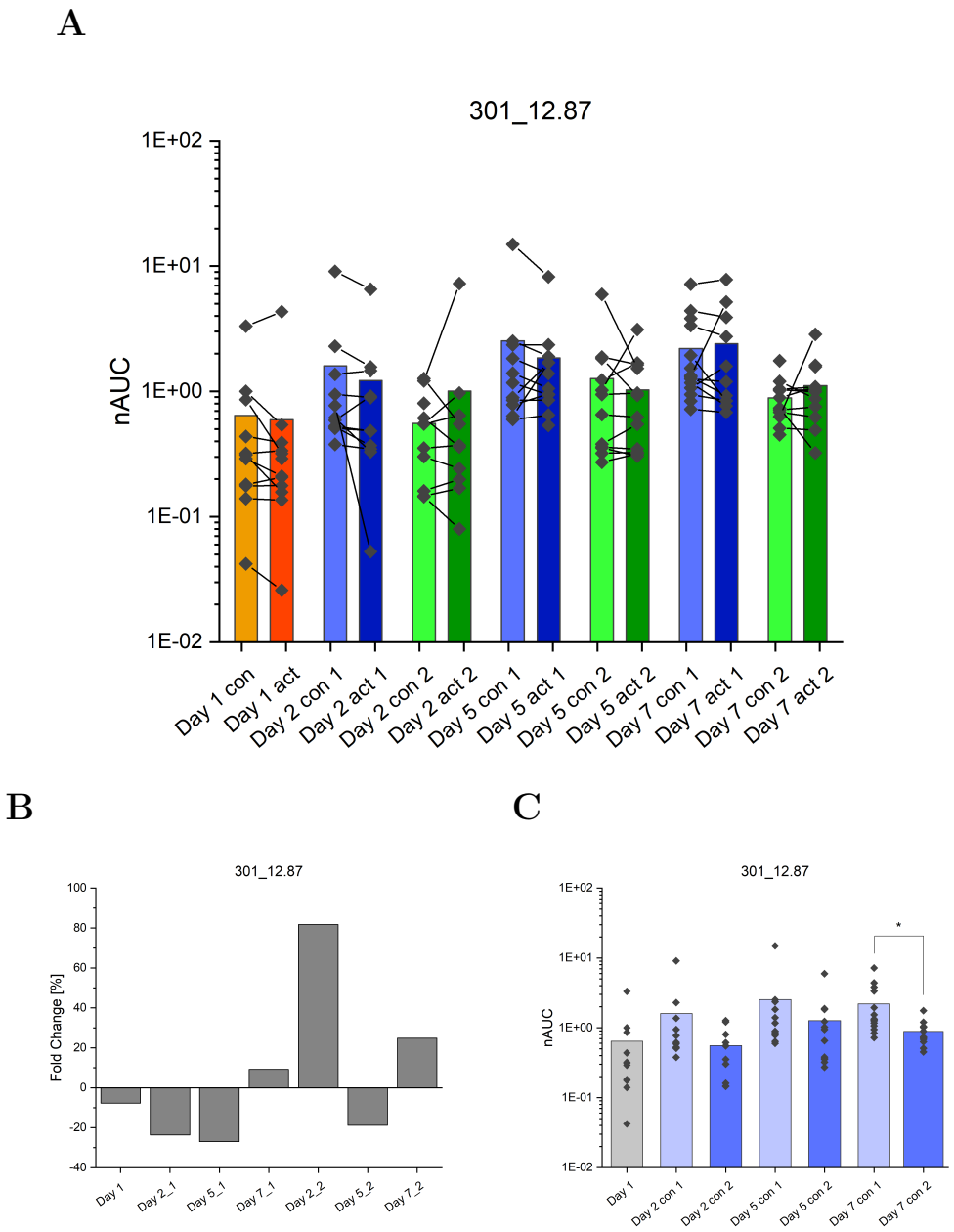

Figure 33: Result of 301_12.87. (A) Bars: Normalised mean peak area of all donors. Dots: Peak area of individual donors. Day 1: con (light orange), act (dark orange). Treatment 1 at day 2, 5 and 7: con (light blue), act (dark blue). Treatment 2 at day 2, 5 and 7: con (light green), act (dark green). Lines are connecting con and act of the same donor. (B) Fold change: Difference in act compared to con. (C) Result of paired t-test of con from both treatments. Significant changes are tagged with "*" (p-value < 0.05), "**" (p-value < 0.01) and "***" (p-value < 0.005).

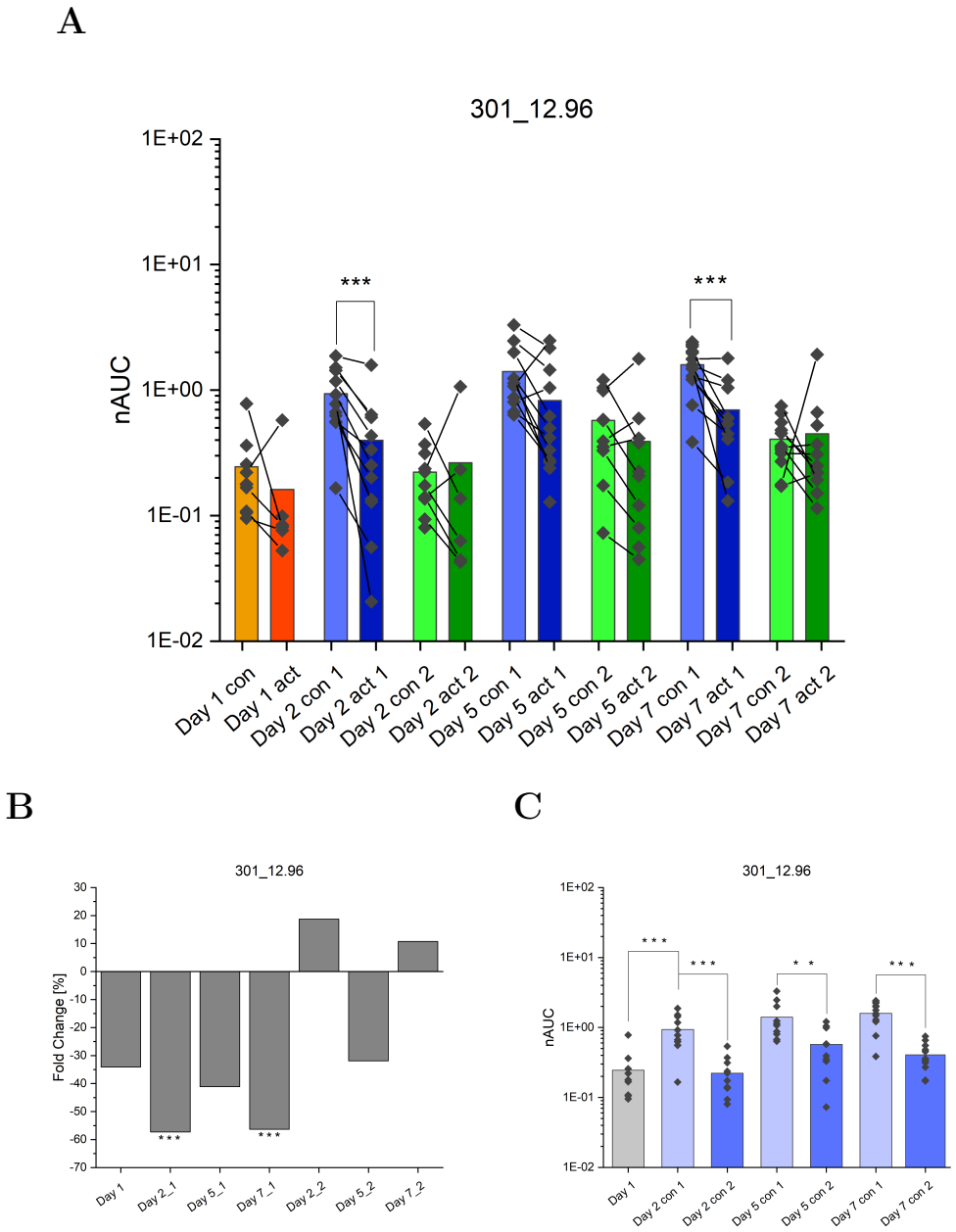

Figure 34: Result of 301_12.96. (A) Bars: Normalised mean peak area of all donors. Dots: Peak area of individual donors. Day 1: con (light orange), act (dark orange). Treatment 1 at day 2, 5 and 7: con (light blue), act (dark blue). Treatment 2 at day 2, 5 and 7: con (light green), act (dark green). Lines are connecting con and act of the same donor. (B) Fold change: Difference in act compared to con. (C) Result of paired t-test of con from both treatments. Significant changes are tagged with "*" (p-value < 0.05), "**" (p-value < 0.01) and "***" (p-value < 0.005).

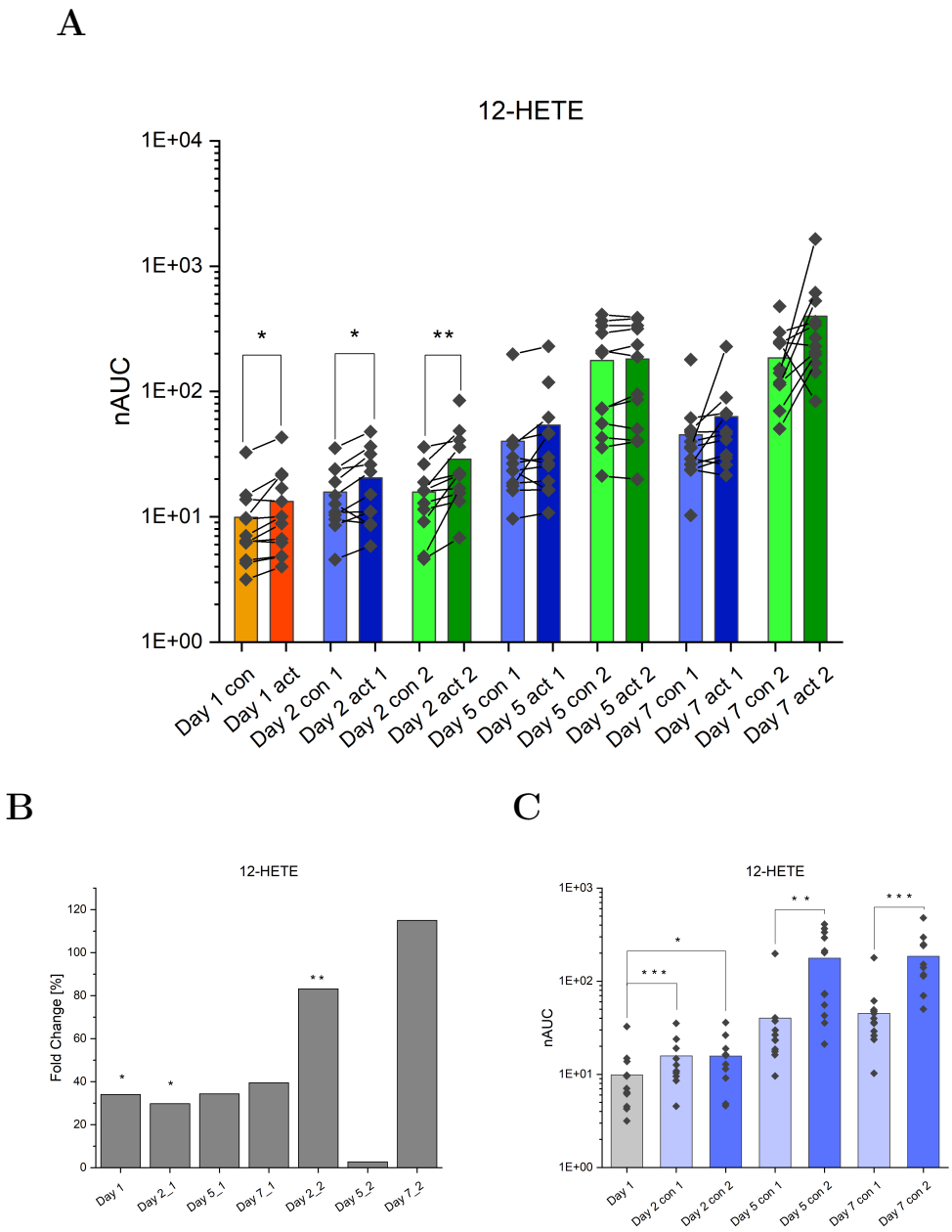

Figure 35: Result of 12-HETE. (A) Bars: Normalised mean peak area of all donors. Dots: Peak area of individual donors. Day 1: con (light orange), act (dark orange). Treatment 1 at day 2, 5 and 7: con (light blue), act (dark blue). Treatment 2 at day 2, 5 and 7: con (light green), act (dark green). Lines are connecting con and act of the same donor. (B) Fold change: Difference in act compared to con. (C) Result of paired t-test of con from both treatments. Significant changes are tagged with "*" (p-value < 0.05), "**" (p-value < 0.01) and "***" (p-value < 0.005).

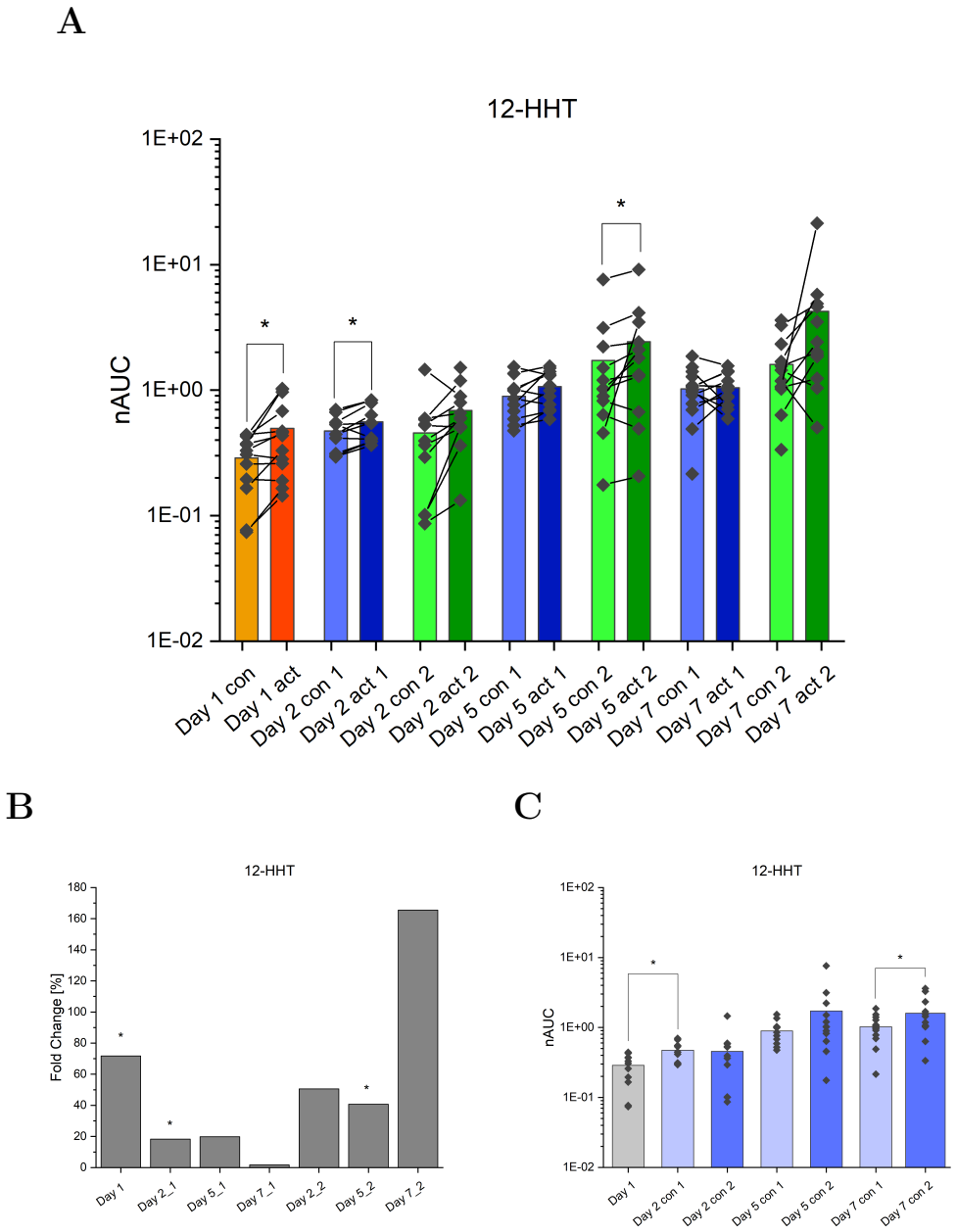

Figure 36: Result of 12-HHT. (A) Bars: Normalised mean peak area of all donors. Dots: Peak area of individual donors. Day 1: con (light orange), act (dark orange). Treatment 1 at day 2, 5 and 7: con (light blue), act (dark blue). Treatment 2 at day 2, 5 and 7: con (light green), act (dark green). Lines are connecting con and act of the same donor. (B) Fold change: Difference in act compared to con. (C) Result of paired t-test of con from both treatments. Significant changes are tagged with "*" (p-value < 0.05), "**" (p-value < 0.01) and "***" (p-value < 0.005).

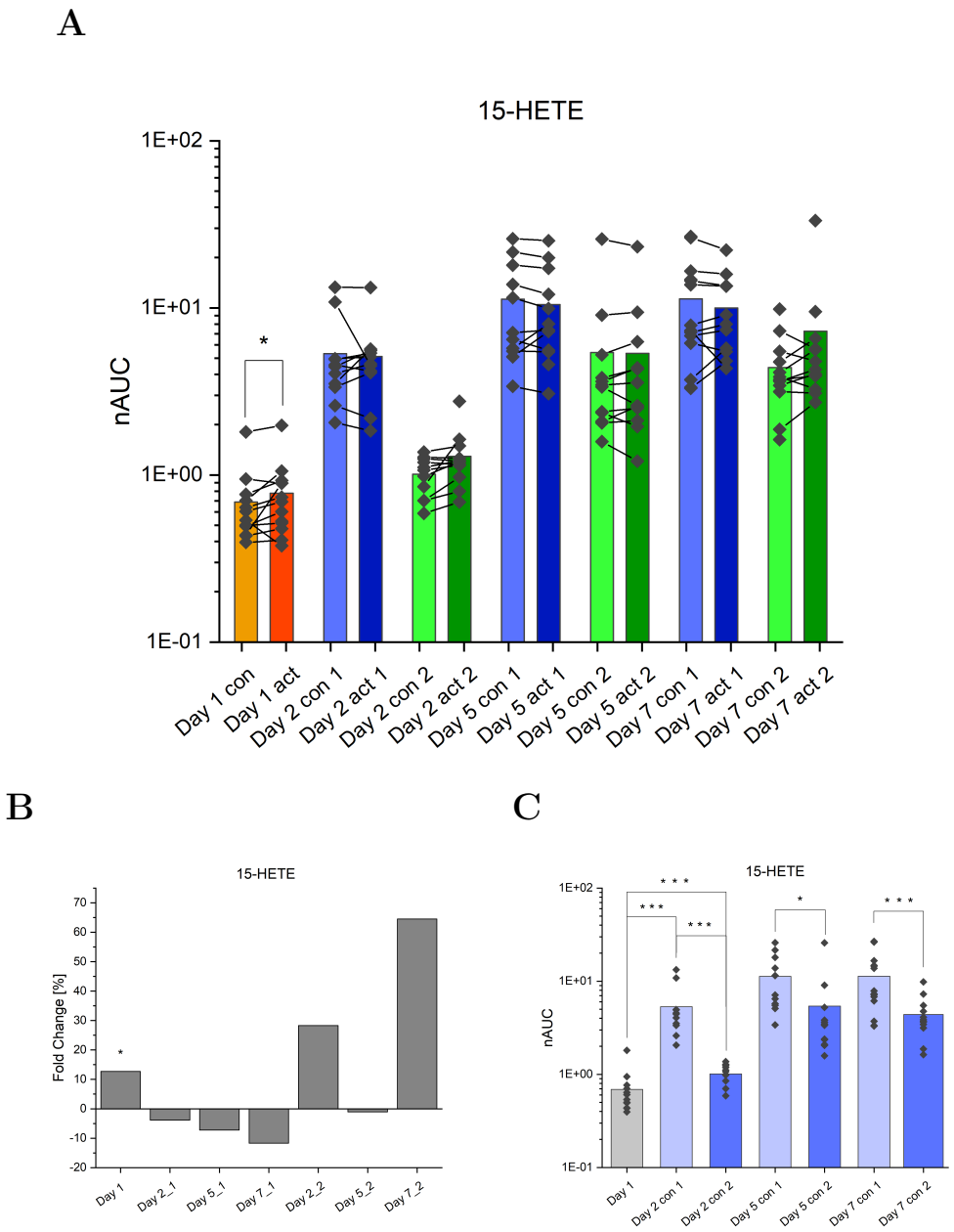

Figure 37: Result of 15-HETE. (A) Bars: Normalised mean peak area of all donors. Dots: Peak area of individual donors. Day 1: con (light orange), act (dark orange). Treatment 1 at day 2, 5 and 7: con (light blue), act (dark blue). Treatment 2 at day 2, 5 and 7: con (light green), act (dark green). Lines are connecting con and act of the same donor. (B) Fold change: Difference in act compared to con. (C) Result of paired t-test of con from both treatments. Significant changes are tagged with "*" (p-value < 0.05), "**" (p-value < 0.01) and "***" (p-value < 0.005).

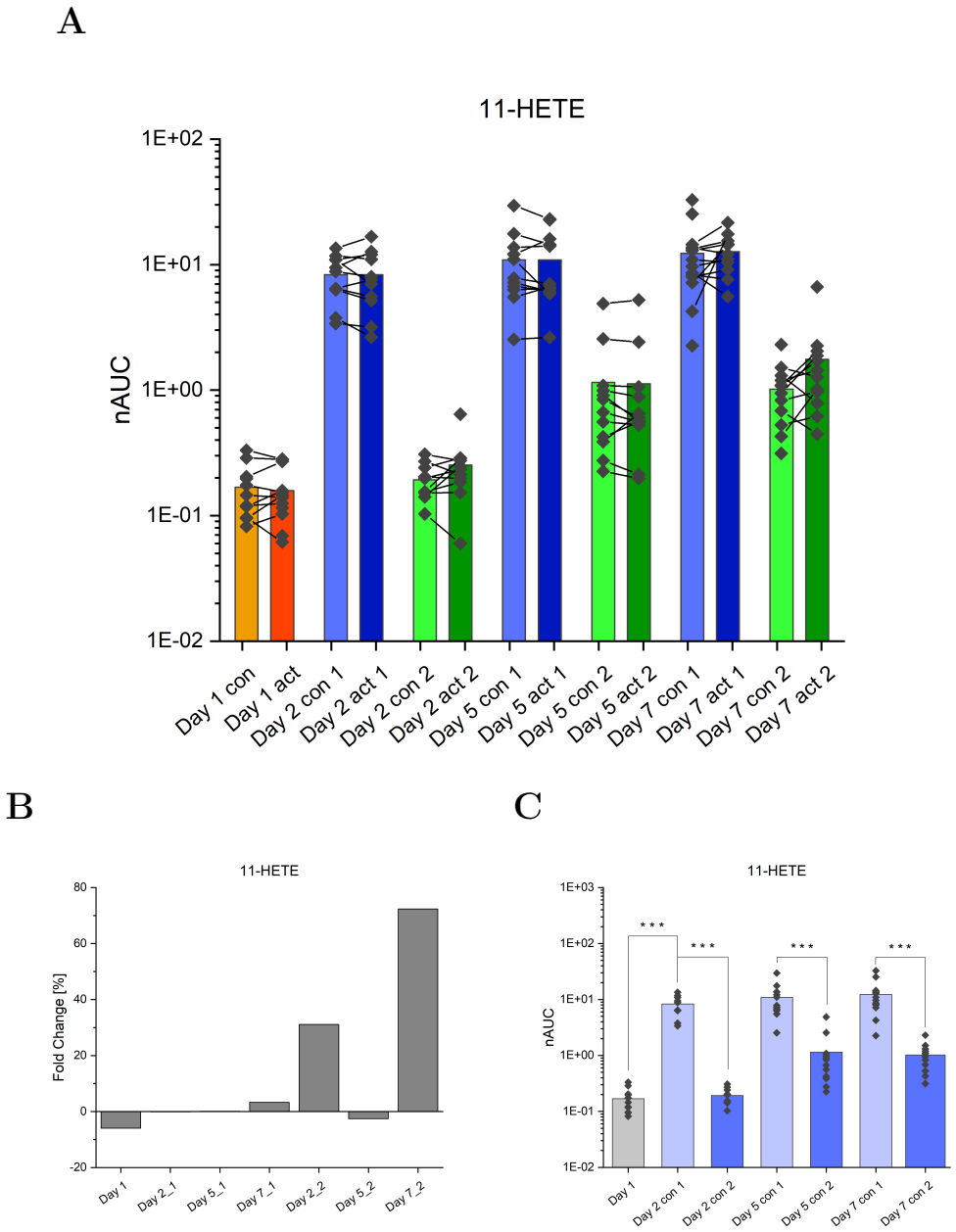

Figure 38: Result of 11-HETE. (A) Bars: Normalised mean peak area of all donors. Dots: Peak area of individual donors. Day 1: con (light orange), act (dark orange). Treatment 1 at day 2, 5 and 7: con (light blue), act (dark blue). Treatment 2 at day 2, 5 and 7: con (light green), act (dark green). Lines are connecting con and act of the same donor. (B) Fold change: Difference in act compared to con. (C) Result of paired t-test of con from both treatments. Significant changes are tagged with "*" (p-value < 0.05), "**" (p-value < 0.01) and "***" (p-value < 0.005).

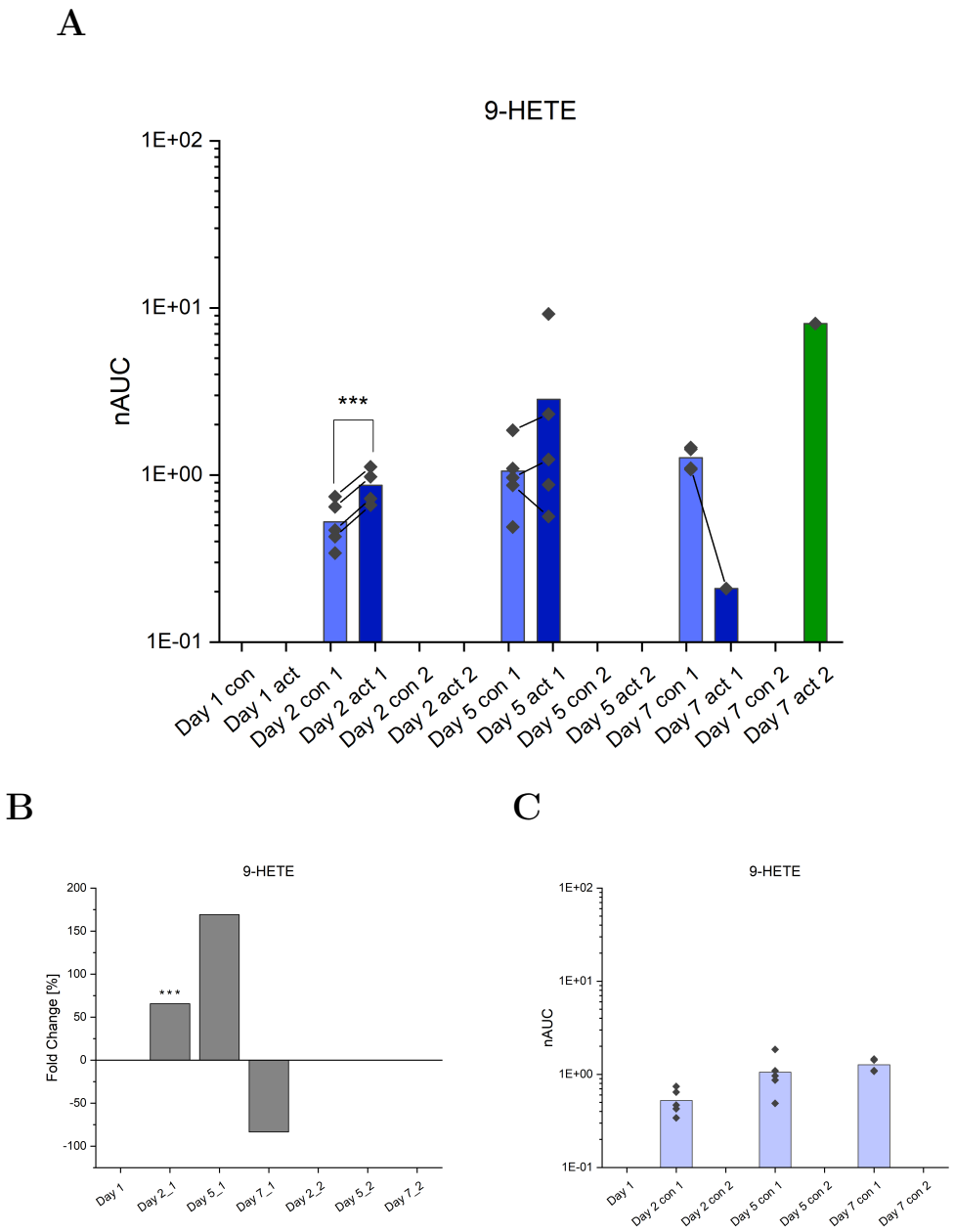

Figure 39: Result of 9-HETE. (A) Bars: Normalised mean peak area of all donors. Dots: Peak area of individual donors. Day 1: con (light orange), act (dark orange). Treatment 1 at day 2, 5 and 7: con (light blue), act (dark blue). Treatment 2 at day 2, 5 and 7: con (light green), act (dark green). Lines are connecting con and act of the same donor. (B) Fold change: Difference in act compared to con. (C) Result of paired t-test of con from both treatments. Significant changes are tagged with "*" (p-value < 0.05), "**" (p-value < 0.01) and "***" (p-value < 0.005).

5 Summary

Platelets are the smallest cells in mammalian blood and are mainly derived from megakaryocytes in the bone marrow and the lungs. These cells are circulating up to 10 days in the bloodstream, which is regulated by their own apoptotic program. They are sensing injured blood vessel endothelium and a clot formed via platelet aggregation is clogging the leakage. Platelet transfusion in thrombocytopenic patients is leading to a reduction of bleeding, but due to their short life time the therapeutic effect is prompt decreasing. The platelets are stored as concentrates in plastic bags with agitation allowing gas exchange at room temperature up to 5 days storage time, which is ensured via different pathogen inactivation techniques. Those treatments should protect the platelet concentrates from viral or bacterial contamination, which would lead to potential transfusion-related sepsis and other transfusion associated graft-versus-host diseases.

Eicosanoids are belonging to the lipid subclass of FAs and are mainly derived from enzymatic metabolism of AA, DHA and EPA via COX, LOX and CYP. This group of molecules is involved in various processes in the body like inflammation or cancer, but some of them are also regulating platelet aggregation. Since activated platelets are releasing over 300 bioactive molecules including eicosanoids, this work is comparing the eicosanoid releasates of platelets concentrates derived from blood samples of 14 donors. Each concentrate was split into two samples, of which one was treated via amotosalen/UVA (treatment 1) and one via cesium-137 (treatment 2).

As reference levels the untreated samples were collected at day 1, directly before treatment. After receiving the treatment, the concentrates were stored up to day 7 with sample collection at day 2, 5 and 7. After retrieving the samples from the general hospital, the platelet concentrates were split into an inactivated control group and an activated group, which was activated via ionomycin and $CaCl_2$. Eicosanoids were obtained via SPE with reversed phase cartridges and analysis was performed via LC-MS. Herein, analyte separation was executed through an UPLC system, which was coupled to a Q Exactive™ HF Hybrid Quadrupole-Orbitrap™ Mass Spectrometer with an ESI source. Samples were measured in negative ion mode to identify the eicosanoids due to their carboxylic functional groups. Fragmentation was obtained in a HCD cell with 24 eV collision energy.

Data analysis was performed via the TraceFinder™ 4.1 Software packages from Thermo Scientific™ by developing a compound database containing the exact mass of the analytes. Herein, the internal standards were used as reference. Via a paired t-test significant changes could be identified between the control and activated state of each molecule at the corresponding days

and by calculating the fold change in percent. To detect significant changes between the initial states from both treatments, the control states of treatment 1 was compared with treatment 2 via a paired t-test as well. In both paired t-tests p-values below 0.05 were distinguished as significant changes.

The comparison of both pathogen inactivation techniques, the INTERCEPT Blood System^{TM} utilizing amotosalen/UVA and the second treatment using radioactive ^{137}Cs, is demonstrating significant differences between them. The most significant difference between both techniques may be the resulting AA isobar 303_12.72, which could not be detected in untreated samples, nor after treatment 2. Only after treatment 1 this unidentified isobar was detectable. The other AA isobars were indicating higher levels in treatment 1, which was also observed within EPA and its isobars, while DHA and its isobar were showing similar levels or higher levels in treatment 2.

Since 12-HETE is one of the most secreted molecules by activated platelets, their activation via ionomycin was leading to significantly increased levels in the activated groups at the first two days with similar levels at day 2 for both treatments. During ongoing storage within the platelets treated with cesium-137 significantly higher amounts of 12-HETE were detected. A similar pattern was found for 12-HHT with similar control levels at day 2 and higher levels at day 5 and 7 for treatment 2. For 15-HETE and 11-HETE the UVA-based treatment was leading to much higher levels with significantly higher control levels at almost all days. 9-HETE was detected in several donors on all days receiving the INTERCEPT Blood System^{TM} and only in one activated sample at day 7 treated with cesium-137. Therefore, treatment 1 seems to induce free-radical stress to the platelets.

The comparison of the untreated samples at day 1 and of the samples at day 2, after receiving the two different treatments at day 1 and one day of storage time, was indicating significantly increased levels for the AA isobars, 303_12.83 and 303_13.33, for EPA and the EPA isobars, 301_12.20, 301_12.45, 301_12.66 and 301_12.96, for 11-, 12- and 15-HETE and for 12-HHT in the amotosalen/UVA-based treatment 1. Since 11-, 12- and 15-HETE and 12-HHT are enzymatically formed eicosanoids, the UVA-based treatment seems to have an impact on the enzyme activity.

In conclusion, it can be stated, that there are significant differences between the two pathogen inactivation techniques and that the INTERCEPT Blood System^{TM} has an effect on lipids, as mentioned in section 2.1.4 amotosalen should not interact with lipids and proteins, but it seems not to be valid to UVA [58]. But also the formation of the eicosanoid precursor molecules or even the chemical structure of these isobaric forms has to be studied.

Abstract

Platelets are participating in many processes within the body, but their most important role is being involved in wound healing due to their ability of aggregation and therefore clogging injured blood vessels with the formed clot. Storing platelets as concentrates for transfusion to patients is important and thus pathogen inactivation techniques are required to ensure the safety of the patients.

Due to the fact, that eicosanoids are regulating platelet aggregation, this work has focused on the effects of the two most common pathogen inactivation techniques, the INTERCEPT Blood System^{TM} utilizing amotosalen/UVA and the second treatment using radioactive ^{137}Cs, on platelet activation by detecting some of the most released eicosanoids by platelets and their precursors like AA.

Samples were collected from 14 donors at day 1, 2, 5 and 7. After collecting an untreated sample, the concentrates received the treatments at day 1 and were stored up to day 7. The platelet concentrates were split into two groups, one group is representing the controlled state, while the second group is representing the activated one. In vitro activation was induced by $CaCl_2$ and ionomycin, proteins were precipitated over night in EtOH (1:5) at -20°C. Eicosanoids were enriched during a reversed-phase SPE, separation and analysis were executed via an UPLC system coupled to a Q Exactive^{TM} HF Hybrid Quadrupole-Orbitrap^{TM} Mass Spectrometer with an ESI source working in negative ionisation mode. Data analysis was performed with the TraceFinder^{TM} 4.1 Software packages from Thermo Scientific^{TM} by developing a compound database. The integrated peaks have been checked manually and the areas were normalised to the mean area of the internal standard molecules. A paired t-test was executed to show significant changes between the control and activated groups, which was also indicated in percent by the calculated fold change, and another paired t-test was performed to compare the control groups of both treatments.

The evaluation of eicosanoid releasates in platelet concentrates consequent to the two different pathogen inactivation techniques resulted in the observation of several eicosanoid precursor isobars, of which one was only detected in the INTERCEPT Blood System^{TM}. But also within some other eicosanoids significant differences could already be detected at day 2 after receiving the treatment. Changes during ongoing storage time have been identified as well. Comparing the samples at day 1 and day 2, significant changes in the control state of all enzymatically formed eicosanoids, which have been investigated, were found in treatment 1 and additionally the control group levels of two isobars of AA, of EPA and of four EPA isobars were significantly

enhanced in treatment 1. The formation of the non-enzymatically generated 9-HETE after receiving the amotosalen/UVA-based treatment 1 through all days seems to be caused by free-radical, oxidative stress within the platelets.

Zusammenfassung

Plättchen sind an einer Vielzahl von Prozessen im menschlichen Körper involviert, aber ihre wichtigste Rolle ist die Beteiligung an der Wundheilung durch ihre Fähigkeit zu aggregieren und somit verletzte Blutgefäße mit dem gebildeten Pfropfen zu verschließen. Die Lagerung von Plättchen in Form von Konzentraten um sie Patienten mittels einer Transfusion zu verabreichen ist von großer Bedeutung, wodurch Pathogeninaktivierungsverfahren unerlässlich sind um die Sicherheit für den Patienten gewährleisten zu können.

Da Eicosanoide einen regulatorischen Effekt auf die Plättchenkoagulation aufweisen, stützt sich diese Arbeit auf den Einfluss auf die Aktivierung von Plättchen durch die zwei am häufigsten verwendeten Pathogeninaktivierungstechniken, dem INTERCEPT Blood System^{TM}, welches Amotosalen in Verbindung mit UVA einsetzt, und einer weiteren Methode, welche die Inaktivierung von Pathogenen mittels radioaktivem ^{137}Cs erreicht. Hierbei sollen einige von Plättchen am häufigsten freigesetzten Eicosanoide samt ihrer Ausgangsmoleküle wie die Arachidonsäure untersucht werden.

Die Proben wurden von 14 Donoren an Tag 1, 2, 5 und 7 gesammelt. Nach dem Sammeln einer unbehandelten Probe an Tag 1 erfolgte die Pathogeninaktivierung und die Konzentrate wurden bis Tag 7 gelagert. Die Plättchenkonzentrate wurden in zwei Gruppen aufgeteilt, wobei ein Teil in vitro aktiviert wurde, während der andere Teil ohne Aktivierung als Kontrollgruppe fungierte. Eine Aktivierung der Plättchen wurde durch Zugabe von $CaCl_2$ und Ionomycin herbeigeführt und die Proteine wurden über Nacht mit kaltem EtOH (1:5) bei -20°C präzipitiert. Eicosanoide wurden durch eine Umkehrphasen-Festphasenextraktion angereichert, die chromatographische Trennung und die Analyse erfolgten mittels einem UPLC System gekoppelt an ein Q Exactive^{TM} HF Hybrid Quadrupol-Orbitrap^{TM} Massenspektrometer mit einer Elektrosprayionisation, welche in negativem Ionenmodus arbeitete. Die Datenanalyse wurde mit der TraceFinder^{TM} 4.1 Software von Thermo Scientific^{TM} durchgeführt, indem zu Beginn eine Komponenten-Datenbank aufgestellt wurde. Die integrierten Peaks wurden manuell überprüft und die daraus resultierende Peakfläche wurde auf den Mittelwert der Fläche aller internen Standards normiert. Ein gepaarter t-Test wurde durchgeführt um signifikante Unterschiede zwischen Kontrollgruppe und aktivierter Gruppe anzuzeigen. Dies wurde durch eine Berechnung der relativen Veränderung der Expressionswerte (fold change) zwischen der Kontrollgruppe und der dazugehörigen aktivierten Gruppe zusätzlich in Prozent dargestellt werden. Signifikante Unterschiede zwischen den Werten der Kontrollgruppe beider Behandlungsmethoden konnten durch einen weiteren gepaarten t-

Test ermittelt werden.

Die Evaluierung der Eicosanoid-Freisetzung in Plättchenkonzentraten infolge zweier verschiedener Pathogeninaktivierungstechniken führte zu der Identifikation von mehreren isobaren Formen der Eicosanoid-Verläufermoleküle, von denen eine isobare Form der Arachidonsäure weder in den unbehandelten Proben von Tag 1, noch in den Proben von Behandlung 2, sondern ausschließlich in den mittels INTERCEPT Blood System^{TM} behandelten Proben detektiert werden konnte. Zudem konnten an Tag 2 bei den anderen untersuchten Eicosanoiden ebenfalls signifikante Unterschiede nach der erfolgten Behandlung beobachtet werden. Zusätzlich konnten Veränderungen mit fortschreitender Lagerungsdauer nachgewiesen werden. In einem Vergleich der Proben von Tag 1 und Tag 2 konnten signifikante Veränderungen in den Kontrollgruppen von allen untersuchten, enzymatisch geformten Eicosanoiden in Behandlung 1 festgestellt werden. Zudem waren die Level der Kontrollgruppe von zwei AA-Isobaren, EPA und vier EPA-Isobaren ebenfalls in Behandlung 1 signifikant erhöht. Nach Behandlung 1 mittels Amotosalen/UVA konnte an allen untersuchten Tagen das nicht-enzymatisch gebildete 9-HETE nachgewiesen werden. Dies scheint durch oxidativen Stress ausgelöst von freien Radikalen in den Blutplättchen hervorgerufen zu werden.

References

[1] J. Ringwald, R. Zimmermann, and R. Eckstein, Transfusion Medicine Reviews **20**, 158 (2006).

[2] J. W. Semple, J. E. Italiano, and J. Freedman, Nature Reviews Immunology **11**, 264 (2011).

[3] E. Lefrançais, G. Ortiz-Muñoz, A. Caudrillier, B. Mallavia, F. Liu, D. M. Sayah, E. E. Thornton, M. B. Headley, T. David, S. R. Coughlin, et al., Nature **544**, 105 (2017).

[4] H. H. Versteeg, J. W. M. Heemskerk, M. Levi, and P. H. Reitsma, Physiological Reviews **93**, 327 (2013).

[5] P. E. J. van der Meijden and J. W. M. Heemskerk, Nature Reviews Cardiology **16**, 166 (2018).

[6] S. S. SMYTH, R. P. MCEVER, A. S. WEYRICH, C. N. MORRELL, M. R. HOFFMAN, G. M. AREPALLY, P. A. FRENCH, H. L. DAUERMAN, and R. C. B. and, Journal of Thrombosis and Haemostasis **7**, 1759 (2009).

[7] A. D. Michelson, Journal of Thrombosis and Thrombolysis **16**, 7 (2003).

[8] G. J. Gasic, T. B. Gasic, and C. C. Stewart, Proceedings of the National Academy of Sciences **61**, 46 (1968).

[9] O. Elaskalani, M. Berndt, M. Falasca, and P. Metharom, Cancers **9**, 94 (2017).

[10] V. B. O'Donnell, R. C. Murphy, and S. P. Watson, Circulation Research **114**, 1185 (2014).

[11] L. Löfgren, M. Ståhlman, G.-B. Forsberg, S. Saarinen, R. Nilsson, and G. I. Hansson, Journal of Lipid Research **53**, 1690 (2012).

[12] B. Ogretmen and Y. A. Hannun, Nature Reviews Cancer **4**, 604 (2004).

[13] W. L. Smith, D. L. DeWitt, and R. M. Garavito, Annual Review of Biochemistry **69**, 145 (2000).

[14] H. Kühn and V. B. O'Donnell, Progress in Lipid Research **45**, 334 (2006).

[15] V. S. Hanna and E. A. A. Hafez, Journal of Advanced Research **11**, 23 (2018).

[16] E. A. Dennis and P. C. Norris, Nature Reviews Immunology **15**, 511 (2015).

[17] W. L. Smith, Biochemical Journal **259**, 315 (1989).

[18] N. Nathoo, Journal of Clinical Pathology **57**, 6 (2004).

[19] D. Wang and R. N. DuBois, Nature Reviews Cancer **10**, 181 (2010).

[20] D. Ribatti and E. Crivellato, Leukemia Research **31**, 1339 (2007).

[21] J. G. White, in *Platelets* (Elsevier, 2013), pp. 117–144.

[22] O. Sonmez and M. Sonmez, Porto Biomedical Journal **2**, 311 (2017).

[23] E. C. Josefsson, M. R. Dowling, M. Lebois, and B. T. Kile, in *Platelets* (Elsevier, 2013), pp. 51–65.

[24] M. Koupenova, L. Clancy, H. A. Corkrey, and J. E. Freedman, Circulation Research **122**, 337 (2018).

[25] A. J. Gale, Toxicologic Pathology **39**, 273 (2010).

[26] E. M. Bevers, P. Comfurius, and R. F. Zwaal, Biochimica et Biophysica Acta (BBA) - Biomembranes **736**, 57 (1983).

[27] L. M. Beaulieu and J. E. Freedman, in *Platelets* (Elsevier, 2013), pp. 313–342.

[28] A. V. de Abreu, M. T. Rondina, A. S. Weyrich, and G. A. Zimmerman, in *Platelets* (Elsevier, 2013), pp. 733–766.

[29] G. L. Klement, E. Shai, and D. Varon, in *Platelets* (Elsevier, 2013), pp. 487–502.

[30] H. Gerhardt, in *VEGF in Development* (Springer New York, ????), pp. 68–78.

[31] G. McDowell, I. Temple, C. Li, C. Kirwan, N. Bundred, C. McCollum, I. Burton, S. Kumar, and G. Byrne, Anticancer Res **25**, 3963 (2005).

[32] J. S. Palumbo, Blood **105**, 178 (2005).

[33] E. M. Golebiewska and A. W. Poole, Blood Reviews **29**, 153 (2015).

[34] P. Massini and U. Näf, Biochimica et Biophysica Acta (BBA) - Biomembranes **598**, 575 (1980).

[35] J. M. E. M. Cosemans, S. E. M. Schols, L. Stefanini, S. de Witt, M. A. H. Feijge, K. Hamulyak, H. Deckmyn, W. Bergmeier, and J. W. M. Heemskerk, Blood **117**, 651 (2010).

[36] W. W. Duke, JAMA **250**, 1201 (1983).

[37] C. H. W. Leeksma and J. A. Cohen, Journal of Clinical Investigation **35**, 964 (1956).

[38] J.-P. Cazenave, H. Isola, C. Waller, I. Mendel, D. Kientz, M. Laforêt, J.-P. Raidot, G. Kandel, M.-L. Wiesel, and L. Corash, Transfusion **51**, 622 (2010).

[39] E. M. Hersh, JAMA **193**, 105 (1965).

[40] A. H. MINOR and L. BURNETT, Blood **7**, 693 (1952).

[41] P. L. Perrotta, J. Parsons, H. M. Rinder, and E. L. Snyder, in *Platelets* (Elsevier, 2013), pp. 1275–1303.

[42] J. Kaiser-Guignard, G. Canellini, N. Lion, M. Abonnenc, J.-C. Osselaer, and J.-D. Tissot, Blood Reviews **28**, 235 (2014).

[43] M. S. Y. Ng, J.-P. Tung, and J. F. Fraser, Transfusion Medicine Reviews **32**, 144 (2018).

[44] N. Tynngård, Transfusion and Apheresis Science **41**, 97 (2009).

[45] H. Ohto and K. E. Nollet, Transfusion and Apheresis Science **44**, 321 (2011).

[46] S. Murphy and F. Gardner, Blood **46**, 209 (1975).

[47] S. Murphy, R. Kahn, S. Holme, G. Phillips, W. Sherwood, W. Davisson, and D. Buchholz, Blood **60**, 194 (1982).

[48] T. Simon, E. Nelson, R. Carmen, and S. Murphy, Transfusion **23**, 207 (1983).

[49] H. Gulliksson, A. Shanwell, A. Wikman, A. Reppucci, S. Sallander, and A. Udén, Vox Sanguinis **61**, 165 (1991).

[50] C. Edenbrandt and S. Murphy, Blood **76**, 1884 (1990).

[51] M. Lozano, F. Knutson, R. Tardivel, J. Cid, R. M. Maymó, H. Löf, H. Roddie, J. Pelly, A. Docherty, C. Sherman, et al., British Journal of Haematology **153**, 393 (2011).

[52] S. L. Stramer, F. B. Hollinger, L. M. Katz, S. Kleinman, P. S. Metzel, K. R. Gregory, and R. Y. Dodd, Transfusion **49**, 1S (2009).

[53] J. A. Grass, D. J. Hei, K. Metchette, G. D. Cimino, G. P. Wiesehahn, L. Corash, and L. Lin, Blood **91**, 2180 (1998).

[54] L. J. Dumont, J. P. AuBuchon, P. Whitley, L. H. Herschel, A. Johnson, D. McNeil, S. Sawyer, and J. C. Roger, Transfusion **42**, 847 (2002).

[55] J. P. AuBuchon, H. Taylor, S. Holme, and E. Nelson, Transfusion **45**, 1356 (2005).

[56] N. Tynngård, M. Studer, T. L. Lindahl, M. Trinks, and G. Berlin, Transfusion **48**, 1669 (2008).

[57] P. D. Mintz and G. Wehrli, Bone Marrow Transplantation **44**, 205 (2009).

[58] J. Irsch and L. Lin, Transfusion Medicine and Hemotherapy **38**, 19 (2011).

[59] S. Marschner and R. Goodrich, Transfusion Medicine and Hemotherapy **38**, 8 (2011).

[60] P. Sandgren, F. Tolksdorf, W. G. Struff, and H. Gulliksson, Vox Sanguinis **101**, 35 (2010).

[61] P. D. Mintz, Transfusion **51**, 1369 (2011).

[62] S. Leitman and P. Holland, Transfusion **25**, 293 (1985).

[63] R. Mallhi, A. Biswas, J. Philip, and T. Chatterjee, Medical Journal Armed Forces India **72**, 19 (2016).

[64] L. Lin, R. Dikeman, B. Molini, S. A. Lukehart, R. Lane, K. Dupuis, P. Metzel, and L. Corash, Transfusion **44**, 1496 (2004).

[65] D. van Rhenen, Blood **101**, 2426 (2002).

[66] R. R. Tice, D. Gatehouse, D. Kirkland, and G. Speit, Mutation Research/Genetic Toxicology and Environmental Mutagenesis **630**, 50 (2007).

[67] V. Ciaravino, Seminars in Hematology **38**, 12 (2001).

[68] R. P. Horgan and L. C. Kenny, The Obstetrician & Gynaecologist **13**, 189 (2011).

[69] V. W. Davis, O. F. Bathe, D. E. Schiller, C. M. Slupsky, and M. B. Sawyer, Journal of Surgical Oncology **103**, 451 (2010).

[70] M. Holčapek, G. Liebisch, and K. Ekroos, Analytical Chemistry **90**, 4249 (2018).

[71] E. Fahy, S. Subramaniam, H. A. Brown, C. K. Glass, A. H. Merrill, R. C. Murphy, C. R. H. Raetz, D. W. Russell, Y. Seyama, W. Shaw, et al., Journal of Lipid Research **46**, 839 (2005).

[72] G. van Meer and A. I. P. M. de Kroon, Journal of Cell Science **124**, 5 (2010).

[73] T. Hartmann, J. Kuchenbecker, and M. O. W. Grimm, Journal of Neurochemistry **103**, 159 (2007).

[74] D. A. Slatter, M. Aldrovandi, A. O'Connor, S. M. Allen, C. J. Brasher, R. C. Murphy, S. Mecklemann, S. Ravi, V. Darley-Usmar, and V. B. O'Donnell, Cell Metabolism **23**, 930 (2016).

[75] W. L. Smith, Trends in Biochemical Sciences **33**, 27 (2008).

[76] K. van Leyen, in *Primer on Cerebrovascular Diseases* (Elsevier, 2017), pp. 86–89.

[77] H. Tallima, K. Hadley, and R. E. Ridi, in *An Overview of Tropical Diseases* (InTech, 2015).

[78] E. J. Neufeld and P. W. Majerus, Journal of Biological Chemistry **258**, 2461 (1983).

[79] W. J. Brown, K. Chambers, and A. Doody, Traffic **4**, 214 (2003).

[80] J. Balsinde, M. V. Winstead, and E. A. Dennis, FEBS Letters **531**, 2 (2002).

[81] E. A. Dennis, J. Cao, Y.-H. Hsu, V. Magrioti, and G. Kokotos, Chemical Reviews **111**, 6130 (2011).

[82] P. C. Norris and E. A. Dennis, Proceedings of the National Academy of Sciences **109**, 8517 (2012).

[83] F. Fitzpatrick and R. Soberman, Journal of Clinical Investigation **107**, 1347 (2001).

[84] W. L. Smith and R. C. Murphy, in *Biochemistry of Lipids, Lipoproteins and Membranes* (Elsevier, 2016), pp. 259–296.

[85] F. Bosetti, Journal of Neurochemistry **102**, 577 (2007).

[86] H. Kuhn, S. Banthiya, and K. van Leyen, Biochimica et Biophysica Acta (BBA) - Molecular and Cell Biology of Lipids **1851**, 308 (2015).

[87] P. K. Ines, Frontiers in Bioscience **13**, 2833 (2008).

[88] Y. K. Denisenko, E. G. L. Lobanova, T. P. Novgorodtseva, T. A. Gvozdenko, and A. V. Nazarenko (2015).

[89] R. K. Saini and Y.-S. Keum, Life Sciences **203**, 255 (2018).

[90] R. C. Block, A. Abdolahi, X. Tu, S. N. Georas, J. T. Brenna, R. P. Phipps, P. Lawrence, and S. A. Mousa, Prostaglandins, Leukotrienes and Essential Fatty Acids **96**, 17 (2015).

[91] B. McAdam, I. Mardini, A. Habib, A. Burke, J. Lawson, S. Kapoor, and G. FitzGerald, Journal of Clinical Investigation **105**, 1473 (2000).

[92] C. M. Jenkins, A. Cedars, and R. W. Gross, Cardiovascular Research **82**, 240 (2008).

[93] M. H. Shishehbor, R. Zhang, H. Medina, M.-L. Brennan, D. M. Brennan, S. G. Ellis, E. J. Topol, and S. L. Hazen, Free Radical Biology and Medicine **41**, 1678 (2006).

[94] B. T. Kalish, M. W. Kieran, M. Puder, and D. Panigrahy, Prostaglandins & Other Lipid Mediators **104-105**, 130 (2013).

[95] M. Rosolowsky and W. B. Campbell, Biochimica et Biophysica Acta (BBA) - Lipids and Lipid Metabolism **1299**, 267 (1996).

[96] M. Crescente, L. Menke, M. V. Chan, P. C. Armstrong, and T. D. Warner, British Journal of Pharmacology (2018).

[97] C. Vijil, C. Hermansson, A. Jeppsson, G. Bergström, and L. M. Hultén, PLoS ONE **9**, e88546 (2014).

[98] S. H. Lee, M. V. Williams, R. N. DuBois, and I. A. Blair, Journal of Biological Chemistry **280**, 28337 (2005).

[99] J. M. Bailey, R. W. Bryant, J. Whiting, and K. Salata, Journal of Lipid Research **24**, 1419 (1983).

[100] B. Porro, P. Songia, I. Squellerio, E. Tremoli, and V. Cavalca, Journal of Chromatography B **964**, 26 (2014).

[101] F. A. Fitzpatrick, M. D. Ennis, M. E. Baze, M. A. Wynalda, J. E. McGee, and W. F. Liggett, Journal of Biological Chemistry **261**, 15334 (1986).

[102] E. Hill, F. Fitzpatrick, and R. C. Murphy, British Journal of Pharmacology **106**, 267 (1992).

[103] L. L. Mazaleuskaya, A. Salamatipour, D. Sarantopoulou, L. Weng, G. A. FitzGerald, I. A. Blair, and C. Mesaros, Journal of Lipid Research **59**, 564 (2018).

[104] Y. Gus-Brautbar and D. Panigrahy, The Journal of Experimental Medicine **211**, 10081 (2014).

[105] M. A. Bachelor and G. Bowden, Seminars in Cancer Biology **14**, 131 (2004).

[106] J. Zhang and G. T. Bowden, Photochem. Photobiol. Sci. **11**, 54 (2012).

[107] D. Hanson and V. DeLeo, Journal of Investigative Dermatology **95**, 158 (1990).

[108] C. F. Poole, TrAC Trends in Analytical Chemistry **22**, 362 (2003).

[109] W. W. Christie, Advances in Lipid Methodology **1**, 1 (1992).

[110] V. Camel, Spectrochimica Acta Part B: Atomic Spectroscopy **58**, 1177 (2003).

[111] V. Ruiz-Gutiérrez and M. Pérez-Camino, Journal of Chromatography A **885**, 321 (2000).

[112] M. Sandoval-Riofrio, Ph.D. thesis (2017).

[113] M. C. McMaster, *LC/MS* (John Wiley & Sons, Inc., 2005).

[114] Y. Hasin, M. Seldin, and A. Lusis, Genome Biology **18** (2017).

[115] D. Tsikas, Journal of Chromatography B **1012-1013**, 211 (2016).

[116] S. Fekete, J. Schappler, J.-L. Veuthey, and D. Guillarme, TrAC Trends in Analytical Chemistry **63**, 2 (2014).

[117] M. E. Swartz, Journal of Liquid Chromatography & Related Technologies **28**, 1253 (2005).

[118] C. K, Anal Chem Ind J. **16**, 114 (2016), ISSN 0974-7419.

[119] R. Harkewicz and E. A. Dennis, Annual Review of Biochemistry **80**, 301 (2011).

[120] R. D. Smith, J. A. Loo, C. G. Edmonds, C. J. Barinaga, and H. R. Udseth, Analytical Chemistry **62**, 882 (1990).

[121] J. H. Gross, *Mass Spectrometry* (Springer Berlin Heidelberg, 2011).

[122] R. A. Scheltema, J.-P. Hauschild, O. Lange, D. Hornburg, E. Denisov, E. Damoc, A. Kuehn, A. Makarov, and M. Mann, Molecular & Cellular Proteomics **13**, 3698 (2014).

[123] C. D. Kelstrup, R. R. Jersie-Christensen, T. S. Batth, T. N. Arrey, A. Kuehn, M. Kellmann, and J. V. Olsen, Journal of Proteome Research **13**, 6187 (2014).

[124] J. V. Olsen, J. C. Schwartz, J. Griep-Raming, M. L. Nielsen, E. Damoc, E. Denisov, O. Lange, P. Remes, D. Taylor, M. Splendore, et al., Molecular & Cellular Proteomics **8**, 2759 (2009).

[125] V. G. Tusher, R. Tibshirani, and G. Chu, Proceedings of the National Academy of Sciences **98**, 5116 (2001).

[126] A. S. B. S. Everitt, *The Cambridge Dictionary of Statistics* (Cambridge University Press, 2015), ISBN 0521766990.